

# **Identification of Damping Contribution from Power System Controllers**

**Mahdi Banejad**

**B.Eng (Electrical Engineering)**

**M.Eng (Electrical Engineering)**

**This thesis was submitted as a requirement for the degree of**

**Doctor of Philosophy**

**Built Environment and Engineering Research Centre**

**School of Electrical and Electronic Systems Engineering**

**Faculty of Built Environment and Engineering**



**Queensland University of Technology**

**June 2004**





QUEENSLAND UNIVERSITY OF TECHNOLOGY  
DOCTOR OF PHILOSOPHY THESIS EXAMINATION

**CANDIDATE NAME:** *Mahdi Banejad*

**FACULTY:** *Built Environment and Engineering*

**SCHOOL:** *Electrical and Electronic Systems Engineering*

**CENTRE:** *Built Environment and Engineering Research Centre*

**PRINCIPAL SUPERVISOR:** *Professor Gerard Ledwich*

**ASSOCIATE SUPERVISORS:** *Dr Edward Palmer*  
*Professor Boualem Boashash*

**THESIS TITLE:** *Identification of Damping Contribution from Power System Controllers*

*Under the requirements of PhD regulations, Section 16, it is hereby certified that the thesis of the above-named candidate has been examined. On advice from the Principal Supervisor and Faculty Head of Postgraduate Research Studies, I recommend on behalf of the University that the thesis be accepted in fulfilment of the conditions for the award of the degree of Doctor of Philosophy.*

*m. Mahendran*  
.....  
Professor Mahendran  
Acting Chair of Research Degrees Committee

*17. 06. 2004*  
.....  
Date



## **Keywords**

Power system eigenvalue, load modelling, resonant frequency, inter-machine oscillations, inter-area oscillations, cross-correlation, autocorrelation, damping contribution, sensitivity analysis, static var compensator, synchronous generator, induction motor, rotor angle.



# Abstract

With the growth of power system interconnections, the economic drivers encourage the electric companies to load the transmission lines near their limits, therefore it is critical to know those limits well. One important limiting issue is the damping of inter-area oscillation (IAO) between groups of synchronous machines. In this Ph.D. thesis, the contribution of power system components such as load and static var compensators (SVC) that affect the IAO of the power system, are analysed. The original contributions of this thesis are as follows:

## **1-Identification of eigenvalues and mode shapes of the IAO:**

In the first contribution of this thesis, the eigenvalues of the IAO are identified using a correlation based method. Then, the mode shape at each identified resonant frequency is determined to show how the synchronous generators swing against each other at the specific resonant frequencies.

## **2-Load modelling and load contribution to damping:**

The first part of this contribution lies in identification of the load model using cross-correlation and autocorrelation functions. The second aspect is the quantification of the load contribution to damping and sensitivity of system eigenvalues with respect to the load.

## **3- SVC contribution to damping:**

In this contribution the criteria for SVC controller redesign based on complete testing is developed. Then the effect of the SVC reactive power on the measured power is investigated.

All of the contributions of this thesis are validated by simulation on test systems. In addition, there are some specific application of the developed methods to real data to find a.) the mode shape of the Australian electricity network, b.) the contribution of the Brisbane feeder load to damping and c.) the effect of the SVC reactive power of the Blackwall substations on the active power supplying Brisbane.



# Table of Contents

<b>Keywords.....</b>	<b>i</b>
<b>Abstract.....</b>	<b>iii</b>
<b>List of Figures.....</b>	<b>xi</b>
<b>List of Tables.....</b>	<b>xvii</b>
<b>List of Symbols and Abbreviations .....</b>	<b>xix</b>
<b>Authorship.....</b>	<b>xxi</b>
<b>Acknowledgements.....</b>	<b>xxiii</b>
<b>Chapter 1: Introduction.....</b>	<b>1</b>
1.1 Significance and Motivation of this Research.....	1
1.2 Approaches and Aims.....	4
1.3 The Original Contributions of this Thesis.....	5
1.4 Organization of this Thesis.....	7
1.5 Publication Arising from this Thesis.....	9
1.6 Summary.....	11
<b>Chapter 2: Literature Review of Damping of Inter-area             Oscillations.....</b>	<b>13</b>
2.1 Introduction.....	13
2.2 Power System Representation in the IAO.....	13
2.3 Mode Shape and Participation Factor.....	18
2.4 Correlation Based System Transfer Function Identification.....	20

2.5 Inter-area Oscillation studies.....	22
2.5.1 Review of the Inter-area Oscillations.....	22
2.5.2 Spectral Methods in IAO Studies.....	23
2.5.3 The Effect Power System Stabilizer on IAO.....	24
2.5.4 Prony's Method.....	25
2.5.5 Energy Concept Approach in IAO Studies.....	28
2.6 Review of Load Modeling.....	29
2.6.1 IEEE Load Modeling.....	29
2.6.2 Modeling of Induction Motors.....	30
2.6.3 Dynamic Load Modeling.....	34
2.6.4 Component Based and Measurement Based Load Modeling..	35
2.7 The Effect of Load on IAO.....	36
2.7.1 The Mutual Interaction between Load and Power System.....	37
2.7.2 The effect of Load Modulation on IAO Damping.....	38
2.8 Review of SVC Modeling.....	39
2.9 The Effect SVC on IAO.....	41
2.10 Summary.....	44

### **Chapter 3: Correlation Based Mode Shape**

<b>Identification.....</b>	<b>45</b>
3.1 Introduction.....	45
3.2 Theory of the Correlation Based Method Mode Shape Identification Method.....	46
3.2.1 Characterizing Power System Disturbances.....	46
3.2.2 Plant Description.....	48
3.2.3 Power System Impulse Response.....	49
3.2.4. Response of the White Noise Driven Power System.....	52
3.2.5. Response of a Power System to White Noise Plus and Impulse .....	54

3.2.6. Using Non-analytic Process.....	55
3.3 Algorithm of the Correlation Based Mode Shape Identification (CBMSI) Method.....	56
3.4 Simulation Results of the CBMSI Method .....	61
3.4.1 Eigenvalue analysis of a Test Power System.....	61
3.4.2. Simulation Results.....	62
3.5 Results of the CBMSI Method on Real Data.....	70
3.5.1. Results due to Power system Disturbance.....	70
3.5.2. Results from Normal Operating Conditions.....	73
3.6 Summary.....	80
<b>Chapter 4: Load Contribution to Damping.....</b>	<b>81</b>
4.1 Introduction.....	81
4.2 The Concept of Load Contribution to Damping.....	82
4.3 State Space Representation of the Power Systems.....	83
4.4 Sensitivity of Power System Mode with Respect to Load Parameters.....	87
4.5 Load Model Identification in IAO.....	89
4.5.1 Describing the Load Effect on Power System Using Block Diagram Representation.....	89
4.5.2 Correlation Based Analysis of the Load Effect on the Power system.....	91
4.6 Algorithm of the Eigenvalue Sensitivity to Load (ESL) Method.....	97
4.7 Simulation Results of the ESL Method.....	99
4.8 Results of the ESL Method on Real Data.....	107
4.9 Summary.....	112

<b>Chapter 5: SVC Contribution to Damping.....</b>	<b>115</b>
5.1 Introduction.....	115
5.2 The Basic concepts of SVC Contribution to Damping.....	116
5.3 SVC Controller Redesign Based on Complete Testing.....	119
5.3.1 The Essence of Redesign of SVC Controller.....	119
5.3.2 Theory of redesign of SVC Controller.....	122
5.4 Algorithm of the SVC Controller Redesign Based on Complete Testing.....	125
5.5 Simulation Results for SVC Controller Redesign Based on Complete Testing.....	127
5.6 SVC controller Redesign Based on Normal Operation (Simplified Case) .....	132
5.7 SVC controller Redesign Based on Normal Operation (General Case).....	140
5.7.1 System Description.....	141
5.7.2 Examination of Approaches to Analyze.....	142
5.8 Identification of System in Normal Operation with SVC.....	145
5.8.1: Algorithm and Simulation of the Partial Fraction Expansion Approach.....	145
5.8.2: Algorithm and Simulation of the Decorration Approach....	148
5.9 Real data Analysis.....	150
5.10 Summary.....	154

<b>Chapter 6: Summary, Conclusion and Recommendation for Future Research.....</b>	<b>157</b>
6.1 Summary.....	157
6.2 Conclusion.....	161
6.3 Recommendation for Future Research.....	162
6.3.1 The Effect of Automatic Voltage Regulator to Damping.....	162
6.3.2 Examining the Effect of Location of Load on the Analysis of the Load Contribution to Damping.....	164
6.3.3 Investigation the effect of other AC Transmission Devices to Damping.....	167
6.3.4 Characterization of the Time Variation of Load.....	168
<b>References.....</b>	<b>169</b>
<b>Appendix A.....</b>	<b>185</b>
<b>Appendix B.....</b>	<b>189</b>
<b>Appendix C.....</b>	<b>191</b>



# List of Figures

Figure 1.1: A single machine connected to infinite bus.....	3
Figure 1.2: The contribution of load to damping.....	4
Figure 2.1: Time frames for dynamic phenomena of the power systems [2] .....	14
Figure 2.2: A linear system with a random variable input.....	21
Figure 2.3: Feedback representation of load dynamic effect in the power systems [81].....	37
Figure 2.4: The response of the real power of a dynamic load to step change in voltage [3] .....	38
Figure 2.5: The V-I characteristic of SVC [90] .....	40
Figure 2.6: A simplified model of an SVC [1].....	40
Figure 2.7: The extended Philips-Hoeffron model with SVC [97].....	42
Figure 2.8: The schematic diagrams for SVC including voltage and damping control blocks [97].....	43
Figure 3.1: A power system with one inputs and two outputs.....	48
Figure 3.2: The schematic diagram of the power system with inputs and outputs.....	57
Figure 3.3: The autocorrelation of rotor angle $\delta_l$ of the test power system.....	63
Figure 3.4: The cross-correlation of $\delta_l$ and $\delta_3$ of the test power system.....	64

Figure 3.5: The <i>FFT</i> of autocorrelation of the generator angle $\delta_2$ and the fitted curves of the test system.....	64
Figure 3.6: Mode shape plot at $f=1.4Hz$ obtained from the two methods, a) eigenvalue analysis, b.) CBMSI method.....	68
Figure 3.7: Mode shape plot at $f=2.1Hz$ obtained from the two methods, a) eigenvalue analysis, b.) CBMSI method.....	69
Figure 3.8: The real data of power flow across the South Australia power line following the braking resistor event 00:44:51 on the 22 <sup>nd</sup> of January 2001.....	71
Figure 3.9: The autocorrelation of the power flow of a power line for the real data.....	71
Figure 3.10: The magnitude of the <i>FFT</i> of the autocorrelation of the power flow of the load centers in Australian electricity network following the braking resistor test.....	72
Figure 3.11: The magnitude of the voltage and current of one hour data started the time 00.00 of the 22 <sup>nd</sup> of May 2002.....	74
Figure 3.12: The autocorrelation of the Brisbane voltage angle .....	75
Figure 3.13: The cross-correlation of voltage angle of Brisbane and Sydney voltage angle .....	75
Figure 3.14: The magnitude of the <i>FFT</i> of autocorrelation of bus voltage angle of the load centers.....	76
Figure 3.15: Mode shape for real data at the first resonant frequency.....	78
Figure 3.16: Mode shape for real data at the second resonant frequency....	78
Figure 3.17: Mode shape for real data at the third resonant frequency.....	79

Figure 4.1: A single machine connected to infinite bus.....	82
Figure 4.2: Load contribution to damping, a) static load, b) dynamic load.....	83
Figure 4.3: The connection of generator $i$ and load $i$ and to the rest of the network.....	84
Figure 4.4: A block diagram of power system to show load dynamics a.) complete model, b.) simplified model.....	90
Figure 4.5: A simplified diagram of the test power system including a dynamic load at each generator terminal.....	101
Figure 4.6: The frequency response of the identified model for load 2 of the test power system.....	103
Figure 4.7: The plot of the contribution of the load $L_I$ to damping at $f = 1.4 \text{ Hz}$ for the test power system.....	106
Figure 4.8: The plot of the contribution of the load $L_I$ to damping at $f = 2.1 \text{ Hz}$ for the test power system.....	106
Figure 4.9: The Brisbane feeder load contribution to damping at $f = 0.299 \text{ Hz}$ .....	111
Figure 4.10: The Brisbane feeder load contribution to damping at $f = 0.439 \text{ Hz}$ .....	111
Figure 4.11: The Brisbane feeder load contribution to damping a $f = 0.740 \text{ Hz}$ .....	112

Figure 5.1: The effect of load to damping, a.) SVC with given controller parameters, b.) SVC with the updated controller parameters.....	117
Figure 5.2: Power system block diagram including the effect of reactive power of SVC on the measured power.....	118
Figure 5.3: The diagram of single machine connected to the infinite bus with SVC and induction motor.....	121
Figure 5.4: The phase shift diagram of contribution of $P_I$ to damping, a.) without SVC, b.) with SVC.....	121
Figure 5.5: The delta equivalent of Figure 5.3.....	124
Figure 5.6: The magnitude of the $FFT$ of autocorrelation of the generator bus voltage angle changes for the test power system.....	128
Figure 5.7: The magnitude and phase of identified transfer function between $Q$ of the SVC and $\delta$ for the test power system.....	129
Figure 5.8: The phase shift fit diagram of the test power system (for SVC: $k_I = 0$ and $k_2 = 0.3$ ).....	130
Figure 5.9: The phase shift of the change in the vectors when $k_2$ increases from $0$ to $0.3$ , meanwhile $k_I = 0$ , for the test power system.....	131
Figure 5.10: Power system block diagram representing the effect of reactive power of SVC on the load active power.....	133

Figure 5.11: A load modulated test system to investigate the effect of the reactive power of SVC on active power of find.....	142
Figure 5.12: frequency response of the identified transfer function $T_t(\omega)$ .....	147
Figure 5.13: The frequency response of the identified transfer function $F(\omega)$ obtained using partial fraction expansion approach .....	147
Figure 5.14: The frequency response of the identified transfer function $T(\omega)$ obtained when the synchronous generator is frozen .....	148
Figure 5.15: The frequency response of the identified transfer function $T(\omega)$ obtained when the generator is running using the decorrelation approach.....	149
Figure 5.16: The reactive power of SVC from Blackwall substation of SVC.....	150
Figure 5.17: The active power flow past Blackwall substation to Brisbane .....	151
Figure 5.18: The frequency response of the identified transfer function $T_t(\omega)$ for the real data.....	153
Figure 5.19: The frequency response of the identified transfer function $T_P(\omega)$ for the real data.....	153

Figure 5.20: The frequency response of the identified transfer function

$\Gamma(\omega)$  for the real data.....154

Figure 6.1: The contribution of produced magnetic flux load to damping.164

Figure 6.2: The diagram of the connection of the general dynamic load  $P_{Lij}$

between generator  $i$  and generator  $j$  .....165

# List of Tables

Table 3.1: The actual and estimated eigenvalues of the test power system.	65
Table 3.2: The actual and estimated resonant frequencies of the test power system.....	65
Table 3.3: The value of the elements of $\bar{\varphi}_k$ associated with $f = 1.4 Hz$ obtained from the two methods: eigenvalue analysis and the CBMSI based method for the test power system.....	67
Table 3.4: The value of the elements of $\bar{\varphi}_k$ associated with $f = 2.1 Hz$ obtained from the two methods: eigenvalue analysis and the CBMSI based method for the test power system.....	67
Table 3.5: The power system eigenvalues estimated from power flow of the load centers in Australian electricity network following the braking resistor test.....	72
Table 3.6: The estimated system frequencies corresponding to Table 3.5...	73
Table 3.7: The power system eigenvalues identified form one hour of the normal operating data .....	77
Table 3.8: The power system resonant frequencies power identified form one hour of the normal operating data .....	77
Table 4.1: The chosen and estimated the loads parameters for the test power system .....	104

Table 4.2: The actual and estimated sensitivity of the power system	
eigenvalues when all loads are present.....	104
Table 4.3: The value of load contribution to damping for the test power	
system.....	105
Table 4.4: The sensitivity of the eigenvalues of the real data with respect to	
the Brisbane feeder load.....	110
Table 4.5: The value of load contribution to damping at the three identified	
resonant frequencies .....	110
Table 5.1: The change in the vectors when $k_2$ increases for the test power	
system.....	131

# List of Symbols and Abbreviations

$\mathfrak{F}$	Fourier transform operator
$FFT$	Fast Fourier transform
$\tau$	Time lag
$E[ \ ]$	Expected value
$s$	Complex frequency variable in the Laplace domain
$t$	Time
$\omega$	Frequency variable in the Fourier domain
$Hz$	Hertz
$Deg.$	Degree
$rad$	Radian
$Sec.$	Second
$t$	Time
$h(t)$	Function in the time domain
$\mathbf{H}(s)$	Function in the Laplace domain
$\mathbf{H}(\omega)$	Function in the Fourier domain
$\Phi$	Right modal matrix
$\Psi$	Left modal matrix
$u_s(t)$	Unit step response
IAO	Inter-area oscillations
COI	Centre of inertia

SVC	Static var compensator
CBMSI	Correlation based mode shape identification
ESL	Eigenvalue sensitivity to load
ARMA	Autoregressive moving average
EMTP	Electromagnetic transient program
PSS	Power system stabilizer
FSM	Frequency spectrum method
DC	Direct current
AC	Alternative current
UPFC	Unified power system controller
TCSC	Thyristor controlled series capacitor
TCR	Thyristor controlled reactor
FC	Fixed capacitor
LIED	Index location for effective damping
PID	Proportional-Integral-Derivative

## **Authorship**

The work continued in this thesis has not been published previously submitted for a degree or diploma at this or any other educational institution. To the best of my knowledge and belief, this thesis contains no material previously published or written by another person except where due reference is made.

Signed.....

....

# Acknowledgements

First and foremost, my sincerest and deepest thanks to God, the most compassionate and merciful, who helped me during my doctoral studies.

I would like to extend my appreciation to my principal supervisor, Prof. Gerard Ledwich, from the depth of my heart. Prof. Ledwich was very patient, kind and helpful during my Ph.D. period. He has been one of the best teachers throughout my academic career. His endless support guided me to complete this thesis. I would also like to thank my associate supervisors, Prof. Boualem Boashash and Dr. Ed Palmer, for their valuable support and help while working in the Signal Processing Research Lab. I am very grateful for their valuable comments.

I would like to express my deepest appreciation to the government of the Islamic Republic of Iran and Shahrood University for awarding this Ph.D. scholarship. I particular thank Prof. Javad Farhoudi, the Iranian scientific counsellor in Australia, for his continuing support.

I would like to extend my appreciation to Powerlink Queensland for providing real data used in this thesis.

I would also like to thank the administration staff, secretarial staff and postgraduate students of the School of Electrical and Electronic Systems Engineering, for providing a helpful environment.

Finally, I would like to express my deepest gratitude to my wife, Khadigeh, and my sons, Alireza and Amireza, for their patience and encouragement. This gratitude extends to my entire family for their support of my research.



## **Chapter 1: Introduction**

### **1.1 Significance and Motivation of this Research**

Due to the expansion of loads in power systems and increasing the power system interconnections, the economic drivers encourage loading the transmission lines near their limits. Therefore, it has become more important to know those limits well. One limiting issue is the damping of inter-area oscillations (IAO) between groups of machines.

In a multi-machine power system, rotor angle stability or in short, angle stability refers to the ability of the power system to maintain synchronization. In a power system, the rotors of all of the machines must be synchronised. This implies that the frequency of stator currents and voltages of all of machines must be the same [1]. In the steady state condition, the input mechanical power is equal to the output electrical power in each machine and speed is kept constant. If a perturbation, such as load changes, occurs in the power system, the equilibrium point would not be maintained. Consequently, for a short time the rotor angle of the generators will change.

In other words, accelerations can occur when there is lack of equality of input and output power for each generator. Because the acceleration of the rotor depends largely on angle differences, the oscillations can occur. There are two types of modes in the IAO: local and inter-area modes. Local modes are associated with the swinging of one generator against the rest of the system. In the inter-area modes, generators in one area swing against the generators of the other area [2].

Lack of sufficient damping torque causes the amplitude of the oscillatory modes to increase and this could result in excessive power oscillations. Therefore, understanding the IAO is essential in power systems studies. An important component of this is the determination of the effect of power system components such as load and static var compensators (SVC) on damping of the IAO. Accurate identification of these effects leads to more reasonable and reliable decision making during normal and emergency situations. The importance of the estimation rises as the complexity of the network increases. By increasing the IAO damping, the stability and reliability of supplying customer demand are maintained and a greater confidence in approaching transfer limit of power flow across major links can be achieved.

The involvement of load to damping is explained from a test power system shown in Figure 1.1. In this figure, a synchronous generator is connected to the infinite bus through a transmission line and there is a load connected to the generator terminals. In the first case, the load is considered as a resistive load. In this case, if there is a step change in the voltage terminals of

generator, the load power  $P_L$  increases instantly. Thus, at the resonant frequency of the IAO, the changes in the load power are in phase with the voltage changes. Since the voltage changes in the test system are anti-phase with the changes of the generator bus voltage angle, then the active power changes of the resistive load do not contribute to damping.

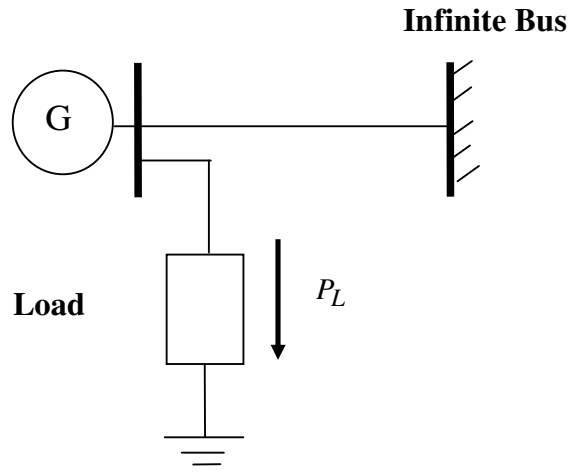


Figure 1.1: A single machine connected to infinite bus

Now consider the case that the load is a dynamic load. In this situation, if a step change of voltage occurs, then due to the dynamics of the load, the load power does not increase instantly [3]. Therefore, at the IAO resonant frequency, the load changes are not in phase with the voltage angle changes and there is phase shift as shown in Figure 1.2. As can be seen in Figure 1.2, load has a component in the direction of  $\dot{\delta}$  or damping torque. Thus, according to this figure, the load contributes positively to damping.

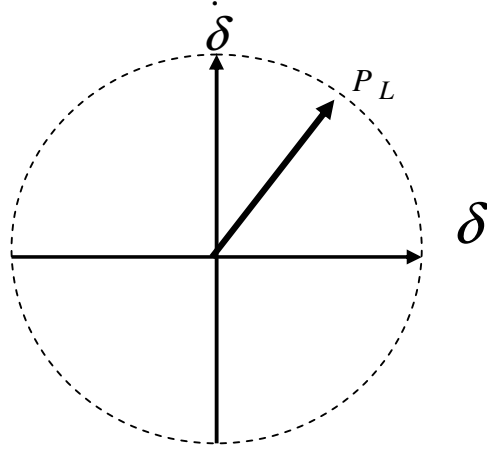


Figure 1.2: The contribution of load to damping

In this thesis a method of quantifying load contribution to damping is developed and a criterion is proposed to achieve the maximum load contribution to damping, i.e. the load contribution to damping is  $90^\circ$  ahead of  $\delta$  at the resonant frequency of the IAO.

## 1.2 Approaches and Aims

The main aspects of this thesis are to develop tools for validation of the contribution of load and SVC to the IAO. The focus is on the electromechanical modes between synchronous generators in the electrical network and in particular on the inter-area modes. The tool is based on small signal disturbances of the network and the contributions are to be analysed for each of the electromechanical oscillatory modes. This tool is for learning of the modal contribution from background disturbances caused by customer load variations and large disturbances such as line outage. The knowledge of the spectral properties of the customer load variations enables

identification of the modal frequencies and mode shapes. In particular, the main aims of this thesis are

- Identification of eigenvalues and mode shape of the IAO of the power systems.
- Load model identification and determination of load contribution to damping.
- Redesigning the SVC controller to achieve maximum damping and identifying the effect of reactive power of SVC on the load.

### 1.3 Original Contributions of this Thesis

The original contributions of this thesis are

- **Developing an algorithm to find mode shape of power system [4-5]**

As a result of these studies, for the first time, the power system engineer can compare an off-line computer model continuously with the actual power system response using normal operating data. Previously, a special test would need to be performed to understand the power system situation at one instant. In this contribution, the eigenvalues of the IAO are identified using a correlation based method. Then, the mode shape at each identified resonant frequency is determined to show how the synchronous generators swing against each other (Chapter 3).

- **Load model identification [6-7]**

The customer load is the power system component that has the most uncertainty in its model parameters. This original contribution demonstrates how the load model parameters can be updated continuously from normal

operating data. Both local and remote load perturbations are employed in identifying the load contribution to damping. The load model is represented by a transfer function that relates the rate of bus voltage angle changes to the measured active power of the load. This transfer function is identified using the autocorrelation and cross-correlation functions (Chapter 4).

- **Developing an algorithm to find load contribution to damping [8]**

The load dynamics effect is one of the most challenging issues in the IAO. Updating the load model in real time helps us to identify continuously the load contribution to damping. In this contribution of the thesis, the load contribution to damping is quantified using autocorrelation and cross-correlation functions. Then, the sensitivity of eigenvalues of the IAO of power system with respect to the load is determined using the right and left eigenvector (Chapter 4).

- **Developing an algorithm to redesign the SVC controller Based on complete testing [9-11]**

Power electronic devices such as SVC are the main tools for suppressing disturbances in transmission networks. The SVC works indirectly by controlling its reactive power which then influences the load and thus can suppress the power system oscillations. This original thesis contribution involves redesigning SVC controller on the basis of complete testing (no restrictions to the changes of the SVC control). The results of applying the suggested method provide the information that is needed to redesign the SVC controller to achieve the maximum load contribution to damping (Chapter 5).

- **Investigating the effect of SVC reactive power on the measured load active power using normal operating data**

In this contribution, the redesign of the SVC controller with the purpose of increasing load contribution to damping can be performed using the normal operating data. A transfer function showing the relationship between the reactive power of the SVC controller and the active power load determined is identified (Chapter 5).

## **1.4 Organization of this Thesis**

On the basis of the aims presented in Section 1.2, the organization of this thesis is as follows:

Chapter 2 is devoted to the review of the main concepts of the IAO and the representation of the power system in the IAO studies. The literature review about the load and SVC modelling is reviewed. Also, the effects of load and SVC on the IAO are discussed in this chapter.

In chapter 3, a method which is called correlation based mode shape identification (CBMSI), is developed to find the resonant frequencies and mode shape plots of the power systems on the basis of the autocorrelation and cross-correlation functions. A mode shape plot of a multi-machine power system shows how the generators of the power system swing against each other. In this chapter firstly, it is proven that by using the response of the generator voltage angles to the combination of large disturbance and costumer load variations, the phase difference and relative magnitude of the generator rotor angle can be determined and as a result the mode shape is

specified at that resonant frequency. In the CBMSI method, the resonant frequencies are identified by means of autocorrelation function, and the mode shape plot is formed using autocorrelation and cross-correlation functions. Then, the CBMSI method is simulated and validated on a multi-machine test system. Finally, the resonant frequencies and mode shape plot for the real data of the Australian electricity network are determined.

The contribution of load to damping of the IAO is studied in Chapter 4. In this chapter, the eigenvalue sensitivity to load (ESL) method is developed to investigate the effect of load in a closed loop system. In the ESL method, after identifying the load model, the contribution of load in damping is determined by finding the component of the load which lies in the direction of damping power. Then, the changes of the power system eigenvalues due to the presence of the load are determined using the ESL method.

The effect of SVC on damping is analysed in Chapter 5. In this chapter, two methods are developed to redesign the SVC controller to increase the damping of the IAO. The first method is based on complete testing and a criterion of SVC control design is introduced to achieve maximum damping of power system using appropriate feedback signals. Then, the suggested method is simulated on a test power system and the results show how the gain of the feedback controllers should be changed to get the maximum contribution to damping. In the second method which is based on normal operation, firstly, the influence of reactive power of the SVC on the active power of the load is studied. Then, after developing the theory, an algorithm is presented to find the effect of SVC reactive power on the load active

power. Then, a simulation is performed on a mainly load modulated test system to identify the transfer function representing the effect of reactive power of the SVC on active power of the load using two approaches: partial fraction expansion approach [12] and decorrelation approach. The information regarding the effect of the SVC reactive power on the active power can be used to design the SVC controller to increase the damping of the IAO. Results of the simulation show the validity of the method. At the end of this chapter, the effect of SVC on the real active power for the real data is investigated.

Finally the conclusion and some suggestions for the future studies in this area are given in Chapter 6.

## **1.5 Publication Arising from this Thesis**

### **Conference Papers**

1. M. Banejad, G. Ledwich, P.O'Shea and E. Palmer, "On Line Determination of Mode Shape of a Power System", The 6<sup>th</sup> International Transmission and Distribution Conference: Distribution 2001, Brisbane, Australia, Nov. 2001.
2. M. Banejad, G. Ledwich, "Correlation-Based Mode Shape Determination of a Power System", 2002 IEEE International Conference on Acoustics, Speech and Signal Processing: ICASSP2002, Orlando, Florida, USA, 12-17 May, 2002.
3. M. Banejad, G. Ledwich, "Correlation-Based Identification of the Effects of the Loads on Oscillatory Modes", Australian Universities Power

System Engineering Conference: AUPEC 2002, Melbourne, Australia. Oct. 2002.

4. M. Banejad, G. Ledwich, “Quantification of Load Contribution to Damping of a Power System”, 17<sup>th</sup> International Power System Conference, Tehran, Iran, 2002.

5. M. Banejad, G. Ledwich, “Analysis of SVC Contribution to Damping of a Power System Including Induction Motor Effects”, The 6<sup>th</sup> International Power Engineering Conference, Singapore, May 2003.

6. M. Banejad, G. Ledwich, “On the Effect of SVC Control Design of Damping of Low frequency Oscillations”, The 38<sup>th</sup> Universities Power Engineering conference: UPEC2003, Sep. 2003, Greece.

7. M. Banejad, G. Ledwich, “Investigation of Load Contribution to Damping in a Multi-machine Power System Based on Sensitivity Analysis”, Australian Universities Power System Engineering Conference: AUPEC 2003, New Zealand, Oct. 2003.

8. M. Banejad, G. Ledwich, “Improving the SVC Contribution to Damping of Low Frequency Oscillations of a Power Systems”, The 7<sup>th</sup> International Transmission and Distribution Conference: Distribution 2003, Adelaide, Australia, Nov. 2003.

### **Technical Report**

1 G. Ledwich, M. Banejad, “Analysis of Blackwall SVC Action Associated with Braking Resistor Tests for QNI Connection”, Report for Powerlink, QUT, Australia, 2001.

### **Journal Paper**

- 1 M. Banejad G. Ledwich, “Quantification of Damping Contribution from Loads”, IEE Part D: Generation, transmission and Distribution. (Submitted).

### **Journal Papers Under Preparation**

- 1 M. Banejad, G. Ledwich, “Correlation-Based Identification of the Resonant Frequencies of Inter-area Oscillations”, To be submitted to the journal “IEEE Transactions on Power Systems”.
- 2 M. Banejad, G. Ledwich, “Improving the SVC Contribution to Damping by Redesigning the SVC Controller”, To be submitted to the journal “IEEE Transactions on Power Systems”.

## **1.6 Summary**

In this chapter, an overview of this thesis including aims, main contributions, and organization the thesis, as well as the publication by the author of this thesis, are explained.

In Chapter 2 the main materials that are needed for the following chapters are given. Chapter 2 covers the power system representation in the IAO, load and SVC modeling. A literature review of the works that have been carried out in the field of load and SVC effects on damping of the IAO is also presented in Chapter 2.



## **Chapter 2: Literature Review of Damping of Inter-area Oscillations**

### **2.1 Introduction**

In this chapter the main concepts that are used in the following chapters are discussed. The concepts are explained in brief, and further discussion can be found in the given references. The literature related to eigenvalues of the inter-area oscillations (IAO), load modeling and static var compensators (SVC) modeling is reviewed and existing methods associated with load and SVC contribution to damping are discussed.

### **2.2 Power System Representation in IAO**

Different power system components have different time responses. The time constants of the power system components range from milliseconds for sub-transient phenomena in synchronous generator to several minutes for boilers in thermal power plants. Different studies are carried out in [2,13-14] to classify the modeling of the power system components in terms of time

response of the components. Figure 2.1 shows the time frames for the different phenomena of the power systems.

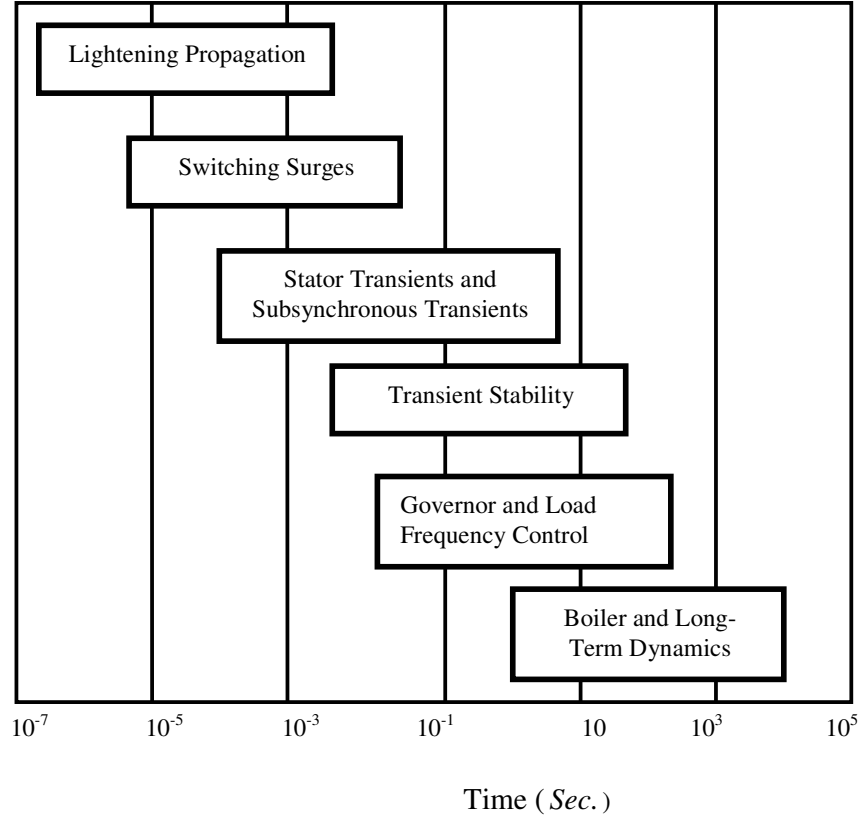


Figure 2.1: Time frames for dynamic phenomena of the power systems [2]

It is discussed in [14] that a new model for simulation should be built up from a set of components with time constants that are important for the phenomenon under investigation. The model should “responds rapidly enough for the impact to be observed before the simulation ends” [14]. In regard to the time scale for the purpose of the IAO studies, shown in Figure 2.1, the simplest model of the synchronous generator that adequately describes the IAO is the classic model [15]. In other words, to validate the methods, the classic model of the synchronous generators is adequate for the

task, and avoids the complexity associated with higher order of the synchronous generator models. If a more detailed synchronous generator is chosen, the nature of the IAO does not change [16].

For a power system including  $n$  generators, the electromechanical equation for generator  $i$  in per unit ( $p.u.$ ) can be written as [15]

$$J_i \ddot{\delta}_i = P_{mi} - P_{ei} - P_{Di} \quad p.u. \quad (2.1)$$

where

$\delta_i$  = rotor angle of generator  $i$

$J_i$  = inertia of generator  $i$

$P_{mi}$  = mechanical power of generator  $i$

$P_{ei}$  = electrical power of generator  $i$

$P_{Di}$  = damping power of generator  $i$

The electric power of generator  $i$  and damping power can be found from the following equations [15]

$$P_{ei} = \sum_{\substack{j=1 \\ j \neq i}}^n \frac{V_i V_j}{x_{ij}} \sin(\delta_i - \delta_j) \quad (2.2)$$

$$P_{Di} = D_i \dot{\delta}_i \quad (2.3)$$

where  $V_i$  and  $V_j$  are the voltage magnitude of bus  $i$  and  $j$  respectively, and

$D_i$  is the damping coefficient of generator  $i$ . Also  $x_{ij}$  is the reactance between bus  $i$  and  $j$ .

Using Equation (2-3) and substituting the appropriate values for all of the terms in Equation (2.1) from [15], then linearizing the result around operating points, yields

$$\ddot{\delta}_i + \frac{1}{J_i} \sum_{j=1}^{n-1} P_{sij} \delta_{ij} + \frac{1}{J_i} D_i \dot{\delta}_i = 0 \quad p.u. \quad i = 1, \dots, n \quad (2.4)$$

where  $P_{sij}$  is the electric power changes of generator  $i$  caused by an angle change between machine  $i$  and  $j$  given in [15]

For convenience,  $\Delta$  is omitted in Equation (2.4). Also,  $\delta_{ij}$  is determined from

$$\delta_{ij} = \delta_i - \delta_j \quad (2.5)$$

The rotor angle  $\delta_i$  in (2.4) shows the absolute changes of the rotor angle  $i$ . Since the relative rotor angle is of interest, rotor angles should be compared with a reference. The angle of centre of inertia (COI) is chosen as the reference angle. The advantages of using the COI angle as the reference angle are a) forming symmetrical swing equations and b) simplicity of use [2]. The angle reference of COI for an  $n$ -machine power system is computed from

$$\delta_{COI} = \frac{\sum_{k=1}^n J_k \delta_k}{\sum_{k=1}^n J_k} \quad (2.6)$$

The rotor angles in the COI referenced system are determined from

$$\delta_{ic} = \delta_i - \delta_{COI} \quad i = 1, \dots, n \quad (2.7)$$

The COI referenced system is used in Chapters 3 and 4 to analyze the simulation results as well as the real data.

Equation (2.4) can be represented by a set of  $n$  linear second-order differential equations or a set of  $2n$  linear first-order differential equations.

By examining the free response of the system, it can be found that the system has  $(n-1)$  pairs of natural frequencies or oscillatory modes and two common modes. Equation (2.4) can be represented in the state space form as

$$\dot{X} = A X \quad (2.8)$$

where

$$X = \begin{bmatrix} \delta_1 & \cdots & \delta_n & \dot{\delta}_1 & \cdots & \dot{\delta}_n \end{bmatrix}^T \quad (2.9)$$

$$A = \begin{bmatrix} 0 & 0 & \cdots & 0 & 1 & 0 & \cdots & 0 \\ 0 & 0 & \cdots & 0 & 0 & 1 & \cdots & 0 \\ \vdots & \vdots & \vdots & \vdots & \vdots & \vdots & \vdots & \vdots \\ 0 & 0 & \cdots & 0 & 0 & 0 & \cdots & 1 \\ \sum_{i=2}^n P_{s1i} & -P_{s12} & \cdots & -P_{s1n} & D_1 & 0 & \cdots & 0 \\ -P_{s21} & \sum_{\substack{i=1 \\ i \neq 2}}^n P_{s2i} & \cdots & -P_{s2n} & 0 & D_2 & \cdots & 0 \\ \vdots & \vdots & \vdots & \vdots & \vdots & \vdots & \vdots & \vdots \\ -P_{sn1} & -P_{sn2} & \cdots & \sum_{\substack{i=1 \\ i \neq n}}^n P_{sni} & 0 & 0 & \cdots & D_n \end{bmatrix} \quad (2.10)$$

The eigenvalues of the matrix  $A$  give the oscillatory modes of the power system IAO.

## 2.3 Mode Shape and Participation Factor

The linearized model of the power system can be represented in the state space form. With regard to Equation (2.8), the right and left eigenvector can be found from Equations (2.11) and (2.12), respectively [1,17-18]

$$\mathbf{A}\phi_i = \lambda_i\phi_i \quad (2.11)$$

$$\psi_i\mathbf{A} = \lambda_i\psi_i \quad (2.12)$$

where

$\lambda_i$  = the  $i^{th}$  eigenvalue

$\phi_i$  = the  $i^{th}$  right eigenvector ( $n \times 1$ )

$\psi_i$  = the  $i^{th}$  left eigenvector ( $1 \times n$ )

The right eigenvector,  $\phi_i$ , shows the extent to which the state variables have a relative activity at a specific excited mode. In the complex right eigenvector, the magnitude of the vector elements gives the magnitude of the relative activity of the state variables, and the phase of the vector elements gives the phase shift of the state variables at a specific excited mode. On the other hand, the left eigenvector,  $\psi_i$ , indicates which combination of the state variables forms the  $i^{th}$  mode and what is the weight of each state variable in forming a mode [1].

The right eigenvectors are used to plot mode shape. The mode shape shows how the synchronous generators swing against each other at a specific power system resonant frequency.

The right modal matrix  $\Phi$  is formed from the right eigenvectors as

$$\Phi = [\phi_1 \quad \dots \quad \phi_i \quad \dots \quad \phi_n] \quad (2.13)$$

Similarly, the left modal matrix can be found from

$$\Psi = [\psi_1^T \quad \dots \quad \psi_i^T \quad \dots \quad \psi_n^T]^T \quad (2.14)$$

It is proven in [1] that the following relations hold for the right and left eigenvector corresponding to eigenvalue  $\lambda_i$

$$\psi_i \phi_j = \begin{cases} d_i & i = j \\ 0 & i \neq j \end{cases} \quad (2.15)$$

where  $d_i$  is non-zero constant.

For convenience, it is customary to normalize these vectors, therefore

Equation (2.15) is changed to

$$\psi_i \phi_j = \begin{cases} 1 & i = j \\ 0 & i \neq j \end{cases} \quad (2.16)$$

Thus if the right and left eigenvectors are normalized, then according to Equation (2.16), then the relationship between the right and left modal matrices can be expressed as

$$\Phi \Psi = I \quad (2.17)$$

where  $I$  is the unity matrix .

There is a relationship between state variables and eigenvalues which is expressed by the participation matrix. The participation matrix,  $P$ , can be found from [19-20]

$$P = \{p_{ki}\} = \{\psi_{ki} \phi_{ki}\} \quad (2.18)$$

where  $\phi_{ki}$  ( $\psi_{ki}$ ) is the  $k^{th}$  element of  $i^{th}$  right (left) eigenvector  $\phi_i$  ( $\psi_i$ ) of the system matrix  $\mathbf{A}$ . The element  $p_{ki}$  shows the degree of participation of the  $k^{th}$  state variable to  $i^{th}$  eigenvalue. The sum of  $p_{ki}$  for the particular mode  $i$  is one [17]. The sensitivity of the  $i^{th}$  eigenvalue with respect to general element,  $a_{kj}$ , of the system matrix  $\mathbf{A}$  can be found from the following equation [20]

$$\frac{\partial \lambda_i}{\partial a_{kj}} = \psi_{ik} \phi_{kj} \quad (2.19)$$

The basic concepts presented in Equation (2.19), have proven useful in [1,17, 21-23] for variations of a single parameter for the system matrix  $\mathbf{A}$ . The major limitation is where a single change of dynamic loads modifying several components of the system matrix  $\mathbf{A}$ .

## 2.4 Correlation Based System Transfer Function

### Identification

One way for identifying a system transfer function is based on correlation functions. Some important aspects of the signal processing used in this thesis are presented in Appendix A [24-27].

It is explained in [28] that averaging the system responses leads to noise rejection. For a single frequency test, if the system responses are multiplied by sine or cosine functions and then the average of the results are computed, the noise level is reduced remarkably. This idea can be extended to the use of the cross-correlation and autocorrelations functions in identifying the system transfer function.

A system with a random variable input  $u(t)$  as an input and output  $y(t)$  is shown in Figure 2.2

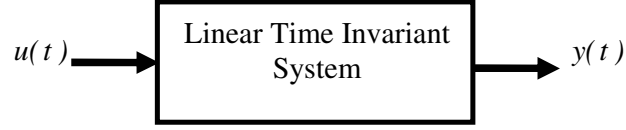


Figure 2.2: A linear system with a random variable input

In Figure 2.2,  $u(t)$  is an ensemble member of process  $U(t)$  (see Appendix A). The impulse response of this system is denoted by  $h(t)$ , then the transfer function of this system between input and output,  $\mathbf{H}(\omega)$  can be found from the following equation [24]

$$\mathbf{H}(\omega) = \frac{\Im[C_{uy}(\tau)]}{\Im[R_{uu}(\tau)]} \quad (2.20)$$

where

$C_{uy}(\tau)$  = the cross-correlation of  $u$  and  $y$

$R_{uu}(\tau)$  = the autocorrelation of  $u$

$\tau$  = time lag

$\Im$  = the Fourier transform operator [29]

## **2.5 Inter-area Oscillation studies**

In this section the inter-area oscillations (IAO) are discussed briefly. Then some methods that have been suggested by researchers to identify the resonant frequencies and damping of the IAO are discussed.

### **2.5.1 Review of the Inter-area Oscillations**

Damping of power system oscillations plays a significant role not only in increasing the line power capacity but also for stabilization of the power system, particularly in weakly coupled systems. As the power systems are operating near their stability limits, there is a more frequent occurrence of problems of low frequency oscillations. Some changes in power systems like line outage and customer load variation can initiate low frequency oscillations. As explained in Chapter 1, there are two types of low frequency oscillations: local and inter-area oscillations. Local oscillations are oscillations associated with a single generator. The oscillations are well recognized and have frequencies in the range of  $1$  to  $3\text{ Hz}$ . Inter-area oscillations are associated with groups of generators and have frequencies usually less than  $1\text{ Hz}$  [30-31].

The phenomena of the inter-area modes were investigated in [32] by determining the dominant modes following a large disturbance. The authors of [32] determined the eigenvalues and eigenvectors of the system from the free motion of the system following a large disturbance. Then, they used the “dominance measure” concept to determine the dominant modes. The dominance measure is determined from the left eigenvector and the value of

the state variable values at the end of the disturbance. A group of the generators is considered coherent if the phase angle of the dominance measures in this group differ by no more  $20^0$  to  $30^0$ . In order to determine the dominant mode in each group, the modes are sorted descendingly according to the magnitude of dominance measure. Finally, the participation of the state variables in the dominant modes are determined.

The effects of line impedance and flow on damping frequencies and mode shapes were investigated in [33]. The authors of [33] analyzed a hypothetical power system with a tie line and concluded that when the tie impedance or power flow is increased, the frequency and damping ratio are decreased. They also concluded with the non-zero tie line power flow, the mode shape changes considerably and the generators of one area no longer oscillate exactly in anti-phase to the generators of the other area.

References [30-33] create a background to analyze the IAO. The method presented in [32] identifies dominant modes of the IAO following a disturbance and it does not use the normal operating data. Reference [33] also gives some examples of mode shape analysis of a real network and the relationship between mode shapes and power flow, which provides a better understanding of the effect of tie line power flow on mode shapes.

### **2.5.2 Spectral Methods in IAO Studies**

Power system mode extraction using spectral analysis was investigated in [34-36]. The method in [34] is based on the Corinthios method [37] and uses Z-transformation identification that allows the modes to be identified directly. In this method, sampling of a recorded continuous time signal

yields a discrete time signal. After that, the Z-transform of the signal is taken. The residue and angle of the poles of the signal in the Z-plane gives the modes of the power system. On the basis of the short-time Fourier transform, a non-parametric method is suggested in [35] to investigate the power system dynamics during disturbances. In this method, the results from the estimation of the time-frequency distributions of the energy of the IAO provide information for modal analysis of the power system dynamics, and for determining the pattern and the dynamics of the power systems. In [36] random load perturbations and the frequency fluctuations are used to generate random power oscillations and excite the modes of a power system. Then, the frequency spectrum method (FSM) identifies the modes. The FSM of power system oscillations of machines and transmission lines can be obtained by expressing the frequency responses of the systems in terms of all operational and control parameters of the systems.

The methods used in [34-36] provide good tools for analyzing the low frequency oscillations of power systems but the problem of quantification of the damping contribution from power system components is still unsolved. Also these methods are off-line and do not use data from the normal operating system.

### **2.5.3 The Effect Power System Stabilizer on IAO**

In order to increase the damping during IAO, power system stabilizers (PSS) are often added to the power system. In fact, PSS uses supplementary signals that could be one of rotor speed deviation, frequency deviation or accelerating power [1-2,16,38-39]. The purpose of PSS is to produce an

electrical torque in phase with rotor speed. A common input of PSS is rotor speed deviation and the output is fed to the exciter of the generator. The PSS consists of three blocks; gain, wash out filter and phase compensation block. In the early 1960's, the preliminary application of PSS was done on four hydraulic power plants and the input signals for PSS were taken from the shaft speed [40]. The effect of various location of power system stabilizer (PSS) on inter-area modes and mode shapes is examined in [41], and it is shown in their example that with changes in location of PSS, the mode shapes do not change considerably.

The references in this section explain how to increase damping of the IAO by means of a supplementary signal. It is reported in these papers that PSS increases damping of the IAO. They also emphasize the control of model updating, which is useful for optimizing the dynamic response of PSS by adjusting the PSS parameters. However, they did not discuss the effect of power system controllers such as load and SVC to damping, and the contribution load to damping has not been quantified.

#### 2.5.4 Prony's Method

Prony's method is an off-line technique for identifying the frequencies ( $f_i$ ), damping factors ( $\alpha_i$ ), amplitudes ( $A_i$ ) and phases ( $\phi_i$ ) of a real exponential signal which can be represented as the following [42-43]

$$y[k] = \sum_{i=1}^P A_i \exp[(\alpha_i + j(2\pi f_i + \phi_i))k] \quad k \geq 0 \quad (2.21)$$

Prony's method has been used by many researchers to identify frequencies and damping of modes of electromechanical oscillation in power systems [43-50].

Prony's method is used to find a model for the measured power system response [43]. In [43], the algorithm consists of three steps. In the first step a discrete linear prediction model is fitted to the recorded data. In the next step, the roots of the polynomial associated with the linear prediction model obtained from the previous step, are determined. In the final step, the amplitude and phase at each mode is computed using the roots of Step 2 and complex frequencies. The method in [43] was used to find the resonant frequencies of a generator response in British Columbia to the modulation of an SVC connected to a 500 KV bus. In a study presented in [44], the modal components of the measured power response were determined by applying Prony's method to the power system response to a 1400 MW, 0.5 second braking resistor pulse.

The transfer function of PSS is determined in [45], based on Prony's method. The authors of [45] showed that this design of PSS leads to an increase in damping for both local and inter-area modes in the two test systems that they used in their work.

A comparison between Prony's method and eigenanalysis was made in [46]. In the eigenanalysis presented in [46] the state matrices are computed based on the small perturbation. It was indicated in this work that the two methods have similar results and they are complementary, but caution should be taken in choosing the processing parameters in Prony's method.

Transfer function identification using autoregressive moving average (ARMA) was compared with transfer function identification using Prony's method in [47] and it was concluded that the numerical robustness of ARMA method is better than Prony's method and the ARMA method has the advantage of simplicity. The identification of the oscillatory mode, (which is one contribution of this thesis), is related to transfer function identification. Since the noise content of a signal, limits the accuracy of Prony's method, the performance of Prony's method was improved in [48] using a set of signals. In this analysis a set of signals that have common eigenvalues are considered and Prony's method is applied to all of the signals of the set simultaneously.

Three methods of identifying the oscillatory modes were compared in [49]. The methods were Prony's method, the Eigensystem Realization algorithm, and the Steigh-McBride algorithm. It was concluded in this paper that the first two methods identify linear systems with similar results, which approximate the real system, but for the third method, the Steigh-McBride algorithm, the result is different.

The interleaved Prony's method was proposed in [50] to overcome the difficulties of Prony's method in identifying low and high frequency modes at the same time. It is also shown in this paper that the accuracy of identification of the modal parameters reduces as the level of noise increases.

Prony's method discussed in this section, from [43-50] has the drawback of being noise sensitive. The method is also not applicable to some of the tasks of this thesis such as load and SVC contribution to damping.

### **2.5.5 Energy Concept Approach in IAO Studies**

During the IAO, the relative acceleration of the rotors of the power system generators produce a periodic interchange of mechanical kinetic energy [51]. This interchange of energy following a disturbance was used in [52-53] to determine the damping and resonant frequencies of the IAO. In [52] two concepts of motion modes and energy modes are introduced to study the IAO. The frequencies of the speed oscillations are called motion oscillations. Also energy modes characterize the energy oscillations. The kinetic energy of each generator is described in terms of all power system modes. The mode with the most significant coefficient in the kinetic energy is called the dominant energy mode. The coefficients of the phase of the dominant energy modes for the generator are compared to identify mode shapes.

The concept of modal energy is introduced in the energy approach of the IAO in [53]. A systematic method is developed in [53] to find the IAO eigenvalues by comparing the magnitude and phase of the coefficients of the energy interchange for particular modes of interest. The power system controllers are designed to decrease the energy exchange of the particular modes.

The energy methods approached by [51-53] can be used following a disturbance to characterize the IAO and the methods do not make use of the

normal operating data. These methods also do not discuss quantifying the effects of power system controllers on damping of the IAO.

## 2.6 Review of Load Modeling

Power system loads have impact on power system stability and load modeling has an important role in stability studies of power systems. In this section various models of the loads are studied.

### 2.6.1 IEEE Load Modeling

According to the IEEE Task Force On Load Representation, load can be represented with a static or dynamic model [54]. The static load model is described as an algebraic relationship between the active (or reactive) and the voltage and frequency of the bus at the same time. The static load models mainly represent the resistive load or they can be used as an approximation of the dynamic loads when there are small changes in the load with time. However, in the dynamic load this relationship can be represented by difference or differential equations. It was explained in [55] that different models are considered for different simulations. For example, to use a static model for dynamic simulation, IEEE recommends the following equations

$$\begin{aligned} \frac{P}{P_{frac} P_0} = & K_{PZ} \left( \frac{V}{V_0} \right)^2 + K_{Pi} \left( \frac{V}{V_0} \right) + K_{PC} + K_{Pl} \left( \frac{V}{V_0} \right)^{n_{pv2}} (1 + n_{npf1} \Delta f) \\ & + K_{P2} \left( \frac{V}{V_0} \right)^{n_{pv2}} (1 + n_{npf2} \Delta f) \end{aligned} \quad (2.22)$$

$$\begin{aligned} \frac{Q}{Q_{frac}Q_0} = & K_{qZ} \left( \frac{V}{V_0} \right)^2 + K_{qi} \left( \frac{V}{V_0} \right) + K_{qC} + K_{ql} \left( \frac{V}{V_0} \right)^{n_{pv2}} (1 + n_{nqf1} \Delta f) \\ & + K_{q2} \left( \frac{V}{V_0} \right)^{n_{qv2}} (1 + n_{nqf2} \Delta f) \end{aligned} \quad (2.23)$$

where

$V$  = operating voltage

$V_0$  = rated voltage

$P$  = active power at the operating voltage

$P_0$  = active power at the rated voltage

$P_{frac}$  = the portion of the bus active load that represented by the static model

$Q$  = reactive power at the operating voltage

$Q_0$  = reactive power at the rated voltage

$Q_{frac}$  = the portion of the bus load that represented by the static model.

The other parameters of Equations (2.22) and (2.23) are given in [55].

### 2.6.2 Modeling of Induction Motors

In many cases such as the IAO studies, it is necessary to consider the dynamics of the load components. Induction motors consume nearly %60 to %70 of the total energy produced in power systems. From damping of the IAO point of view, the induction motors are the most influential load in damping. Therefore, the modeling of the induction motors is very important

for the IAO studies. Modeling of induction motors has been discussed in many papers such as [56-61].

The dominant behavior of large induction motors is described in [57] by a first-order voltage model using an integral Manifold [58]. Hung and Dommel in [59] suggested using a synchronous machine model of Electromagnetic Transient Program (EMPTP) to analyze the induction motor transients. Using EMTP to simulate the induction motor is advantageous because it consists of model of many power system components which may consider all transient characteristics of an induction motor.

A probabilistic method for characterization of dynamical modes of induction machine clusters under parametric uncertainties, was introduced in [60]. The method uses a stochastic norm to characterize variations of the model when parametric variations are present. The stochastic norm relates the size of the random matrix of the system to the expected value of the Frobenius norm [61] of the random matrix of the system. The stochastic approach in [60] removes the fast state variables and keeps the interaction between the fast and slow state variables of the motor. This method provides the information that is useful for establishing an aggregate model of the induction motors. The method also determines the suitable order of dynamic model using identification of separate clusters of eigenvalue associated with load dynamics.

A comparison study of the response of a realistic load including two induction motors and the aggregate model of the induction motor was

performed in [62]. In this study, a step decrease in voltage was applied to a realistic load and the aggregate model and the response of two cases were compared. The results show that the aggregate induction motor model of fifth order can better predict the transient responses.

Aspects of voltage dynamics of induction motors were investigated in [63] using a linearized model and the following models were recommended for aggregated loads

- A first order model can be used for active and reactive loads which consist of no dominant large induction motors.
- If the load consists of some dominant large induction motors, a second- or third-order can be used for active power, and first-order model for reactive power.

The validity of different order models was examined in [64] to anticipate the low frequency dynamic response of an induction machine. In reference [64] a perturbation in shaft torque, supply frequency and voltage magnitude are considered. They found that choosing a fifth-order model leads to achieving the high accuracy. In the simulation with the fifth order, validation of the response to all of the perturbation was confirmed in rotor speed, electrodynamic torque, active power, reactive power and stator current responses. The third order model anticipated well all responses to perturbation in torque and frequency up to  $10\text{ Hz}$ . They also found that the first-order speed model could be used to anticipate the rotor speed, electrodynamic torque and active power responses to torque and frequency

perturbation up to  $3\text{ Hz}$ . They concluded a third-order model is a good compromise between accuracy and simplicity in power system analysis.

The singular perturbations method is used in [65-68] to model the effects of variations of frequency in induction motors. The singular perturbations method deals with the slow and fast states rather than the original model [66]. In particular, this method is useful for studying phenomena which have a large difference in their frequency components. For example, the transients of the network have the natural frequency of more than  $60\text{ Hz}$ . On the other hand, the natural frequencies of in the rotor angle transient lies in the range of  $0.2 - 3\text{ Hz}$ . Therefore, this method is called “two time scale analysis” [65]. The authors of [66] used a singularly perturbed model to remove the state variables with small time constants. In the model, the fast and slow state variables described a first order mode separately. In the method presented in [67], in spite of eliminating the fast states, the model keeps the interaction between the low and fast transients. The idea of the singular perturbation model is extended in [68] to eliminate the fast state variables in an induction motor model. The advantages of the method are reduction in the simulation time and retaining the nature of the state variables. This method can also determine the interaction between the fast and slow motor dynamics. In the simulation performed in [68], it was observed that when there remarkable changes in the system frequency occur, ignoring the rate of changes of stator and rotor in different models produce a great error. However, the singularly perturbed model of the

induction motor can describe the dynamic of these state variables efficiently.

### 2.6.3 Dynamic Load Modeling

Since the dynamic aspects of electric load influence the performance of the power system in angle stability, dynamic load modeling has been investigated by many researchers including [3,68-73].

The general load model was proposed in [3,69]. The load is described as a non-linear dynamic model in [3,69]. This model agreed with the experiments in the laboratory and was presented as

$$T_P \dot{P}_d + P_d = P_s(V) + K_P(V) \dot{V} \quad (2.24)$$

where  $P_d$  is demand power and the static part of the load and represented by  $P_s(V)$ . In this equation  $P_s$  and  $K_P$  are two non-linear algebraic equations, and  $K_d$  is a linear time constant. It is shown in [3] that the solution of Equation (2.25) for the step change in the load voltage can be obtained from

$$P_d(t) = P_s(V_l) + [P_s(V_l) - \frac{1}{T_P} K_P(V_0) + P_s(V_l) P_d - \frac{1}{T_P} K_P(V_l)] e^{-\frac{(t-t_0)}{T_P}} \quad (2.25)$$

where  $V_0$  and  $V_l$  are the load voltage before and after the step change, respectively. The load equation for different loads such as induction motor and tap changer action can be derived from Equation (2.25). Based on Equation (2.25), an aggregate dynamic load model for field measurements, obtained following a reduction in the voltage [69]. In another work

described in [74] the effect of phase voltage changes on nonlinear dynamic load were investigated and the following points are observed:

- The change of the voltage angle has no influence on the static load such as resistive load and pure reactive load.
- The sharp change of the voltage angle causes active power changes of the rotating electric machines such as induction motors.

#### **2.6.4 Component Based and Measurement Based Load Modeling**

There is another classification of dynamic load modeling in the time domain which contains two approaches: the component based approach and the measurement approach. In the component-based approach, the dynamic characteristics of all of the components are used to create the load model. However, in the measurement based approach, the load model is built up from the gathered information of the field measurements.

The measurement based load modeling was discussed in [1,70,75-79]. In [79] the parameters of the equivalent dynamic load model are obtained from field data using the Kalman filter [80]. The method presented in [79] does not need the value of the individual load parameters. The least square method was used in [70] to find the load model parameters using the recorded field data. In the load model, the active and reactive power is expressed in terms frequency and voltage deviations. The authors of [70] showed that the second-order model better describes response of the Taipower system than the first-order.

The component based approach load modeling was studied in [75-78]. In [77] the dynamic of a single motor model and two-motor model are extracted. Then, the derived dynamic load models are used to simulate two events. After that, the dynamic load models are replaced by a composite load (static and static) and the events are simulated using the composite load. The comparison of the results reveals that by using a single-motor or two-motor model, the reactive power responses are improved considerably compared to the composite load. In [78] the effect of load model on low frequency oscillations was investigated. In this paper the total dynamic loads were represented by an equivalent-single motor. It was concluded that during unstable inter-area oscillations, the single-motor equivalent motor has the largest oscillation compared to composite load (static and dynamic) or exponential load model.

The references that have been discussed in this section can be used to establish a load model to indicate firstly how the oscillations influence load dynamics and secondly what the load contribution is to damping. In this thesis, the load model is formed by the recorded data. This is clearly a measurement based category.

### **2.7 The Effect of Load on IAO**

The literature review regarding the effect influence of load on the IAO is discussed in this section. Firstly, the mutual interaction of load and power system is studied. Then some methods of using load modulation are described.

### 2.7.1 The Mutual Interaction between Load and Power System

In [21, 81, 82], the mutual interaction between load and power system was investigated by considering the effect of load dynamics on damping through a feedback path as shown in Figure 2.3. In this figure,  $\Delta P$  and  $\Delta V$  a real power disturbance and bus voltage respectively. The effect of  $\Delta V$  on the load is shown by  $\Delta P_d$ . It was also studied in [81] that the power system transfer function power consists of static and dynamic parts. The static part is associated with power flow Jacobian and the dynamic indicates the dynamics of the synchronous generators, power system controllers and load.

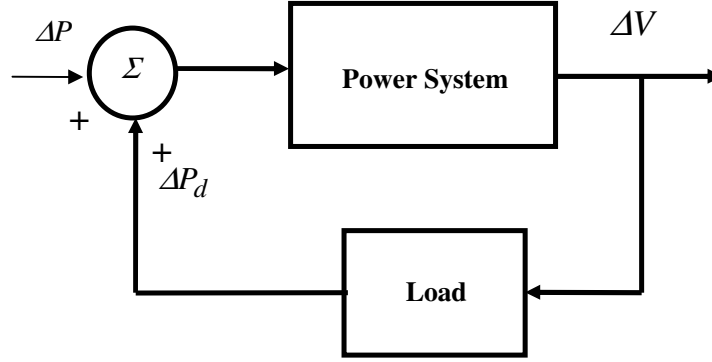


Figure 2.3 Feedback representation of load dynamic effect in the power systems [81]

Laboratory tests and field measurements on buses indicated that response of a typical load model to a voltage step change can be presented graphically in Figure 2.4 [3]. The response of the reactive power response to the step voltage change has a similar trend. This figure can be interpreted as follows.

When there is a step change in voltage, since the slip of the induction motor cannot be changed suddenly, the load acts a like static load and therefore there is a step change in the demand power  $P_d$ . As the time proceeds the load recovers to a new steady state value, because of the slip changes.

The references discussed in subsections, provide a generic load model that relates the load active power to the load voltage model. However, they do not describe a load model that relates the rate of bus voltage angle to the active load power, which is needed in determining the load contribution to damping.

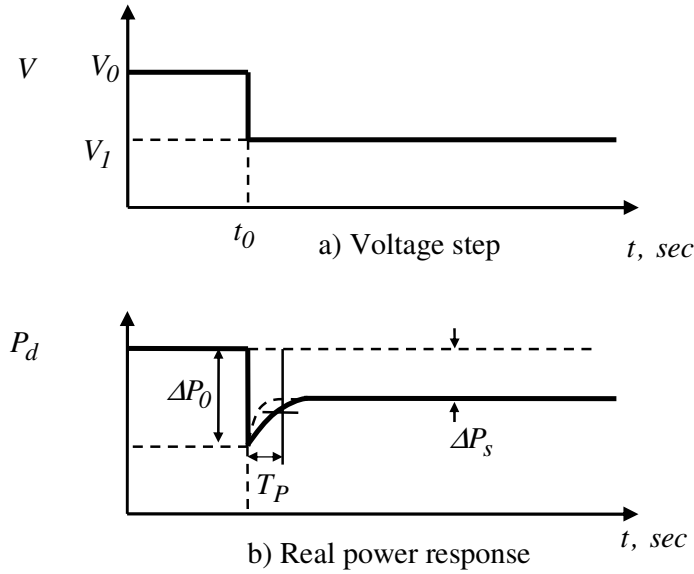


Figure 2.4: The response of the real power of a dynamic load to step change in voltage [3]

### 2.7.2 The effect of Load Modulation on IAO Damping

The effect of load modulation on the IAO was studied in [83-88]. The effect of load modulation on the IAO was investigated in [83]. In this paper, two areas of a power system are connected together and in the pathway HVDC

equipment is placed. As far as the AC system is concerned, this DC link appears as a fully controllable load. Results of [83] show that the active load modulation can improve the damping if the demand active load is modulated in phase with the speed of the generator that has the shortest mass-scaled electrical distance from the converter. The direct control of the active load was discussed in [87] to damp the IAO. The author of [87] suggested using the local frequency to control the active load in order to change the IAO damping. It was shown in [86] that by using active load modulators that control less than one percent of the base load, damping of both local and inter and inter-area modes are improved significantly. Results of a field test in [88] show that the on-off control of the active load is more effective than the sinusoidal modulation of the active load.

The references that are described in this Subsection provide a good background for analyzing the effect of load dynamic on damping. However, they do not present a load model that can be used to quantify load contribution to damping. Also they do not consider the sensitivity of eigenvalues of the IAO with respect to load.

## **2.8 Review of SVC Modeling**

This section deals with modeling of static var compensators (SVC) and the effect SVC on the IAO.

Some reasons for utilization of SVCs in power systems are control of temporary over voltages, prevention of voltage collapse, enhancement of transient stability and increasing damping of the system oscillations. By controlling the switching of SVC, it behaves like a capacitor or inductor

generates or consumes reactive power [20,89]. Figure 2.5 shows the V-I characteristics of SVC.

In the active region of Figure 2.5, according to the slope of the characteristic, the voltage is regulated by changing the current and reactive power. As shown in this figure, the SVC characteristic has two limits: capacitive limits and inductive limits. At its capacitive limit, the SVC acts as a shunt capacitor and at the inductive limit it changed to a shunt reactor [90]. Figure 2.6 shows the simplified model of an SVC consisting of a thyristor controlled reactor (TCR) and a fixed capacitor (FC).

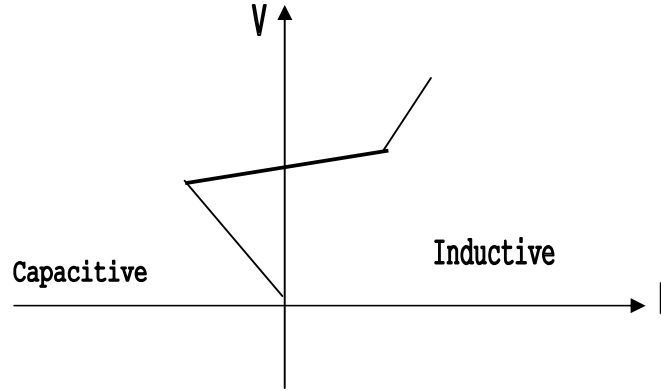


Figure 2.5: The V-I characteristic of SVC [90]

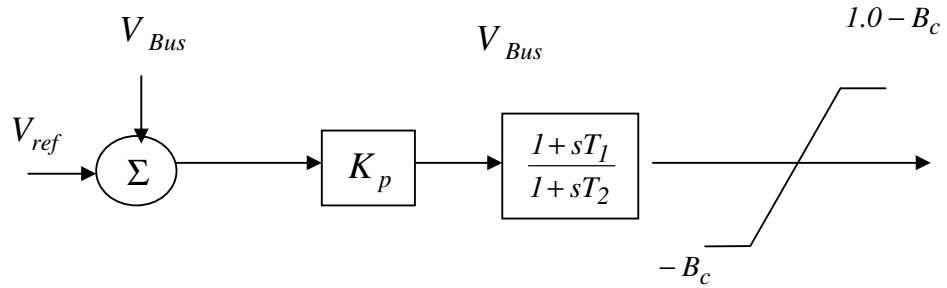


Figure 2.6: A simplified model of an SVC [1]

Static var compensator systems are usually designed to meet individual system load requirements. Therefore, in stability studies a detailed model of SVC is needed. More information for modeling of SVC are given in [90].

## **2.9 The Effect SVC on IAO**

The primary aim of SVC application in power systems is to keep bus voltage at or close to a constant level. However, it was found that SVC could improve damping of low frequency oscillations [91-96].

In a study carried out by Choudhry, et al. [92], a method on the basis of reactive modulation was suggested to improve the dynamic performance of power systems. They designed a reactive power system modulation controller with a gain corresponding to rotor speed deviation to reduce the damping. In their study, 50% of load was considered as static load and described as a nonlinear function of load bus voltage, and 50% of the load was dynamic load which is described by a fifth-order model of the induction motor.

The impact of load on the damping of controllable series capacitor (CSC) and SVC was investigated in [93]. It was shown in this paper that with increasing transmission line loading, the damping effects of a CSC is higher than of a SVC.

In [94] an adaptive static var compensator was used to damp synchronous generator oscillations. In this method, the performance of a self-tuning PID controller is compared to a fixed-gain PID controller. The results show that the controllers had a good capability in damping. However, the self-tuning controller is more effective than the fixed-gain controller, because the self

tuning PID controller could modify its parameters in real time on the basis of the on-line measurement.

An indicator called index location for effective damping (LIED) was introduced by Okamoto et al. [95]. In their method, effective location of SVC was determined using modal controllability to improve the damping of the IAO. They concluded that if SVC is located at the point where LIED is large for weak damping mode, then by suitable control of SVC, the mode can be stabilized.

To find the damping effect of SVC, an extended Philips-Hoeffron model was used in [96-98]. The extended Philips-Hoeffron model of a synchronous generator with SVC is illustrated in Figure 2.7.

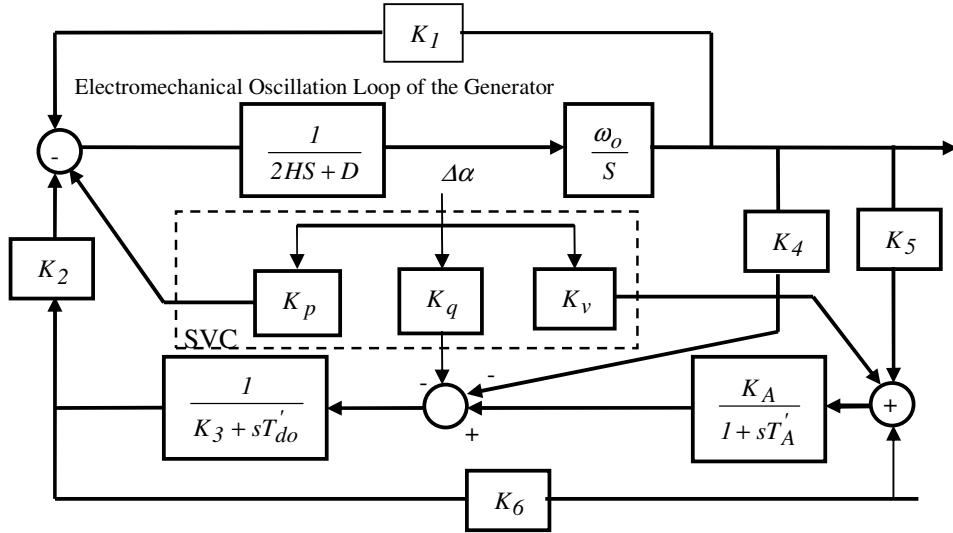


Figure 2.7: The extended Philips-Hoeffron model with SVC [97]

The authors in [96] showed that the SVC improves damping of the IAO directly and indirectly. The block  $K_q$  in Figure 2.7 shows the direct SVC contribution to damping. The indirect effect of SVC contribution to

damping applies through the blocks  $K_V$  and  $K_q$  in Figure 2.7. Usually the direct effect of SVC on damping is much greater than its direct effect. It was also reported in [96] that SVC improves both transient stability (first swing stability) and oscillation stability and more damping can be achieved by choosing a higher gain of  $K_q$  in the SVC controller. They also came to the conclusion that when the power system operates at higher load condition, the SVC operates more efficiently. Figure 2.8 illustrates the thyristor-control reactor, fixed capacitor and damping control system in the SVC. As can be seen in the figure, the damping signal is one of the inputs of the thyristor firing circuit

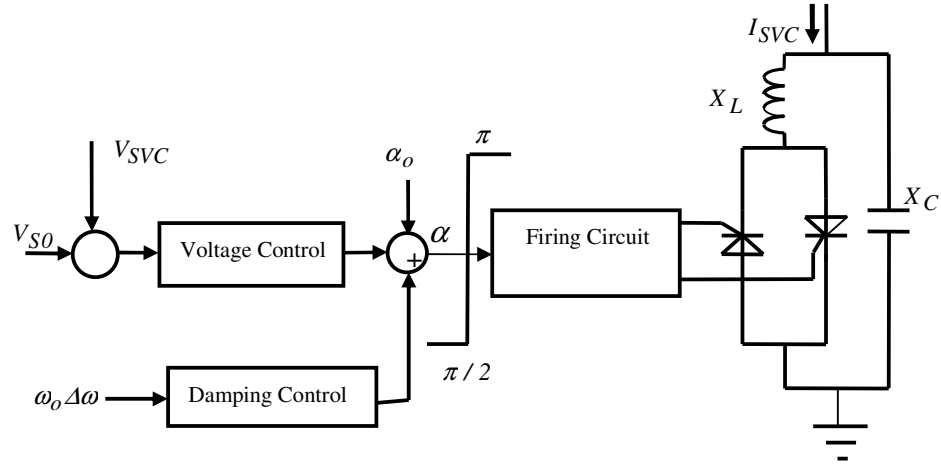


Figure 2.8: The schematic diagrams for SVC including voltage and damping control blocks [97]

The effect of SVC on a given mode was investigated by controllability and observability characteristics in [99] using a singular value decomposition method to determine the best location of SVC. They also examined the effect of load on performance of damping of SVC by controllability analysis. They observed when the load model is a kind of constant power,

the controllability of critical modes decreases. Chen et al. in [100] showed that SVC is more effective in damping of oscillations of single machine power system than PSS. A robust control strategy based on energy function was examined in [101] to improve power system stabilizer properties using thyristor controlled series (TCSCs) and SVCs. The controller is robust with respect to system loading, system configuration and fault type and location. In the references relating to SVC application in damping, there are good points that give some insights about how an SVC can improve the damping torque in the power systems, the best place for SVC. Also some methods to improve the performance of SVC in damping are introduced. However, the effects of SVC on load contribution to damping are not fully investigated in these papers, also they do not present a method to redesign the SVC controller to increase the load contribution to damping. These papers do not develop a model to consider the effect of SVC reactive power on the measured power, which can be used in redesigning of the SVC on the basis of the operating data to increase damping of the IAO.

## **2.10 Summary**

The basic materials that are needed for the following chapters are reviewed in this chapter. Also the related works to load and SVC modeling and their effect on the IAO are discussed.

In Chapter 3, a method based on cross-correlation and autocorrelation functions is developed to identify the power system eigenvalues of the IAO, and mode shapes of the power systems.

## **Chapter 3: Correlation Based Mode Shape Identification**

### **3.1 Introduction**

In this chapter, the concept of identification of modal frequencies and mode shape of the inter-area oscillations (IAO) on the basis of cross-correlation and autocorrelation is introduced. The correlation based mode shape identification (CBMSI) method is developed in this chapter to identify the eigenvalues and mode shapes of the IAO. The CBMSI uses cross-correlation and autocorrelation of the appropriate time domain signals, and curve fitting in the frequency domain.

It is found that disturbances in the power system as well as customer load variations can be used to identify the mode shape and the contribution of power system controllers to the IAO. Large disturbances of a power system can cause the system to respond as though an impulse had been applied. Continuous disturbances arise because of the customer load changes. This chapter examines both styles of disturbances.

In this chapter after developing the CBMSI method, an algorithm is presented to identify the eigenvalues and mode shapes of the IAO. Then, the CBMSI applied to a test power system, and resonant frequencies, damping and mode of shapes the test power systems are identified. The results of the simulation validate the algorithm.

The resonant frequencies and mode shapes for two different sets of real data are determined using the CBMSI method. The first set is the recorded data following the test events performed on the Australian electricity network. The system response after the test events is treated as an impulse response. The second set of the real data is the measured data from the normal operating system and the measurements are treated as the integral of white noise.

### **3.2 Theory of the Correlation Based Mode Shape Identification Method**

#### **3.2.1 Characterizing the Power System Disturbances**

The power system disturbances are categorized for this thesis into the following classes:

##### **a.) Large Disturbances**

Large disturbances in this thesis are defined as disturbances that are large enough to excite the system, but their duration is short compared to the time constants of the IAO of the power system. Examples of such a large disturbance could be a braking resistor or a short circuit which is cleared

and the system restored to its original state. For a braking resistor test, a high power resistor is connected to a network bus for a short time and then disconnected. The behaviour of the system after the disconnection is used to study the system and is similar to an impulse response test of the system.

#### **b.) Continuous Small Random Disturbances**

The continuous small random disturbances occurring in a power system results in small changes in many power system measurements. The important property of the small random disturbances is that they are usually largely unpredictable, at least over the short time scales of  $0.1$  to  $20$  seconds relevant to the IAO. Consider a power system running in normal conditions, in this case, the customer load changes continuously and unpredictably. Therefore, the changes of the customer load variations behave like a white noise process and as a white noise process, its frequency spectrum is a real positive number, and the energy is distributed, at least over the frequencies relevant to IAO. With large numbers of independent sources, according to the central limit theorem, the probability distribution function of the sum of small random disturbances approaches the Gaussian distribution function. In the most power systems, there are many independent sources of changes in the loading. Thus, the central limit theorem applies and the characteristic of load changes is modeled as a Gaussian random process. Since the changes in the customer load are approximately white noise, the measured power is considered as the integral of white noise [50] over the frequency band of interest.

### 3.2.2 Plant Description

First, we consider a power system with one input and two outputs as the plant shown in Figure 3.1



Figure 3.1: A power system with one inputs and two outputs

In this system, the input could be the occurrence of a significant event or customer load variations. The outputs could be rotor angles of the generators or values from the outputs of power systems controllers, such as SVC.

The transfer function from the single input to each output in Figure 3.1 can be written as

$$\mathbf{H}_1(\omega) = \frac{\mathbf{Y}_1(\omega)}{\mathbf{U}(\omega)} \quad (3.1)$$

$$\mathbf{H}_2(\omega) = \frac{\mathbf{Y}_2(\omega)}{\mathbf{U}(\omega)} \quad (3.2)$$

Equations (3.1) and (3.2) can be written as the ratio of polynomials

$$\mathbf{H}_1(\omega) = \frac{b_1(j\omega)}{a(j\omega)} \quad (3.3)$$

$$\mathbf{H}_2(\omega) = \frac{b_2(j\omega)}{a(j\omega)} \quad (3.4)$$

Then the relationship between the two outputs,  $y_1$  and  $y_2$  can be determined from

$$\frac{\mathbf{Y}_2(\omega)}{\mathbf{Y}_1(\omega)} = \mathbf{G}_1(\omega) = \frac{b_2(j\omega)}{b_1(j\omega)} \quad (3.5)$$

### 3.2.3 Power System Impulse Response

Consider a power system as in Figure 3.1 with an impulse input. The aim of this section is to determine what the relationship is between the two outputs of the plants. Given the transfer functions values of  $H_1$  and  $H_2$  at the resonant frequency as shown in Figure 3.1, the outputs due to the impulse are in the form of

$$y_1(t) = A_1 e^{-\alpha t} \cos(\omega_0 t + \phi_1) u_s(t) \quad (3.6)$$

$$y_2(t) = A_2 e^{-\alpha t} \cos(\omega_0 t + \phi_2) u_s(t) \quad (3.7)$$

where  $\alpha$  is damping coefficient,  $\omega_0$  is angular frequency of the oscillations,  $\phi_1$  and  $\phi_2$  are phase shift of  $y_1$  and  $y_2$ , respectively. In Equations (3.6) and (3.7),  $u_s(t)$  is the unit step response and this shows that only the response for  $t \geq 0$  is of interest.

In the IAO studies, it is assumed that all of the signals being studied are ergodic (refer to Appendix A). The assumption of ergodicity is reasonable for short term power system analysis, because based on statistical observation, the statistical properties of the studied signals do not change significantly during periods of the signals that are studied in this thesis.

The autocorrelation of  $y_1(t)$  could be computed from the following equation [102]

$$R_{y_1 y_1}(\tau) = \int_{t=-\infty}^{\infty} A_1 e^{-\alpha t} \cos(\omega_0 t + \phi_1) u(t) A_1 e^{-\alpha(t+\tau)} \cos(\omega_0(t+\tau) + \phi_1) u(t+\tau) dt \quad (3.8)$$

Then

$$R_{y_I y_I}(\tau) = \begin{cases} \frac{1}{4} A_I^2 e^{-\alpha\tau} \left[ \frac{\cos(\omega_0 \tau)}{\alpha} + \frac{\alpha \cos(\omega_0 \tau + 2\phi_I) - \omega_0 \sin(\omega_0 \tau + 2\phi_I)}{\alpha^2 + \omega_0^2} \right] & \tau \geq 0 \\ \frac{1}{4} A_I^2 e^{\alpha\tau} \left[ \frac{\cos(\omega_0 \tau)}{\alpha} + \frac{\alpha \cos(\omega_0 \tau - 2\phi_I) + \omega_0 \sin(\omega_0 \tau - 2\phi_I)}{\alpha^2 + \omega_0^2} \right] & \tau < 0 \end{cases} \quad (3.9)$$

Also cross-correlation of  $y_I(t)$  and  $y_2(t)$  can be determined as shown in the following equation [102]

$$C_{y_I y_2}(\tau) = \begin{cases} \frac{1}{4} A_I A_2 e^{-\alpha\tau} \left[ \frac{\cos(\omega_0 \tau - \phi_I + \phi_2)}{\alpha} + \frac{\alpha \cos(\omega_0 \tau + \phi_I + \phi_2) - \omega_0 \sin(\omega_0 \tau + \phi_I + \phi_2)}{\alpha^2 + \omega_0^2} \right] & \tau \geq 0 \\ \frac{1}{4} A_I A_2 e^{\alpha\tau} \left[ \frac{\cos(\omega_0 \tau + \phi_I - \phi_2)}{\alpha} + \frac{\alpha \cos(\omega_0 \tau - \phi_I - \phi_2) + \omega_0 \sin(\omega_0 \tau - \phi_I - \phi_2)}{\alpha^2 + \omega_0^2} \right] & \tau < 0 \end{cases} \quad (3.10)$$

Since the aim is to find the relationship between  $y_I$  and  $y_2$  by means of their cross-correlation and autocorrelation, therefore according to Equation (2.20), we divide the Fourier transform of cross-correlation of  $y_I$  and  $y_2$ , by the Fourier transform of autocorrelation of  $y_I$  and compute this ratio at  $\omega = \omega_0$  as

$$\mathbf{G}(\omega_0) = \frac{\mathfrak{F}(C_{y_I y_2})}{\mathfrak{F}(R_{y_I y_I})} \quad (3.11)$$

where  $\omega_0$  is the power system resonant frequency and  $\mathfrak{F}$  the Fourier transform operator. In analysis of sinusoidal signals, it is often found beneficial to consider the analytic associate of the cross-correlation and autocorrelation functions. Therefore, in taking the Fourier transform, we consider the analytic associate of the cross-correlation and autocorrelation

functionss. In doing this, firstly, the Hilbert transform [25] of all terms in Equations (3.9) and (3.10) should be computed. Therefore, the analytic associate of the cross-correlation and autocorrelation functions, are considered in this section.

The Fourier transform of analytic associate of  $C_{y_I y_2}$  at  $\omega = \omega_0$  for  $\tau \geq 0$  could be calculated as

$$\mathbf{C}_{y_I y_2}(\omega_0) = \Im(C_{y_I y_2}(\tau)) \Big|_{\omega=\omega_0} \quad (3.12)$$

The simplified form of Equation (3.12) is

$$\mathbf{C}_{y_I y_2}(\omega_0) = \frac{1}{4} A_I A_2 \left[ \frac{e^{j(-\phi_I + \phi_2)}}{\alpha^2} + \frac{e^{j(\phi_I + \phi_2)} - e^{j(\phi_I + \phi_2 - \frac{\pi}{2})}}{\alpha(\alpha^2 + \omega_0^2)} \right] \tau \geq 0 \quad (3.13)$$

Similarly

$$\mathbf{R}_{y_I y_I}(\omega_0) = \Im(C_{y_I y_I}(\tau)) \Big|_{\omega=\omega_0} \quad (3.14)$$

or

$$\mathbf{R}_{y_I y_I}(\omega_0) = \frac{1}{4} A_I^2 \left[ \frac{1}{\alpha^2} + \frac{e^{j(2\phi_I)} - e^{j(2\phi_I - \frac{\pi}{2})}}{\alpha(\alpha^2 + \omega_0^2)} \right] \tau \geq 0 \quad (3.15)$$

By substituting from (3.13) and (3.15) into (3.11), we have

$$\mathbf{G}(j\omega_0) = \frac{A_2 e^{j\phi_2}}{A_I e^{j\phi_I}} \tau \geq 0 \quad (3.16)$$

Similarly for  $\tau < 0$  we have

$$\mathbf{G}(\omega_0) = \frac{A_2 e^{j\varphi_2}}{A_1 e^{j\varphi_1}} \quad \tau < 0 \quad (3.17)$$

Thus for all values of  $\tau$  we can write

$$\mathbf{G}(\omega_0) = \frac{A_2 e^{j\varphi_2}}{A_1 e^{j\varphi_1}} \quad (3.18)$$

As a result, if we have two signals in the form of Equations (3.6) and (3.7), then the phase difference and the ratio of the amplitude of the two signals can be computed according to Equation (3.18).

### 3.2.4 Response of the White Noise Driven Power System

In this section a white noise driven power system is examined and we aim to determine the relationship between the two outputs of the power system in Figure 3.1, labeled  $y_1$  and  $y_2$ . If we relate  $y_1$  to the white noise input using Equation (3.3), and  $y_2$  to the input white noise using Equation (3.4), then  $y_2$  and  $y_1$  are related by

$$\mathbf{G}(\omega) = \frac{b_2(j\omega)}{b_1(j\omega)} \quad (3.19)$$

with a common driving noise. In general, the numerator and denominator in (3.19) have a common coefficient that cancels each other out. According to Equation (2.20),  $\mathbf{G}(\omega)$  can be found from

$$\mathbf{G}(\omega) = \frac{\Im(C_{y_1 y_2})}{\Im(R_{y_1 y_1})} = \frac{\mathbf{C}_{y_1 y_2}(\omega)}{\mathbf{R}_{y_1 y_1}(\omega)} \quad (3.20)$$

where  $\mathbf{C}_{y_1 y_2}(\omega)$  is the Fourier transform of cross-correlation between  $y_1$  and  $y_2$ , and  $\mathbf{R}_{y_1 y_1}(\omega)$  is the Fourier transform of autocorrelation of  $y_1$ .

To determine  $\mathbf{G}(j\omega)$ , we consider the analytic associate of its numerator and denominator. Thus, for  $\omega \geq 0$  we could write

$$\mathbf{G}(\omega) = \frac{\mathbf{C}_{y_I y_2}(\omega) - j\mathbf{C}_{y_I y_2}(j\omega)}{\mathbf{R}_{y_I y_I}(\omega) - j\mathbf{R}_{y_I y_I}(j\omega)} = \frac{\sqrt{2}\angle -45^\circ \mathbf{C}_{y_I y_2}(\omega)}{\sqrt{2}\angle -45^\circ \mathbf{R}_{y_I y_I}(\omega)} \quad \omega \geq 0 \quad (3.21)$$

Therefore

$$\mathbf{G}(\omega) = \frac{\mathbf{C}_{y_I y_2}(j\omega)}{\mathbf{R}_{y_I y_I}(j\omega)} \quad \omega \geq 0 \quad (3.22)$$

Similarly for  $\omega < 0$  we have

$$\mathbf{G}(j\omega) = \frac{\mathbf{C}_{y_I y_2}(j\omega) + j\mathbf{C}_{y_I y_2}(j\omega)}{\mathbf{R}_{y_I y_I}(j\omega) + j\mathbf{R}_{y_I y_I}(j\omega)} \quad \omega < 0 \quad (3.23)$$

Thus

$$\mathbf{G}(j\omega) = \frac{\mathbf{C}_{y_I y_2}(j\omega)}{\mathbf{R}_{y_I y_I}(j\omega)} \quad \omega < 0 \quad (3.24)$$

With respect to Equation (3.24), we can determine  $\mathbf{G}(\omega)$  at the power system resonant frequency. Thus we can write:

$$\mathbf{G}(j\omega_0) = \frac{\mathbf{C}_{y_I y_2}(\omega_0)}{\mathbf{R}_{y_I y_I}(\omega_0)} \quad (3.25)$$

So, to find the relative magnitude and phase difference between  $y_I$  and  $y_2$  in the white noise driven system, the Fourier transform of the cross-correlation  $y_I$  and  $y_2$  should be divided by the Fourier transform of the autocorrelation  $y_I$ . This derivation is obtained from the analytic associate of the cross-correlation and autocorrelation functions.

**3.2.5 Response of a Power System to White Noise Plus an Impulse**

Consider a white noise driven system with an additional impulse input. If it is assumed that the system is linear, each of the outputs could be divided into response due to impulse input and response due to white noise as

$$y_I = y_{Ii} + y_{Iw} \quad \text{and} \quad y_2 = y_{2i} + y_{2w} \quad (3.26)$$

The autocorrelation of  $y_I$  and cross-correlation of  $y_I$  and  $y_2$  can be shown to be

$$R_{y_I y_I} = R_{y_{Ii} y_{Ii}} + R_{y_{Iw} y_{Iw}} \quad \text{and} \quad C_{y_I y_2} = C_{y_{Ii} y_{2i}} + C_{y_{Iw} y_{2w}} \quad (3.27)$$

where  $R_{y_{Ii} y_{Ii}}$  and  $R_{y_{Iw} y_{Iw}}$  are autocorrelations of  $y_{Ii}$  and  $y_{Iw}$ , respectively. Also  $C_{y_{Ii} y_{2i}}$  is the cross-correlation of  $y_{Ii}$  and  $y_{2i}$  and  $C_{y_{Iw} y_{2w}}$  is the cross-correlation of  $y_{Iw}$  and  $y_{2w}$ . In Equation (3.27), since there is no correlation between the impulse signal and the white noise signal, there is no correlation between the two parts of either output signal. This implies that the cross terms are zero in Equation (3.27). The relationship between  $y_I$  and  $y_2$  can be determined from

$$\mathbf{G}(\omega_0) = \frac{\Im(C_{y_I y_2})}{\Im(R_{y_I y_I})} = \frac{\Im(C_{y_{Ii} y_{2i}}) + \Im(C_{y_{Iw} y_{2w}})}{\Im(R_{y_{Ii} y_{Ii}}) + \Im(R_{y_{Iw} y_{Iw}})} \quad (3.28)$$

This gives the same result as processing white noise or impulse response separately. Equation (3.28) shows the relative magnitude and phase difference of the two outputs  $y_2$  and  $y_I$  at  $\omega_0$ .

### 3.2.6 Using Non-analytic Process

So far the analytic associate of cross-correlation and autocorrelation is considered. In this section, we examine what error will be made if the non-analytic signal of cross-correlation and autocorrelation functions are used.

Firstly, the impulse response is considered. If in Equations (3.9) and (3.10), the non-analytic signal is considered, then Equations (3.13) and (3.15) are changed to the following equations:

$$\mathbf{C}_{y_I y_2}(\omega_0) = \frac{1}{8} A_I A_2 \left[ \frac{e^{j(-\phi_1 + \phi_2)}}{\alpha^2} + \frac{e^{j(\phi_1 + \phi_2)} - e^{j(\phi_1 + \phi_2 - \frac{\pi}{2})}}{\alpha(\alpha^2 + \omega_0^2)} + \frac{e^{j(\phi_1 - \phi_2)}}{\alpha(\alpha + 2j\omega_0)} + \frac{e^{-j(\phi_1 + \phi_2)} - e^{-j(\phi_1 + \phi_2 - \frac{\pi}{2})}}{(\alpha + 2j\omega_0)(\alpha^2 + \omega_0^2)} \right] \tau \geq 0 \quad (3.29)$$

and

$$\mathbf{R}_{y_I y_I}(\omega_0) = \frac{1}{8} A_I^2 \left[ \frac{1}{\alpha^2} + \frac{e^{j2\phi_1} - e^{j(2\phi_1 - \frac{\pi}{2})}}{\alpha(\alpha^2 + \omega_0^2)} + \frac{1}{\alpha(\alpha + 2j\omega_0)} + \frac{e^{-j2\phi_1} - e^{-j(2\phi_1 - \frac{\pi}{2})}}{(\alpha + 2j\omega_0)(\alpha^2 + \omega_0^2)} \right] \tau \geq 0 \quad (3.30)$$

By substituting (3.29) and (3.30) in (3.10) and simplifying

$$\mathbf{G}(\omega_0) = \frac{A_2}{A_I} e^{j(-\phi_1 + \phi_2)} + \frac{A_2}{A_I} e^{j(-\phi_1 + \phi_2)} \frac{\frac{\alpha e^{j2(\phi_1 - \phi_2)}}{(\alpha + 2j\omega_0)} - \frac{\alpha}{(\alpha + 2j\omega_0)}}{1 + \frac{\alpha}{(\alpha + 2j\omega_0)}} \tau \geq 0 \quad (3.31)$$

If we assume  $\alpha \ll \omega_0$ , (which is often found in low damping case power systems), Equation (3.31) becomes

$$\mathbf{G}(\omega_0) = \frac{A_2}{A_1} e^{j(-\phi_1 + \phi_2)} + \frac{A_2}{A_1} e^{j(-\phi_1 + \phi_2)} \frac{\alpha}{2j\omega_0} \left[ e^{j2(\phi_1 - \phi_2)} - 1 \right] \quad \tau \geq 0 \quad (3.32)$$

With comparing (3.32) with (3.18), the bound of relative error due to use of the non-analytic signal is

$$|\varepsilon_r| \leq \frac{\alpha}{2\omega_0} \quad \tau \geq 0, \text{ for } \alpha \ll \omega_0 \quad (3.33)$$

With regards to the nature of the IAO in power systems, the assumption of  $\alpha \ll \omega_0$  is frequently true. Consequently, under this assumption the bound of the error due to a non-analytic signal can be determined according to Equation (3.33). It should be noted that a similar result can be obtained for  $\tau < 0$ .

For the case of a white noise driven system, according to Section 3.2.3., the results will not be changed if the not-analytic signal of the cross-correlation of  $y_1$  and  $y_2$  is used.

### 3.3 Algorithm of the Correlation Based Mode Shape Identification (CBMSI) Method

The procedure for determining the mode shape using the CBMSI method is explained in this section. Let us consider a power system including  $n$  synchronous generators as shown in Figure 3.2. In this system, the

inputs,  $u_1, \dots, u_m$ , could be significant disturbance or customer load variation. The outputs are the generators rotor angle changes,  $\delta_1, \dots, \delta_n$ , and they show the response of the generators rotor angle changes to significant power system disturbance or customer load variations.

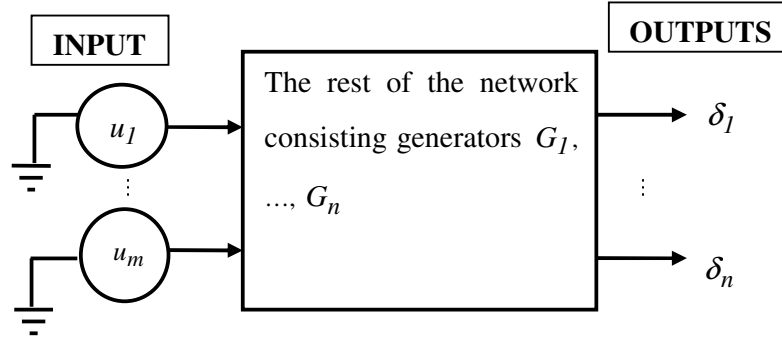


Figure 3.2: Schematic diagram of the power system with inputs and outputs

In general, the transfer function between input  $j$  and an output  $i$ , can be found from

$$\mathbf{H}_{ji}(\omega) = \frac{b_{ji}(j\omega)}{a(j\omega)} \quad (3.34)$$

The least square method is used to find the transfer functions in Equation (3.34) with different numerators and a common denominator. In this method the best set for numerators ( $b_j$ 's) and common denominator ( $a$ ), are identified. This method is called multi-site curve fitting, since it estimates the coefficients of several transfer function with a common denominator.

The system shown in Figure 3.2, has  $2n$  state variables. The first  $n$  state variables are the changes of generator bus voltage angle ( $\delta_1, \dots, \delta_n$ ) and the remaining state are the rate of change of generator bus voltage angle ( $\dot{\delta}_1, \dots, \dot{\delta}_n$ ). The procedure for using the CBMSI is as follows:

### **Step 1: Refining the data**

The response of the rotor angles to customer load variations, as explained in [50], is the integral of white noise. To represent the system as being driven by white noise all output measurements should be differentiated. For a real system with large disturbances, since the duration of the response is short, therefore the customer load variations are often neglected.

### **Step 2: Mapping all of the rotor angles to the COI referenced system**

The rotor angles are mapped to the COI referenced system by subtracting the angle of COI from each of the rotor angles according to Equation (2.7).

### **Step 3: Autocorrelation Computation**

In order to determine the IAO resonant frequencies, which lie in the range of  $0.05$  to  $3$  Hz, the time duration of the autocorrelation is often selected to be  $20$  seconds. To increase the frequency resolution in the frequency domain, the time duration of the autocorrelation could be increased or the signal is zero padded.

### **Step 4: Resonant frequency identification of the IAO of the power system**

The resonant frequencies of the power system can be found by taking the Fast Fourier Transform ( $FFT$ ) [103-104] of the autocorrelation of all of the bus voltage angle differences and using multi-site curve fitting in the

frequency domain. The resonant frequencies are the imaginary parts of the roots of the identified common denominator of Equation (3.34).

#### Step 5: Mode shape plot using eigenvector

Since the eigenvector of a linear system shows how the state variables are related, therefore in this section the relative magnitude and the phase difference of the rotor angles with respect to a reference are computed. Consider the outputs in Figure 3.1, take one generator rotor angle as a reference, e.g. rotor angle  $j$ , in that case we can form the following set of transfer functions

$$\mathbf{H}_i(\omega) = \frac{\Im(\delta_i)}{\Im(\delta_j)} \quad i = 1, \dots, j-1, j+1, \dots, n \quad (3.35)$$

Equation (3.35) can be evaluated with lower noise levels using

$$\mathbf{H}_i(\omega) = \frac{\Im(C_{\delta_j \delta_i}(\tau))}{\Im(R_{\delta_j \delta_j}(\tau))} \quad i = 1, \dots, j-1, j+1, \dots, n \quad (3.36)$$

where  $C_{\delta_j \delta_i}(\tau)$  is the cross-correlation of  $\delta_j$  and  $\delta_i$ . Also  $R_{\delta_j \delta_j}(\tau)$  is the autocorrelation of  $\delta_j$ .

The system has  $2n$  states, so the system also has  $2n$  eigenvectors. The first  $n$  elements of the  $k^{th}$  eigenvector correspond to the changes of generators bus voltage angle. They have the general element  $\bar{\phi}_{ik}$  that can be obtained from

$$\bar{\phi}_{ik} = \begin{cases} \mathbf{H}_i(\omega)|_{\omega=\omega_k} & i = 1, \dots, j-1, j+1, \dots, n \\ I & i = j \end{cases} \quad (3.37)$$

where  $\omega_k$  is the  $k^{th}$  power resonant frequency.

Therefore, if the rotor angle  $j$  is considered as the reference rotor angle, then the mode shape at the power system resonant frequency  $\omega_k$  can be plotted using the elements of the following vector

$$\bar{\varphi}_k = \left\{ \begin{array}{c} \mathbf{H}_1(\omega) \big|_{\omega=\omega_k} \\ \vdots \\ \mathbf{H}_{j-1}(\omega) \big|_{\omega=\omega_k} \\ 1 \\ \mathbf{H}_{j+1}(\omega) \big|_{\omega=\omega_k} \\ \vdots \\ \mathbf{H}_n(\omega) \big|_{\omega=\omega_k} \end{array} \right\} \quad (3.38)$$

Since  $\bar{\varphi}_k$  is a part of the right eigenvector and the eigenvector is not unique and any multiple of any eigenvalue is also an eigenvalue, Equation (3.38) can be written as

$$\bar{\varphi}_k = \left\{ \begin{array}{c} \Im(C \delta_j \delta_1) \big|_{\omega=\omega_k} \\ \vdots \\ \Im(C \delta_j \delta_{j-1}) \big|_{\omega=\omega_k} \\ \Im(R \delta_j \delta_j) \big|_{\omega=\omega_k} \\ \Im(C \delta_j \delta_{j+1}) \big|_{\omega=\omega_k} \\ \vdots \\ \Im(C \delta_j \delta_n) \big|_{\omega=\omega_k} \end{array} \right\} \quad (3.39)$$

### 3.4 Simulation Results of the CBMSI Method

#### 3.4.1 Eigenvalue Analysis of a Test Power System

In this part, the algorithm of the CBMSI method is validated by simulating a linearized test power system. The test power system consists of three generators and nine lines. The specifications of the test power system are given in [15]. The basic model does not include any machine damping. In this case a damping factor,  $D$ , is considered to damp the oscillation of the IAO in the test power system. The damping power for each generator is expressed by

$$P_{Di} = -0.6 \dot{\delta}_i \quad i = 1, \dots, 3 \quad (3.40)$$

Since this test system has three generators, the vector of state variables is formed as

$$X = \begin{bmatrix} \delta_1 & \delta_2 & \delta_3 & \dot{\delta}_1 & \dot{\delta}_2 & \dot{\delta}_3 \end{bmatrix}^T \quad (3.41)$$

Also, the state space presentation of the test system can be written as

$$\dot{X} = \mathbf{A}X + \mathbf{B}U \quad (3.42)$$

where

$\mathbf{A}$  = the system matrix that can be computed according to Equation (2.10)

using Equation (3.40) and data of the test system given in [15]

$X$  = the vector of the state variables

$U$  = the vector of the input sources

The input matrix  $\mathbf{B}$  and the input vector  $U$  and are considered as

$$\mathbf{B} = \begin{bmatrix} 0 & 0 & 0 & \frac{1}{J_1} & 0 & 0 \\ 0 & 0 & 0 & 0 & \frac{1}{J_2} & 0 \\ 0 & 0 & 0 & 0 & 0 & \frac{1}{J_3} \end{bmatrix}^T \quad (3.43)$$

$$U = [u_1 \quad u_2 \quad u_3]^T \quad (3.44)$$

where  $u_1$  to  $u_3$  are three white noise sources.

Since this system consists of three generators, there are two complex modes.

The test system has the following complex eigenvalues

$$-0.3 \pm j8.8015 \quad \text{and} \quad -0.3 \pm j13.4130 \quad (3.45)$$

The resonant frequencies are

$$f_1 = 1.4\text{Hz} \quad \text{and} \quad f_2 = 2.1\text{Hz} \quad (3.46)$$

### 3.4.2. Simulation Results

In applying the algorithm to the test power system, the inputs are white noise sources. The simulation is performed for 30 minutes. In the simulation of the test power system, at first the obtained generator rotor angles mapped to the COI referenced system. Then, the autocorrelation of

the angles are computed. Figure 3.3 shows the autocorrelation of rotor angle  $\delta_1$ . and Figure 3.4 represents the cross-correlation of  $\delta_1$  and  $\delta_3$ .

Then, the *FFT* of the autocorrelations are taken. Multi-site curve fitting in the frequency domain on the of the autocorrelations yields the power system eigenvalues. Figure 3.5 illustrates the *FFT* of autocorrelation of the generator angle  $\delta_2$  and the fitted curves of the test power system. As shown in Figure 3.5, there are two distinct resonant frequencies for the test power system.

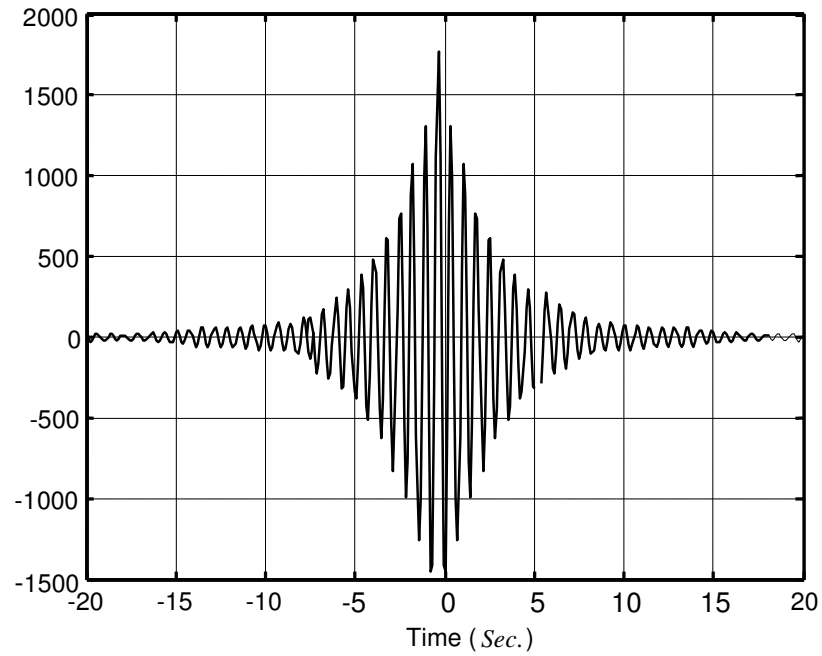


Figure 3.3: The autocorrelation of rotor angle  $\delta_1$  of the test power system

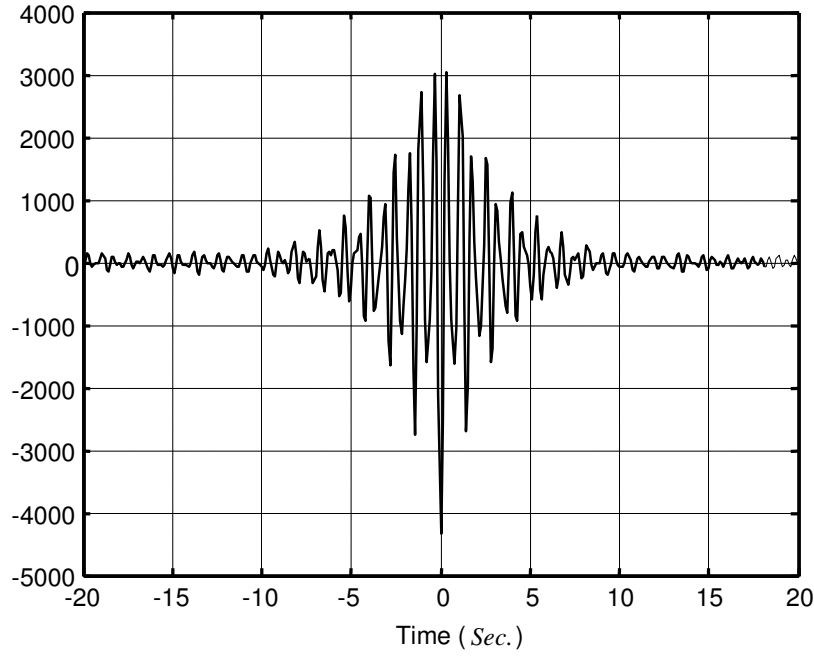


Figure 3.4: The cross-correlation of  $\delta_1$  and  $\delta_3$  of the test power system

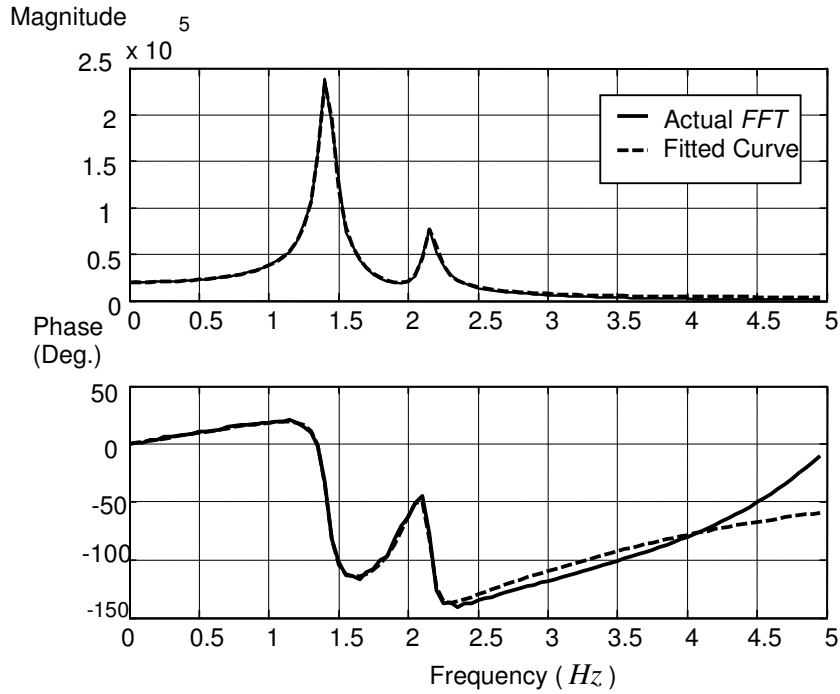


Figure 3.5: The *FFT* of autocorrelation of the generator angle  $\delta_2$  and the fitted curves of the test system

The identified eigenvalues are given in Table 3.1. Also the estimated resonant frequencies are given in Table 3.2. In these two tables, the actual values refer to the values obtained from eigenvalue analysis of the state space model and estimated values indicate the values identified by the CBMSI method.

Table 3.1: The actual and estimated eigenvalues of the test power system

Actual value	Estimated value
$-0.3 + j8.8015$	$-0.3005 + j8.8662$
$-0.3 + j13.4130$	$-0.3272 + j13.3926$

Table 3.2: The actual and estimated resonant frequencies of the test power system

Actual Resonant Frequency (Hz)	Estimated Resonant Frequency (Hz)
1.4008	1.4111
2.1347	2.1315

In the next step, the first half elements eigenvectors of the test power system

,  $\bar{\varphi}_k$ , corresponding to rotor angle state variables, are determined using

Equation (3.39). For this system, at each resonant frequency the elements of the eigenvectors associated with  $\delta_1$ ,  $\delta_2$ ,  $\delta_3$  are denoted by  $V_{\delta_1}$ ,  $V_{\delta_2}$  and  $V_{\delta_3}$ , respectively. These vectors are shown by  $\bar{\varphi}_k = [V_{\delta_1} \ V_{\delta_2} \ V_{\delta_3}]^T$ . For forming the mode shape plot of this system, the rotor angle  $\delta_3$  is considered as the reference rotor angle. According to Equation (3.39), the *FFT* of the autocorrelation of  $\delta_3$  and the *FFT* of the cross-correlation of  $\delta_3$  and other rotor angles are computed, and then evaluated at the specific resonant frequencies to form  $\bar{\varphi}_k$ . The vector  $\bar{\varphi}_k$  are determined from two methods; one method is the eigenvalue analysis and the other method is the CBMSI method proposed in this chapter. The value of  $\bar{\varphi}_k$  obtained from these two methods are compared in Tables 3.3 and 3.4 at power system resonant frequencies of  $1.4 \text{ Hz}$  and  $2.1 \text{ Hz}$ , respectively. Also, the mode shapes that are obtained from these two methods are plotted in Figures 3.6 and 3.7 for the identified resonant frequencies. Tables 3.1 to 3.4 and also Figures 3.5 and 3.7 indicate that the estimated values obtained from the CBMSI method are close to the actual values computed from eigenvalue analysis. This indicates that the CBMSI method can reliably estimate mode shapes as well as eigenvalues of the power system. These results represent the validity of the CBMSI method.

As can be seen in Tables 3.3 and 3.4 there are some phase shifts in angles and changes in magnitude for the eigenvector. This is to be expected, since

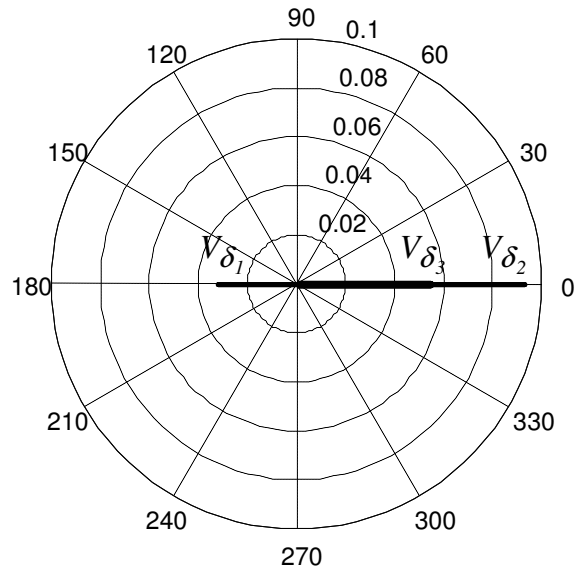
the autocorrelations are based on a finite data length; ideally an infinite length simulation would yield perfect estimates.

Table 3.3: The value of the elements of  $\bar{\varphi}_k$  associated with  $f = 1.4 \text{ Hz}$  obtained from the two methods: eigenvalue analysis and the CBMSI based method for the test power system

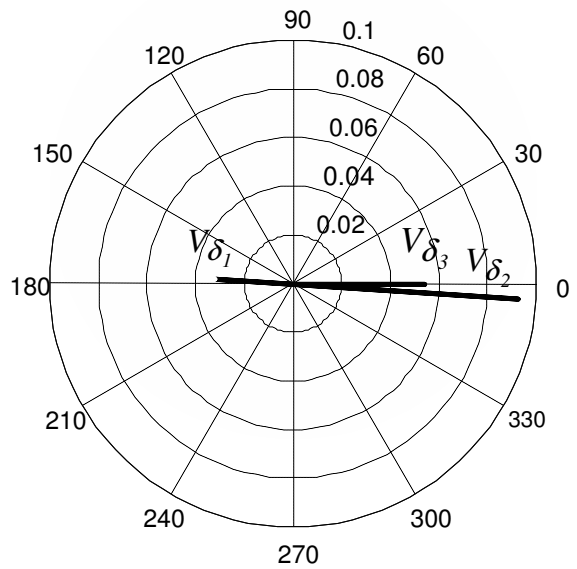
	Eigenvalue Analysis	Correlation Based Method
Generator 1: $V_{\delta_1}$	$0.0322 \angle -180^\circ$	$0.0320 \angle -183.2^\circ$
Generator 2: $V_{\delta_2}$	$0.0933 \angle 0^\circ$	$0.0927 \angle -4.1^\circ$
Generator 3: $V_{\delta_3}$	$0.0546 \angle 0^\circ$	$0.0540 \angle 0^\circ$

Table 3.4: The value of the elements of  $\bar{\varphi}_k$  associated with  $f=2.1 \text{ Hz}$  obtained from the two methods: eigenvalue analysis and the CBMSI method for the test power system

	Eigenvalue Analysis	Correlation Based Method
Generator 1: $V_{\delta_1}$	$0.0028 \angle -180^\circ$	$0.0035 \angle -164.5^\circ$
Generator 2: $V_{\delta_2}$	$0.023 \angle 180^\circ$	$0.0211 \angle 170.6^\circ$
Generator 3: $V_{\delta_3}$	$0.0706 \angle 0^\circ$	$0.0707 \angle 0^\circ$

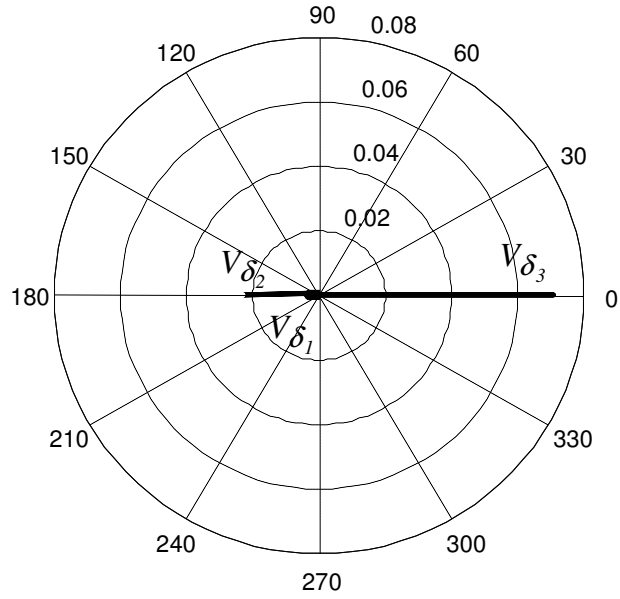


a.) Eigenvalue analysis method

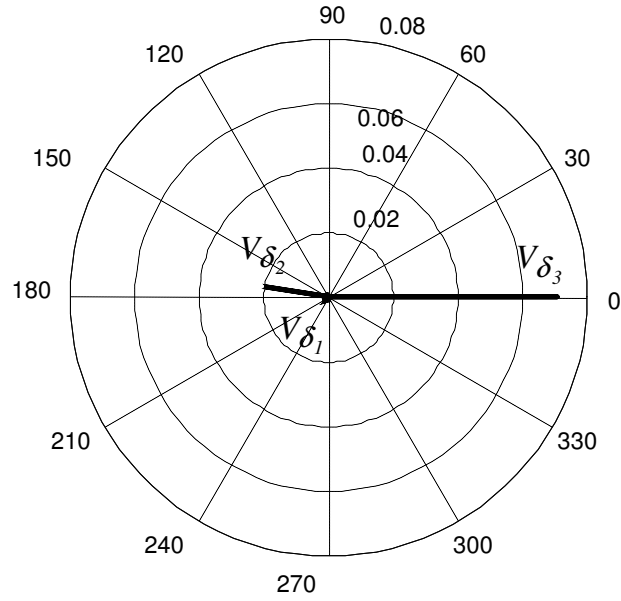


b.) CBMSI method

Figure 3.6: Mode shape plot at  $f=1.4 \text{ Hz}$  obtained from the two methods, a) eigenvalue analysis, b.) CBMSI method



a.) Eigenvalue analysis method



b.) CBMSI method

Figure 3.7: Mode shape plot at  $f=2.1$  Hz, obtained from the two methods,

a) eigenvalue analysis, b.) CBMSI method

## 3.5 Results of CBMSI Method on Real Data<sup>1</sup>

### 3.5.1. Results Due to Power System Disturbance

In this part the recorded data following a braking resistor event are used to find the IAO eigenvalues of the Australian electricity network. The data are power flows along 6 lines in Queensland and Victoria associated with a braking resistor test carried out on the 22<sup>nd</sup> of January 2001. The duration of data captured following the braking resistor event was around 1.5 minutes. Figure 3.8 shows the power flow of a power line in South Australia following a braking resistor event at 00:44:51 on the 22<sup>nd</sup> of January 2001. The autocorrelation of the power flow changes of South Australia line is depicted in Figure 3.9.

After taking the *FFT* of the autocorrelations the resonant frequencies are identified using multi-site curve fitting in the frequency domain. Figure 3.9 shows the *FFT* of the autocorrelation of the load centers. As can be seen in Figure 3.10, there are two dominant resonant frequencies. Tables 3.5 and 3.6 show the power system identified eigenvalues and resonant frequencies, respectively.

---

1-The read data was provided by Powerlink Queensland.

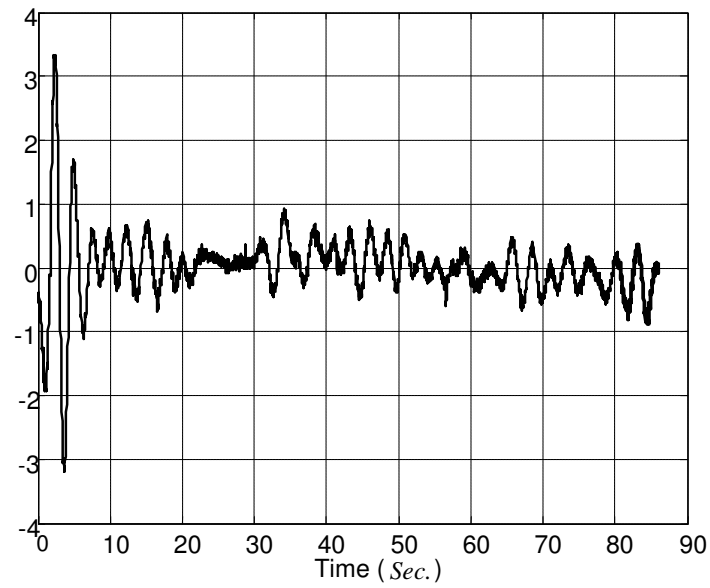


Figure 3.8: The real data of power flow across the South Australia power line following the braking resistor event 00:44:51 on the 22<sup>nd</sup> of January 2001

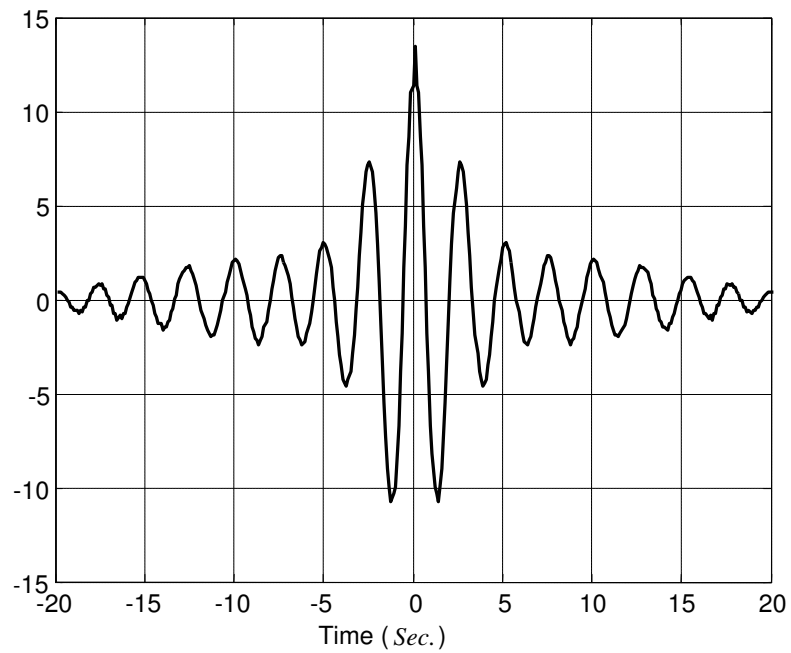


Figure 3.9: The autocorrelation of the power flow of a power line for the real data

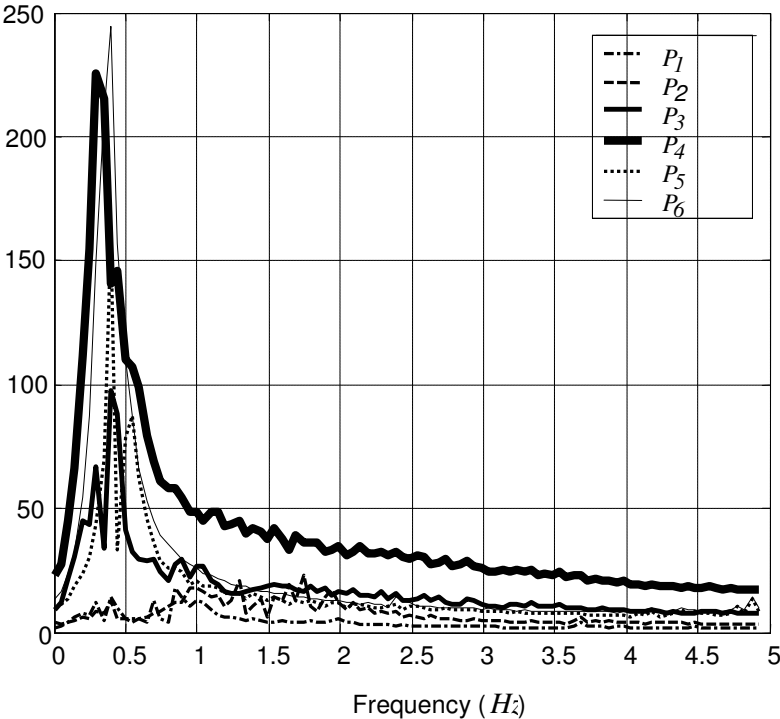


Figure 3.10: The magnitude of the *FFT* of the autocorrelation of the power flow of the load centers in Australian electricity network following the braking resistor test

Table 3.5: The power system eigenvalues estimated from the power flow of the load centers in the Australian electricity network following the braking resistor test

	Estimated Power System Eigenvalues
First Mode	$-0.2733 + j2.0250$
Second Mode	$-0.2406 + j2.5277$

Table 3.6: The estimated system frequencies corresponding to Table 3.5

	Estimated Power System Resonant Frequency ( $Hz$ )
First Mode	<i>0.3223</i>
Second Mode	<i>0.4023</i>

### 3.5.2. Results from Normal Operating Conditions<sup>1</sup>

In this section the power system eigenvalues of the Australian electricity network are identified by applying CBMSI method on real data from normal operating condition. The data consists of the voltage bus angle of the four major load centers: Brisbane, Sydney, Adelaide and Melbourne and some measurements of current flow to loads. All angles are measured with respect to a GPS (Global Positioning System) strobe. The sampling frequency of the real data is  $5\text{ Hz}$  and the duration is one hour starting from the time 00.00 of the 22<sup>nd</sup> of May 2002. The voltage and current of the Brisbane load centre is given in Figure 3.11. The data of this figure was recorded by the angle measurement unit and because of the interfacing system, the values of the vertical axes are not scaled to represent the actual value of the voltage and current magnitude.

---

<sup>1</sup>-The real data was provided by Powerlink Queensland.

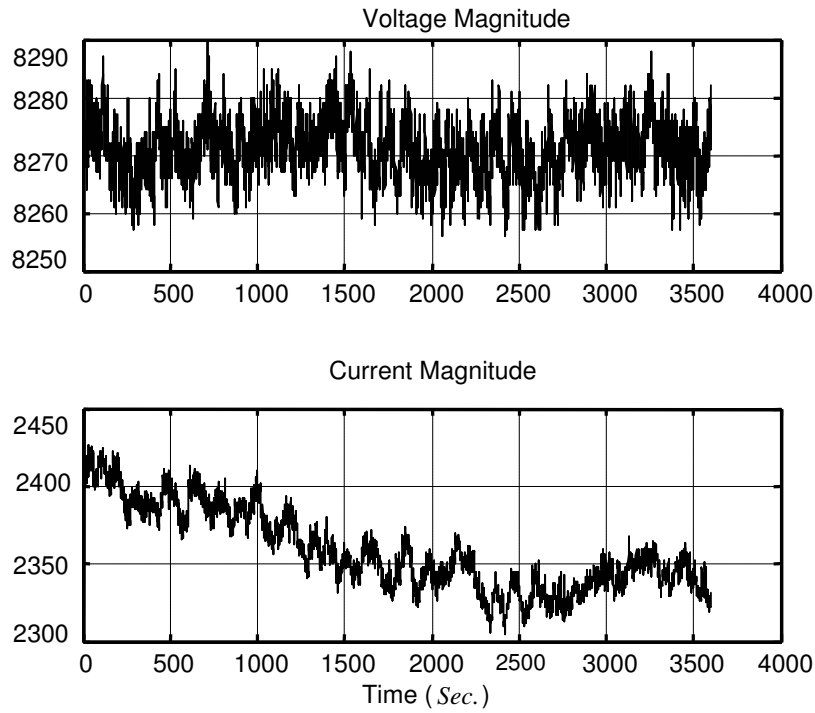


Figure 3.11: The magnitude of the voltage and current of one hour data started the time 00.00 of the 22<sup>nd</sup> of May 2002

The voltage of the four major load centers were analyzed to find the eigenvalues and mode shape of the Australian electricity network. Since the customer load variations are the integral of the white noise, the voltage angles were differentiated to present the measurement as though driven by white noise. In the next step the COI angle is computed and all of the angles were mapped to the COI referenced system. Then the autocorrelation of all of the voltage angles are computed. Figure 3.12 shows the autocorrelation of the voltage angle of the Brisbane load centre. Also the cross-correlation of the voltage angle of Brisbane and the Sydney load centers is depicted in Figure 3.13.

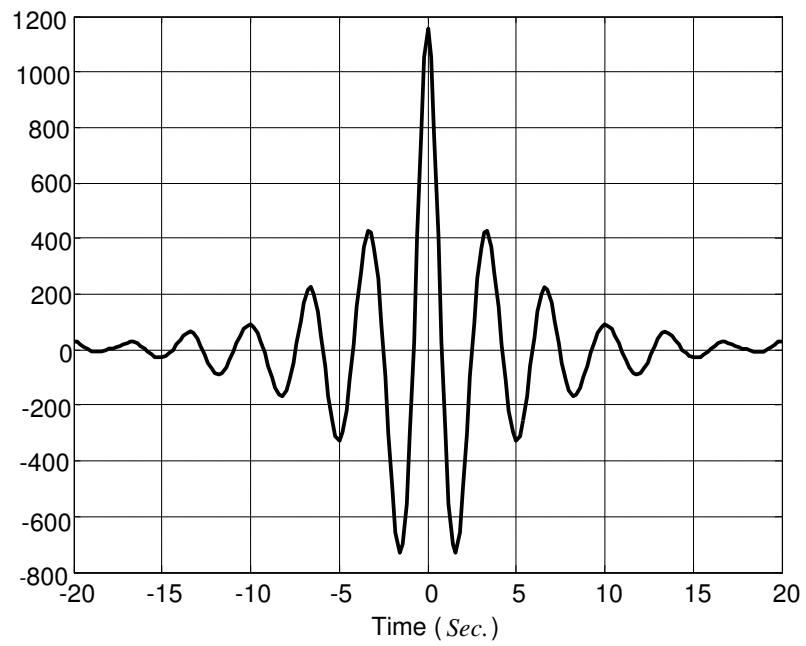


Figure 3.12: The autocorrelation of the Brisbane voltage angle

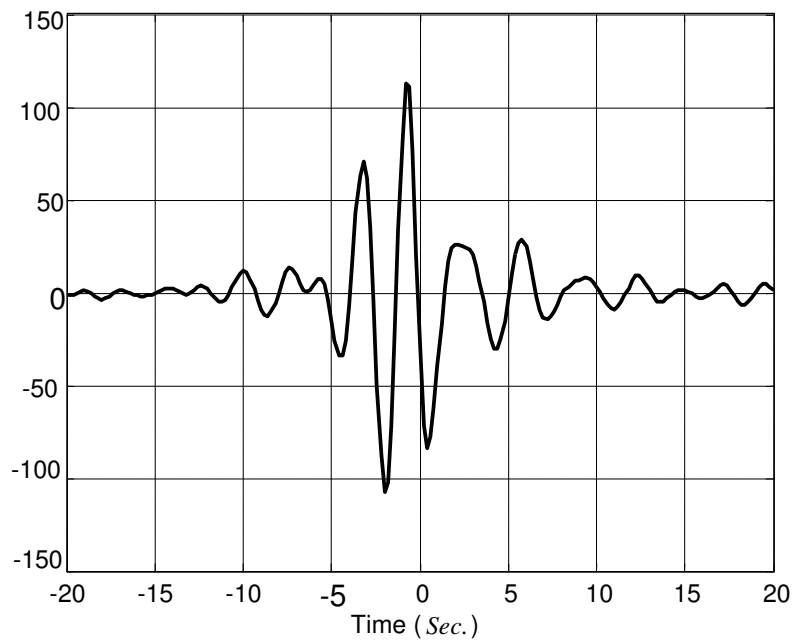


Figure 3.13: The cross-correlation of voltage angle of Brisbane and Sydney  
voltage angle

The power system resonant frequencies are found using multi-site curve fitting *FFT* of autocorrelations of the COI referenced voltage angles of the four major load centers in frequency domain. The time lag of autocorrelation in the real data analysis is chosen 40 seconds, to increase the frequency resolution. Then, the curve fitting is performed over the frequency range of interest as explained in Step 3 of the CBMSI algorithm presented Section 3.3.

The *FFT* of the autocorrelation of load centers are illustrated in Figure 3.14, and the identified eigenvalues and resonant frequencies are given in Tables 3.7 and 3.8 respectively.

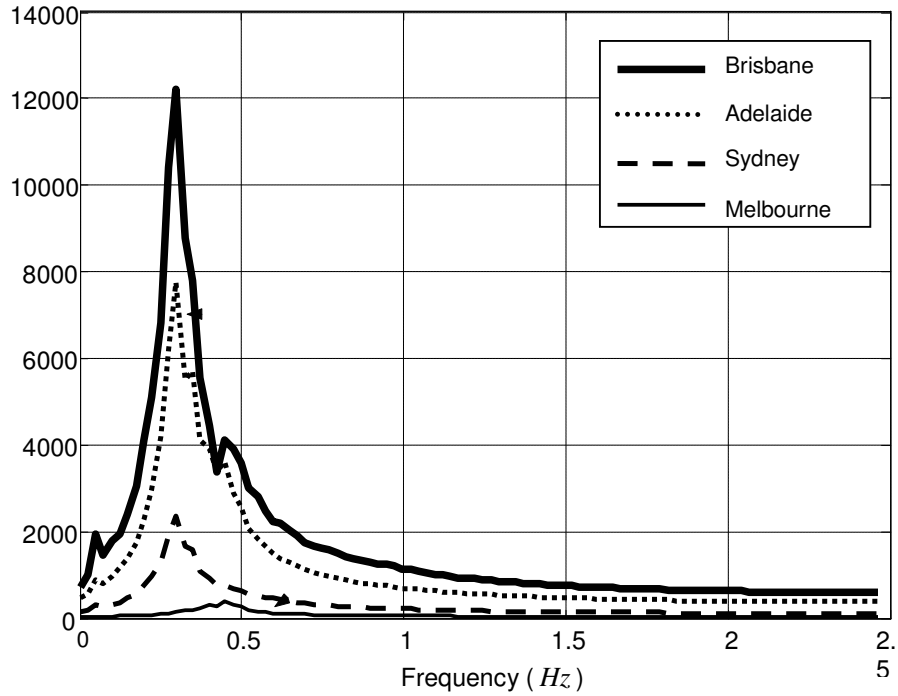


Figure 3.14: The magnitude of the *FFT* of autocorrelation of bus voltage angle of the load centers

Table 3.7: The power system eigenvalues identified from one hour of the normal operating data

Mode	Estimated Power System Eigenvalues
Mode 1	$-0.2255 + j1.8793$
Mode 2	$-0.3512 + j2.7552$
Mode3	$-6.1219 + j4.4677$

As shown in Figure 3.14, the first two modes are dominant in all of the *FFT* of the autocorrelations.

According to Equation (3.39), the mode shape plot at each identified resonant frequency can be determined using autocorrelation and cross-correlations. The mode shape plots for the three estimated resonant frequencies are illustrated in Figures 3.15 to 3.17.

Table 3.8: The power system resonant frequencies identified form one hour of the normal operating data

	Estimated Power System Resonant Frequency ( <i>Hz</i> )
Mode 1	$0.2991$
Mode 2	$0.4385$
Mode 3	$0.7397$

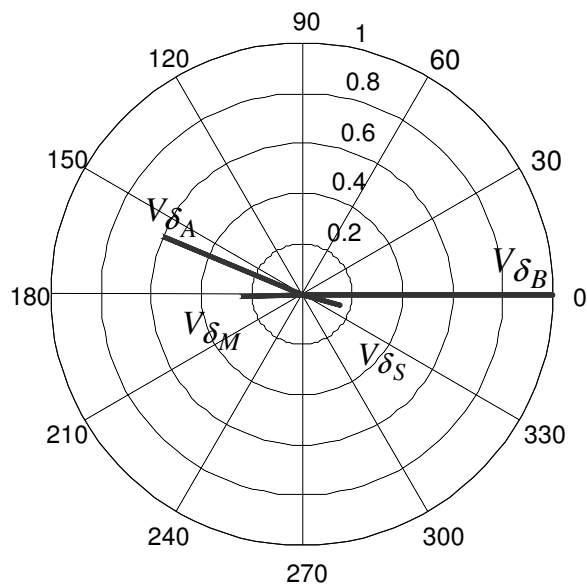


Figure 3.15: Mode shape for the real data at the first resonant frequency

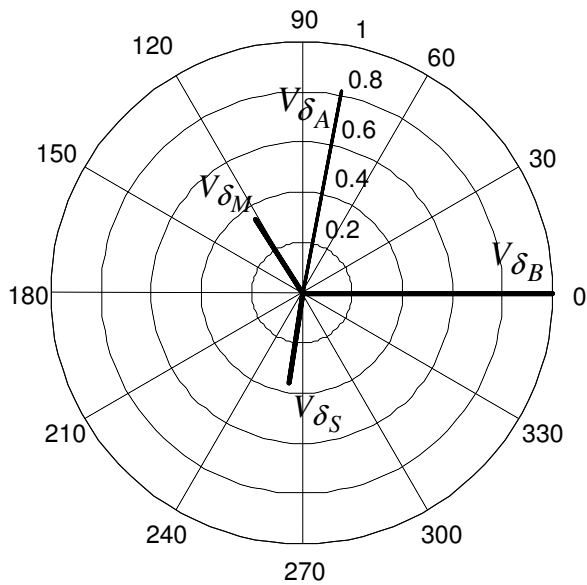


Figure 3.16: Mode shape for the real data at the second resonant frequency

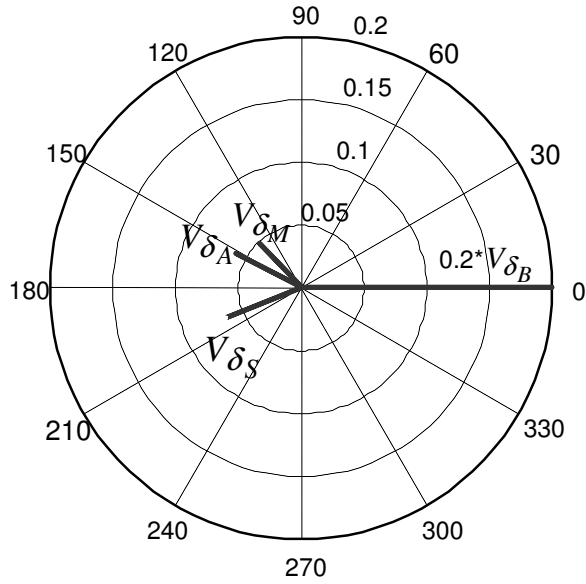


Figure 3.17: Mode shape for the real data at the third resonant frequency

From the mode shape plots in Figures 3.15 to 3.17 the following points can be made:

- At the first resonant frequency, the generators near Brisbane and Sydney load centers in one group are swinging against the generators near the Melbourne and Adelaide load centers in the other group. This happens at the second resonant frequencies in almost the same way.
- The Sydney voltage bus has the smallest contribution at the first resonant frequency.
- At the third resonant frequency, the Sydney, Melbourne and Adelaide load centers swing against the Brisbane load center.

### 3.6 Summary

In this chapter, the CBMSI method based on the autocorrelation and cross-correlation functions is proposed to identify the power system eigenvalues and mode shape. After developing the theory and presenting the algorithm, the CBMSI method is validated by simulating a test power system. The findings of the simulation show that the estimated power system eigenvalues and mode shapes agree with the results obtained by the eigenvalue analysis.

The CBMSI method is applied on two different sets of real data of the Australian electricity network. The first set of real data consisted of the power across 6 major lines of the Australian electricity network following a large disturbance created by a braking resistor event. The response of the system to the braking resistor is considered similar to an impulse response of the power system. From this data the power system resonant frequencies are identified using the correlation based method. The second data set includes magnitude and angle of voltage and current of four major load centers, Brisbane, Sydney, Melbourne and Adelaide, collected from the normal operating conditions for one hour. The power system resonant frequencies are identified using the CBMSI method. Then the mode shape at the each identified resonant frequency of the Australian electricity network, are determined.

## Chapter 4: Load Contribution to Damping

### 4.1 Introduction

This chapter develops a method to identify the effect of the load dynamics on oscillatory modes of the inter-area oscillations (IAO). In particular, the proposed method aims to find the sensitivity of the oscillatory modes with respect to the loads in a multi-machine power system and the extent to which loads can change the eigenvalues of a multi-machine system. In this method, the sensitivity is found by a.) using the identified oscillatory modes of low frequency oscillations, b.) the identified load model, and c.), the right and left modal matrices.

The eigenvalue sensitivity to load (ESL) method presented in this chapter can be applied to the actual power system to continuously learn actual parameters rather than derive them from an off-line model.

A test power system including three generators and nine buses is simulated to validate the algorithm.

This approach is also applied to the IAO of the Australian electricity network and the sensitivity to one particular feeder load is identified.

## 4.2 The Concept of Load Contribution to Damping

In order to explain the effect of load to damping, consider Figure 1.2, which is repeated in Figure 4.1 for convenience.

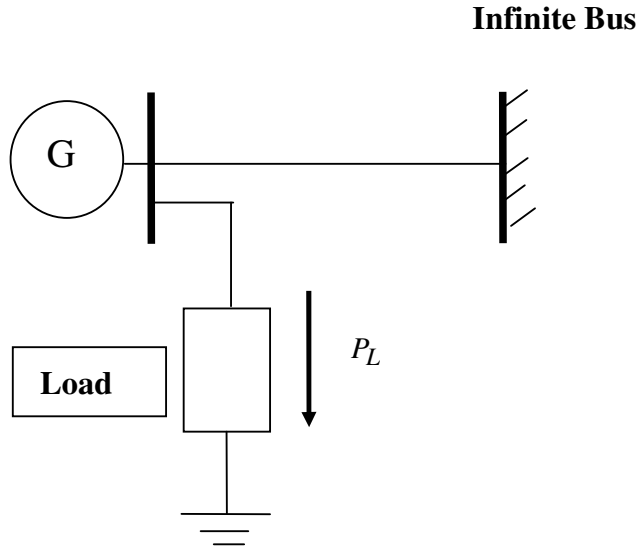


Figure 4.1: A single machine connected to infinite bus

At first consider that the load is static, therefore with a step change in voltage, the load power  $P_L$  changes suddenly. Hence the  $P_L$  changes are in phase with voltage and consequently in phase with  $\delta$  and it has no component in the direction of  $\dot{\delta}$ . Therefore, it does not contribute to damping, because according to Equation (2.3)  $P_L$  should have a component in the direction of  $\dot{\delta}$  in order to contribute to damping. This is shown in Figure 4.2.a.

Now consider the case that the load is a dynamic load like an induction motor. As explained previously due to the motor inertia, there is a phase

shift between the  $P_L$  changes and the voltage changes or between  $P_L$  changes and  $\delta$  changes as shown in Figure 4.2.b. The phase shift in Figure 4.2.b indicates that the load has a component in the direction of  $\dot{\delta}$ . Thus, the induction motor contributes to damping.

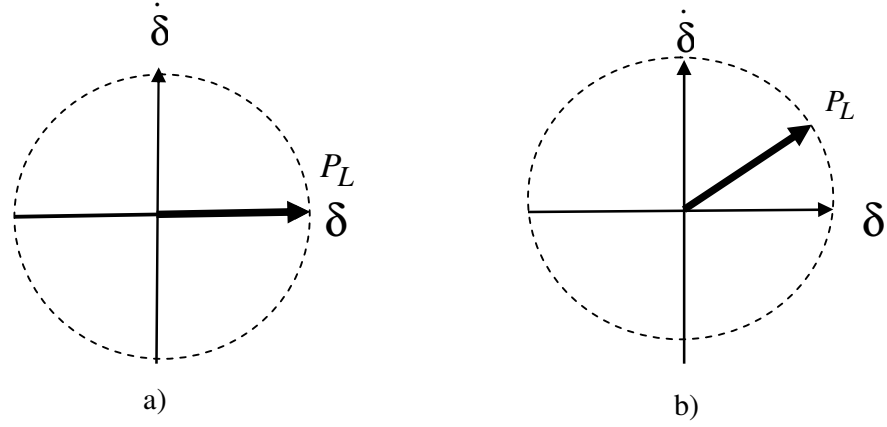


Figure 4.2: Load contribution to damping, a) static load, b) dynamic load

### 4.3 State Space Representation of Power Systems Including Dynamic Loads

As explained in Section 2.2, it is assumed that the perturbation around the operating point is small, such that the variations in the power system can be expressed in the form of a linear state space model. In Section 2.2, the state space representation of the power system in the IAO was studied.

In this section, the modification of the state space model is performed by considering the dynamic loads. Figure 4.3 represents the connection of the generator  $i$  to the rest of the network in an  $n$ -machine power system. For

each generator, a dynamic load is connected to the bus terminal of the generator.

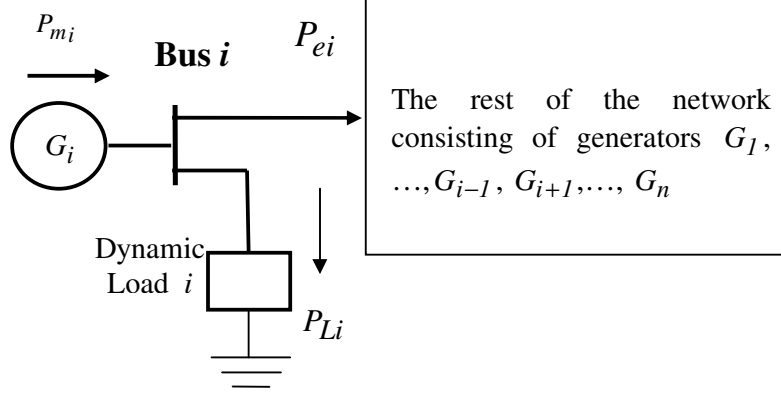


Figure 4.3: The connection of the generator  $i$  and load  $i$  and to the rest of the network

Since the aim is to describe the influence of the loads on the system modes, a load model is developed. This load model relates the rate of machine angle changes to the active power of the load. In particular, since the load is assumed to be located at the generator terminals, only the generator  $i$  affects the load  $i$ . This model shows the load at the generator terminals. This is not strictly true for all power systems but can be approximated in many cases. Where a group of generators are all in proximity of a load, then the aggregate generator representing the group may approximate this condition of loads at the generator terminals. In this simulation, the dynamic load model is chosen as a first order transfer function

$$P_{Li} = \frac{b_i}{a_i + s} \dot{\delta} \quad (4.1)$$

As explained in Chapter 2, the response of the aggregated induction motor model to the step change of the bus voltage angle is exponential. Therefore,

the dependency on frequency,  $\dot{\delta}$ , in the dynamic load model of Equation (4.1) is similar to the response of an induction motor [63,82].

Using the same method in Section 2.2 including dynamic load, Equation (2.4) can be modified as

$$\ddot{\delta}_i + \frac{1}{J_i} \sum_{j=1}^{n-1} P_{sij} \delta_{ij} + \frac{1}{J_i} D_i \dot{\delta}_i + \frac{1}{J_i} P_{Lik} = 0 \quad p.u. \quad i = 1, \dots, n \quad (4.2)$$

Evaluating Equation (4.1) at the  $k^{th}$  power system resonant frequency,  $\omega_k$ ,

and simplifying, an equation relating  $\dot{\delta}_i$  to  $P_{Li}$  at the specific resonant frequency  $\omega_k$ , can be found as

$$P_{Lik} = \alpha_{ik} \left( -\omega_k \sin \theta_i \delta_i + \cos \theta_i \dot{\delta}_i \right) \quad (4.3)$$

where

$$\alpha_{ik} = \frac{b}{\sqrt{a_i^2 + \omega^2}} \quad \text{and} \quad \theta_i = -\tan^{-1} \left( \frac{\omega_k}{a_i} \right) \quad (4.4)$$

in Equation (4.4),  $\alpha_{ik}$  is the load factor of the  $i^{th}$  dynamic load at  $\omega_k$ , and represents the value of the magnitude of the  $i^{th}$  dynamic load, and in the per unit (p.u.) system, it can take any value between zero and one.

It should be noted that to reach Equation (4.3), the following relation has been used

$$\dot{\delta}_i = j\omega_k \delta_i \quad (4.5)$$

where  $j$  is the complex operator.

Substituting Equation (4.3) into Equation (4.2) gives

$$\ddot{\delta}_i + \frac{1}{J_i} \sum_{j=1}^{n-1} P_{sij} \delta_{ij} + \frac{1}{J_i} D_i \dot{\delta}_i + \frac{1}{J_i} \alpha \left( -\omega_k \sin \theta \delta_i + \cos \theta \dot{\delta}_i \right) = 0 \quad p.u$$

$$i = 1, \dots, n$$
(4.6)

The normal approach to represent the state space model in Equation (4.6) is to form the full state space model including the dynamics of the load as given in Equation (4.1). However, it should be noted that as explained in Subsection 3.2.1, the load power has the characteristic of an integral of white noise and this signal excites the system. Then, the power system resonant frequencies are identified using the CBMSI method presented in Chapter 3. According to Equation (4.1), the rate of voltage angle changes,  $\dot{\delta}$ , is used to find the load model. However, energy of the spectrum of the  $\dot{\delta}$  is concentrated at the resonant frequencies of the IAO and is not uniformly distributed in the range of frequencies of interest for which we wish to find the load model. In spite of this, what is important is to find the load model at the resonant frequency and perform the sensitivity analysis which is described in Section 4.4. Thus, the state space representation of Equation (4.6) in the compact form is

$$\dot{X} = \mathbf{A}X + \alpha_{1k} E_1 V_{1k} X + \dots + \alpha_{ik} E_i V_{ik} X + \dots + \alpha_{nk} E_n V_{nk} X \quad (4.7)$$

where

$\mathbf{A}$  = the power system state matrix given in Equation (2.10) and

$$X = \begin{bmatrix} \delta_1 & \delta_2 & \dots & \delta_n & \dot{\delta}_1 & \dot{\delta}_2 & \dots & \dot{\delta}_n \end{bmatrix}^T \quad (4.8)$$

$$E_i = \begin{bmatrix} 0 & 0 & \dots & 0 & 0 & 0 & \dots & -\frac{1}{J_i} & \dots & 0 \end{bmatrix}^T \quad (4.9)$$

$$V_{ik} = \begin{bmatrix} 0 & 0 & \dots & -\omega_k \sin(\theta_i) & \dots & 0 & 0 & 0 & \dots & \cos(\theta_i) & \dots & 0 \end{bmatrix} \quad (4.10)$$

## 4.4 Sensitivity of Power System Mode with Respect to Load Parameters

This section makes use of eigenvalue sensitivity presented in Section 2.3. The limitation of the existing approaches is single parameter variation. As we see in this section there is a need of modification of eigenvalue sensitivity, when there are multiple parameter changes of the system matrix **A**.

In this section we want to know how the eigenvalues of a power system change as the load changes. Now consider the right eigenvector of the power system,  $\phi_k$ , which is characterized by the following equation

$$\left[ \mathbf{A} + \alpha_{ik} (E_{Ik} V_i) + \dots + \alpha_i (E_{ik} V_i) + \dots + \alpha_{nk} (E_{nk} V_n) \right] \phi_k = \lambda_k \phi_k \quad (4.11)$$

The derivative of Equation (4.11) with respect to  $\alpha_{ik}$  can be computed as

$$\begin{aligned} & \left[ \frac{\partial}{\partial \alpha_{ik}} (\mathbf{A} + \alpha_{ik} E_{ik} V_i) \right] \phi_k + \\ & \left[ \mathbf{A} + \alpha_{Ik} (E_{Ik} V_i) + \dots + \alpha_i (E_{ik} V_i) + \dots + \alpha_{nk} (E_{nk} V_n) \right] \frac{\partial \phi_k}{\partial \alpha_{ik}} \quad (4.12) \\ & = \frac{\partial \lambda_k}{\partial \alpha_{ik}} \phi_k + \lambda_k \frac{\partial \phi_k}{\partial \alpha_{ik}} \end{aligned}$$

or

$$E_{ik}V_i\phi_k + (\mathbf{A} + \alpha_{Ik}(E_{Ik}V_I) + \dots + \alpha_{ik}(E_{ik}V_i) + \dots + \alpha_{nk}(E_{nk}V_n)) \frac{\partial \phi_k}{\partial \alpha_{ik}} = \frac{\partial \lambda_k}{\partial \alpha_{ik}} \phi_k + \lambda_k \frac{\partial \phi_k}{\partial \alpha_{ik}} \quad (4.13)$$

Let  $\psi_i$  denotes the  $i^{th}$  left eigenvector, then premultiplying Equation (4.13)

by  $\psi_i$ , the following equation is obtained

$$\psi_k E_{ik}V_i\phi_k + \psi_k [\mathbf{A} + \alpha_{Ik}(E_{Ik}V_I) + \dots + \alpha_{ik}(E_{ik}V_i) + \dots + \alpha_{nk}(E_{nk}V_n)] \frac{\partial \phi_k}{\partial \alpha_{ik}} = \psi_k \frac{\partial \lambda_k}{\partial \alpha_{ik}} \phi_k + \psi_k \lambda_k \frac{\partial \phi_k}{\partial \alpha_{ik}}$$

According to Equation (2.16), we have

$$\psi_k \frac{\partial \lambda_k}{\partial \alpha_{ik}} \phi_k = \frac{\partial \lambda_k}{\partial \alpha_{ik}} \quad (4.14)$$

Also, from the definition of the right eigenvector the following equation can be written as.

$$\psi_k [(\mathbf{A} + \alpha_{Ik}(E_{Ik}V_I) + \dots + \alpha_{ik}(E_{ik}V_i) + \dots + \alpha_{nk}(E_{nk}V_{nk})) - \lambda_k I] \phi_k = 0 \quad (4.15)$$

Therefore, the sensitivity of the  $k^{th}$  eigenvalue with respect to the  $i^{th}$  load (per dynamic load unit) is

$$\frac{\partial \lambda_k}{\partial \alpha_{ik}} = \psi_k E_{ik}V_i\phi_k \quad (4.16)$$

Therefore the changes in the  $k^{th}$  eigenvalue,  $\Delta \lambda_k$ , due to presence of the  $i^{th}$  load can found from

$$\Delta \lambda_k = \psi_k E_{ik}V_i\phi_k \Delta \alpha_{ik} \quad (4.17)$$

## 4.5 Load Model Identification in IAO

### 4.5.1 Describing the Load Effect on Power System Using

#### Block Diagram Representation

In order to investigate the effects of the load characteristics on the IAO, consider the block diagram in Figure 4.4. In this block diagram, the measured power,  $P$ , includes some of the system “noise disturbance” which are customer load changes within the feeder. There are two inputs  $w$  and  $z$  for the block diagram shown in Figure 4.4. Input  $w$  represents the local customer load perturbation and input  $z$  shows the remote customer load perturbation. In the other word, at any resonant frequency, the mode is partly excited by local load variations or feedback power system controller influences, and partly from other loads or other power system controllers [8]. The local and remote excitation of the system oscillations are labeled  $w(t)$  and  $z(t)$  respectively. Since the load can be modeled as the integral of white noise [50], the power system with local and remote disturbances can be represented as in Figure 4.4.a. In this model  $w$  and  $z$  are uncorrelated white noises. The model in Figure 4.4.a, can be simplified to the representation shown in Figure 4.4.b. In Figure 4.4 the transfer function  $\frac{m(s)}{n(s)}$  is included to represent the different effect of load perturbation from remote locations on the system response.

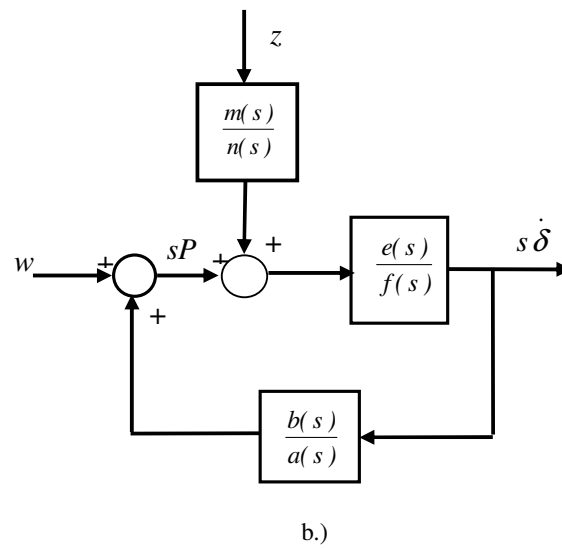
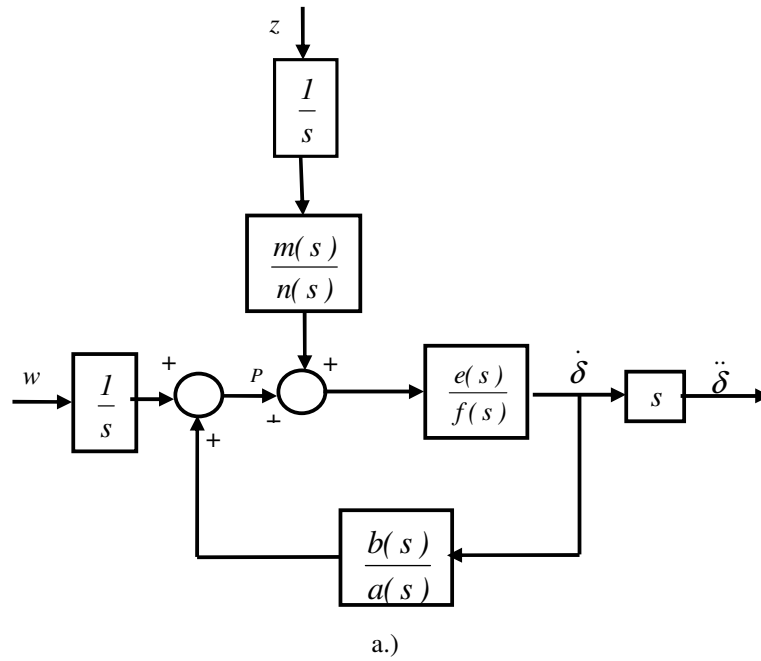


Figure 4.4: Block diagram of power system to show load dynamics a.) complete model, b.) simplified model

### 4.5.2 Correlation Based Analysis of the Load Effect on the Power system

The influence of the load on the power system is investigated analytically in this section.

With regard to Figure 4.4 we can write

$$s \dot{\boldsymbol{\delta}}(s) = \frac{e(s)a(s)}{a(s)f(s) - b(s)e(s)} \left( \frac{m(s)}{n(s)} \mathbf{z}(s) + \mathbf{w}(s) \right) \quad (4.18)$$

$$s \dot{\mathbf{P}}(s) = \frac{f(s)a(s)n(s)\mathbf{w}(s) + e(s)b(s)m(s)\mathbf{z}(s)}{n(s)(a(s)f(s) - b(s)e(s))} \quad (4.19)$$

Equations (4.18) and (4.19) can be written as

$$\dot{\boldsymbol{\delta}}(s) = \mathbf{H}_{11}(s)\mathbf{w}(s) + \mathbf{H}_{12}(s)\mathbf{z}(s) \quad (4.20)$$

$$\mathbf{P}(s) = \mathbf{H}_{21}(s)\mathbf{w}(s) + \mathbf{H}_{22}(s)\mathbf{z}(s) \quad (4.21)$$

where

$$\mathbf{H}_{11}(s) = \frac{e(s)a(s)}{a(s)f(s) - b(s)e(s)} \frac{m(s)}{n(s)} \quad (4.22)$$

$$\mathbf{H}_{12}(s) = \frac{e(s)a(s)}{a(s)f(s) - b(s)e(s)} \quad (4.23)$$

$$\mathbf{H}_{21}(s) = \frac{f(s)a(s)n(s)}{n(s)(a(s)f(s) - b(s)e(s))} \quad (4.24)$$

$$\mathbf{H}_{22}(s) = \frac{e(s)b(s)m(s)}{n(s)(a(s)f(s) - b(s)e(s))} \quad (4.25)$$

Equations (4.18) and (4.19) in time domain can be expressed as

$$\dot{\boldsymbol{\delta}}(t) = \int_{-\infty}^{\infty} h_{11}(\xi_{11}) \mathbf{w}(t - \xi_{11}) d\xi_{11} + \int_{-\infty}^{\infty} h_{12}(\xi_{12}) \mathbf{z}(t - \xi_{12}) d\xi_{12} \quad (4.26)$$

$$P(t) = \int_{-\infty}^{\infty} h_{21}(\xi_{21}) w(t - \xi_{21}) d\xi_{21} + \int_{-\infty}^{\infty} h_{22}(\xi_{22}) z(t - \xi_{22}) d\xi_{22} \quad (4.27)$$

where  $h_{11}$ ,  $h_{12}$ ,  $h_{21}$  and  $h_{22}$ , are the impulse responses of  $\mathbf{H}_{11}(s)$ ,  $\mathbf{H}_{12}(s)$ ,  $\mathbf{H}_{21}(s)$  and  $\mathbf{H}_{22}(s)$ , respectively.

The desired load model, which is the transfer function between  $\dot{\delta}$  and  $P$  in the frequency domain,  $\mathbf{H}_L(\omega)$ , can be computed according to (2.20)

$$\mathbf{H}_L(\omega) = \frac{\Im \left[ C_{\dot{\delta}P}(\tau) \right]}{\Im \left[ R_{\dot{\delta}\dot{\delta}}(\tau) \right]} \quad (4.28)$$

where  $C_{\dot{\delta}P}(\tau)$  is the cross-correlation of  $\dot{\delta}$ , and  $R_{\dot{\delta}\dot{\delta}}(\tau)$  is the Fourier

transform of the auto-correlation of  $\dot{\delta}$  [8]. The cross-correlation function  $C_{\dot{\delta}P}(\tau)$  and autocorrelation function  $R_{\dot{\delta}\dot{\delta}}(\tau)$  can be found from the

following equations (see Appendix A)

$$C_{\dot{\delta}P}(\tau) = E[\dot{\delta}(t) P(t + \tau)] \quad (4.29)$$

$$R_{\dot{\delta}\dot{\delta}}(\tau) = E[\dot{\delta}(t) \dot{\delta}(t + \tau)] \quad (4.30)$$

where  $E$  is the expected value.

Substituting (4.26) and (4.27) into (4.29) and (4.30) respectively, yields

$$C_{\delta P}(\tau) = E \left\{ \left[ \int_{-\infty}^{\infty} h_{11}(\xi_{11}) w(t - \xi_{11}) d\xi_{11} + \int_{-\infty}^{\infty} h_{12}(\xi_{12}) z(t - \xi_{12}) d\xi_{12} \right] \right. \\ \left. \left[ \int_{-\infty}^{\infty} h_{21}(\xi_{21}) w(t + \tau - \xi_{21}) d\xi_{21} + \int_{-\infty}^{\infty} h_{22}(\xi_{22}) z(t + \tau - \xi_{22}) d\xi_{22} \right] \right\} \quad (4.31)$$

or

$$C_{\delta P}(\tau) = E \left\{ \int_{-\infty}^{\infty} h_{11}(\xi_{11}) w(t - \xi_{11}) d\xi_{11} \int_{-\infty}^{\infty} h_{21}(\xi_{21}) w(t + \tau - \xi_{21}) d\xi_{21} \right\} \\ + E \left\{ \int_{-\infty}^{\infty} h_{11}(\xi_{11}) w(t - \xi_{11}) d\xi_{11} \int_{-\infty}^{\infty} h_{22}(\xi_{22}) z(t + \tau - \xi_{22}) d\xi_{22} \right\} \\ + E \left\{ \int_{-\infty}^{\infty} h_{12}(\xi_{12}) z(t - \xi_{12}) d\xi_{12} \int_{-\infty}^{\infty} h_{21}(\xi_{21}) w(t + \tau - \xi_{21}) d\xi_{21} \right\} \\ + E \left\{ \int_{-\infty}^{\infty} h_{12}(\xi_{12}) z(t - \xi_{12}) d\xi_{12} \int_{-\infty}^{\infty} h_{22}(\xi_{22}) z(t + \tau - \xi_{22}) d\xi_{22} \right\} \quad (4.32)$$

The expected value from the internal terms of the integrals in (4.32) is taken as

$$C_{\delta P}(\tau) = \int_{-\infty}^{\infty} \int_{-\infty}^{\infty} h_{11}(\xi_{11}) h_{21}(\xi_{21}) E\{w(t - \xi_{11}) w(t + \tau - \xi_{21})\} d\xi_{11} d\xi_{21} \\ + \int_{-\infty}^{\infty} \int_{-\infty}^{\infty} h_{11}(\xi_{11}) h_{22}(\xi_{22}) E\{w(t - \xi_{11}) z(t + \tau - \xi_{22})\} d\xi_{11} d\xi_{22} \\ + \int_{-\infty}^{\infty} \int_{-\infty}^{\infty} h_{12}(\xi_{12}) h_{21}(\xi_{21}) E\{z(t - \xi_{12}) w(t + \tau - \xi_{21})\} d\xi_{12} d\xi_{21} \\ + \int_{-\infty}^{\infty} \int_{-\infty}^{\infty} h_{12}(\xi_{12}) h_{22}(\xi_{22}) E\{z(t - \xi_{12}) z(t + \tau - \xi_{22})\} d\xi_{12} d\xi_{22} \quad (4.33)$$

Since  $w$  and  $z$  are uncorrelated white noise, therefore we have

$$E[w(t) z(t + \tau)] = 0 \quad (4.34)$$

Equation (4.34) holds for all values of time lag,  $\tau$ , [24]. Equation (4.33) is simplified using Equation (4.34) as

$$\begin{aligned}
C_{\dot{\delta}P}(\tau) = & \int_{-\infty}^{\infty} \int_{-\infty}^{\infty} h_{11}(\xi_{11}) h_{21}(\xi_{21}) R_{ww}(\tau + \xi_{11} - \xi_{21}) d\xi_{11} d\xi_{21} \\
& + \int_{-\infty}^{\infty} \int_{-\infty}^{\infty} h_{12}(\xi_{12}) h_{22}(\xi_{22}) R_{zz}(\tau + \xi_{12} - \xi_{22}) d\xi_{12} d\xi_{22} \quad (4.35)
\end{aligned}$$

where  $R_{ww}$  and  $R_{zz}$  are the autocorrelation of  $w(t)$  and  $z(t)$  respectively.

By using the definition of convolution, Equation (4.35) becomes

$$C_{\dot{\delta}P}(\tau) = R_{ww}(\tau) * h_{11}(-\tau) * h_{21}(\tau) + R_{zz}(\tau) * h_{12}(-\tau) * h_{22}(\tau) \quad (4.36)$$

where  $*$  represents the convolution integral operator.

Applying the same method for the autocorrelation of  $\dot{\delta}$ ,  $R_{\dot{\delta}\dot{\delta}}(\tau)$ , gives

$$R_{\dot{\delta}\dot{\delta}}(\tau) = R_{ww}(\tau) * h_{11}(-\tau) * h_{11}(\tau) + R_{zz}(\tau) * h_{12}(-\tau) * h_{12}(\tau) \quad (4.37)$$

Then, the Fourier transform of (4.36) and (4.37) is taken as

$$C_{\dot{\delta}P}(\omega) = R_{ww}(\omega) H_{11}(-\omega) H_{11}(\omega) + R_{zz}(\omega) H_{21}(-\omega) * H_{22}(\omega) \quad (4.38)$$

$$R_{\dot{\delta}\dot{\delta}}(\omega) = R_{ww}(\omega) H_{11}(-\omega) H_{11}(\omega) + R_{zz}(\omega) H_{12}(-\omega) * H_{22}(\omega)$$

$$R_{\dot{\delta}\dot{\delta}}(\omega) = R_{ww}(\omega) H_{11}(-\omega) H_{11}(\omega) + R_{zz}(\omega) H_{12}(-\omega) * H_{12}(\omega) \quad (4.39)$$

Since  $w(t)$  and  $d(t)$  are white noise, their power spectrum densities are flat, Therefore,  $R_{ww}(\omega)$  and  $R_{zz}(\omega)$  can be found from the following equations

$$\mathbf{R}_{ww}(\omega) = W \quad (4.40)$$

$$\mathbf{R}_{zz}(\omega) = Z \quad (4.41)$$

where  $W$  and  $Z$  are real positive constants.

By using  $\mathbf{R}_{ww}(\omega)$  and  $\mathbf{R}_{zz}(\omega)$  from (4.40) and (4.41) respectively,

Equations (4.38) and (4.39) are changed to

$$\mathbf{C}_{\delta p}(\omega) = \mathbf{H}_{11}(-\omega) \mathbf{H}_{21}(\omega) W + \mathbf{H}_{12}(-\omega) * \mathbf{H}_{22}(\omega) Z \quad (4.42)$$

$$\mathbf{R}_{\delta \delta}(\omega) = \mathbf{H}_{11}(-\omega) \mathbf{H}_{11}(\omega) W + \mathbf{H}_{12}(-\omega) * \mathbf{H}_{12}(\omega) Z \quad (4.43)$$

Equations (4.42) and (4.43) can be written in the short form of

$$\mathbf{C}_{\delta p}(\omega) = \mathbf{H}_a(\omega) W + \mathbf{H}_b(\omega) Z \quad (4.44)$$

$$\mathbf{R}_{\delta \delta}(\omega) = \mathbf{H}_c(\omega) W + \mathbf{H}_d(\omega) Z \quad (4.45)$$

where

$$\mathbf{H}_a(\omega) = \mathbf{H}_{11}(-\omega) \mathbf{H}_{21}(\omega) \quad (4.46)$$

$$\mathbf{H}_b(\omega) = \mathbf{H}_{21}(-\omega) \mathbf{H}_{22}(\omega) \quad (4.47)$$

$$\mathbf{H}_c(\omega) = \mathbf{H}_{11}(-\omega) \mathbf{H}_{11}(\omega) \quad (4.48)$$

$$\mathbf{H}_d(\omega) = \mathbf{H}_{12}(-\omega) \mathbf{H}_{21}(\omega) \quad (4.49)$$

The load transfer function is determined by substituting the numerator and denominator of (4.28) by (4.44) and (4.45), respectively. Therefore, the load model can be found from

$$\mathbf{H}_L(\omega) = \frac{\mathbf{H}_a(\omega)W + \mathbf{H}_b(\omega)Z}{\mathbf{H}_c(\omega)W + \mathbf{H}_d(\omega)Z} \quad (4.50)$$

or

$$\mathbf{H}_L(\omega) = \frac{\mathbf{H}_a(\omega)W}{\mathbf{H}_c(\omega)W + \mathbf{H}_d(\omega)Z} + \frac{\mathbf{H}_b(\omega)Z}{\mathbf{H}_c(\omega)W + \mathbf{H}_d(\omega)Z} \quad (4.51)$$

When the overwhelming majority of the modal disturbance does not originate in the feeder load being examined, or in the other words, if  $W \ll Z$ , then the transfer function  $\mathbf{H}_L$  can be approximated by

$$\mathbf{H}_L(\omega) = \frac{\mathbf{H}_b(\omega)}{\mathbf{H}_d(\omega)} \quad (4.52)$$

After substituting  $H_b(\omega)$  from (4.47) and  $H_d(\omega)$  from (4.49) and simplifying, the load transfer function can be expressed as

$$\mathbf{H}_L(\omega) = \frac{b(\omega)}{a(\omega)} \quad (4.53)$$

So, with the condition that  $W$  is much smaller than  $Z$ , the transfer function between  $\delta$  and  $P$  can be identified. Consider the case of monitoring one feeder in a large interconnected system. In this case, the load variations in that feeder will have a much lower effect on the network than the cumulative effect of variations from every other feeder in the entire power system network. Therefore, if the local customer changes are much greater than the remote load changes, the load transfer function  $\mathbf{H}_L(\omega)$  can be found from Equation (4.53).

## 4.6 Algorithm for the Eigenvalue Sensitivity to Load (ESL) Method

On the basis of the theory presented in the previous sections of this chapter, the algorithm of eigenvalue sensitivity to load (ESL) method is developed to determine the load contribution to damping in a multi-machine power system. The algorithm has the following steps:

### Step 1: Identifying the resonant frequencies of the IAO

The CBMSI method was developed in Chapter 3, is used to find the oscillatory modes of the IAO. When using CBMSI method, the COI angle is first computed using Equation (2.6) and then the voltage angles are mapped to the COI reference angle according to (2.7). The voltage angles in the COI referenced system are used by the CBMSI method to find the power system eigenvalues.

### Step 2: Identifying the load model

The load model in the algorithm is found on the basis of cross-correlation and autocorrelation functions from Equation (4.28), with the assumption that the local load disturbance is much smaller than that of remote disturbances.

### Step 3: Determination of the right and left eigenvectors

In Section 3.3, the process of determining the mode shape plot, on the basis of cross-correlation and autocorrelation was developed and explained. The mode shape is plotted using  $\bar{\phi}_k$  as shown in Equation (3.39). It was also

mentioned that  $\bar{\phi}_k$  in (3.39) is a part of  $k^{th}$  right eigenvector,  $\phi_k$ . The right eigenvector  $\phi_k$  can be found with the same method used previously in (3.38) and considering the relationship between the  $\delta$  and  $\dot{\delta}$  described by (4.5) as

$$\phi_k = \begin{bmatrix} 1 \\ \mathbf{H}_2(\omega)|_{\omega=\omega_k} \\ \vdots \\ \mathbf{H}_n(\omega)|_{\omega=\omega_k} \\ j\omega_k \\ j\omega_k \mathbf{H}_2(\omega)|_{\omega=\omega_k} \\ \vdots \\ j\omega_k \mathbf{H}_n(\omega)|_{\omega=\omega_k} \end{bmatrix} \quad (4.54)$$

The right eigenvector  $\phi_k$  in Equation (4.54) is normalized to the first element of the vector.

The right modal matrix is formed as given in Equation (2.13) using Equation (4.54). It should be noted that in an  $n$ -machine system, there are  $(n-1)$  inter-machine frequencies or  $2(n-1)$  complex frequencies but the size of the right modal matrix is  $2n$  by  $2n$ . The remaining eigenvectors correspond to the common modes. One of the common mode frequencies for the model in (4.7) is zero and the other is equal to the system load response time constant. If the load response common mode is called  $\lambda_c$ , then the  $2n$  by  $1$  unnormalized eigenvectors corresponding to common modes can be formed as

$$\phi_{2n-1} = [1 \quad \cdots \quad 1 \quad 0 \quad \cdots \quad 0]^T \quad (4.55)$$

$$\phi_{2n} = [I \quad \cdots \quad I \quad \lambda_c \quad \cdots \quad \lambda_c]^T \quad (4.56)$$

The common mode,  $\lambda_c$ , can be found by fitting a first order model on the *FFT* of the autocorrelation of the COI angle.

According to Equation (2.17), the left modal matrix is the inverse of the right modal matrix. The rows of the left modal matrix are the left eigenvectors.

#### **Step 4: Identification of the load contribution to damping**

By evaluating the identified load transfer function from Equation (4.28) at the power system resonant frequency, the contribution of load to damping is quantified. In fact, this quantification is used to form  $V$  vectors in Equation (4.10).

#### **Step 5: Sensitivity analysis**

In this step, the sensitivity of the eigenvalues with respect to the load factor is determined using Equation (4.16). Indeed, the computed sensitivity shows the extent to which the eigenvalues of the system would be changed in the presence of the load.

### **4.7 Simulation Results of the ESL Method**

This section examines the simulation of the proposed ESL method on a test power system consisting of three generators and nine lines. The same test power system used in Chapter 3, is simulated in this section with some modifications. The test system and its parameters are derived from [15]. Following the steps given in [15], the system can be reduced to a 3-machine system with three lines. In our analysis only the reactive part of the line

impedance is considered. The diagram of the resulting system is illustrated in Figure 4.3. The modifications of the test system of [15] include the three dynamic loads which are placed close to the generator terminals as discussed in Section 4.3.

To validate the sensitivity algorithm, the eigenvalues of the system with the loads and without the loads are determined via a simulation. Then the difference between the two separate sets is considered as the actual sensitivity. These values are then compared to the values that are to be obtained by means of the sensitivity analysis which is described in Section 4.4 in Equation (4.17). The test system is excited with three white noise sources in such a way that each of the sources is located near a generator bus.

In this simulation, the load connected at each generator bus, is considered in the form of

$$\frac{P_{Li}}{\dot{\delta}_i} = \frac{b_i}{a_i + s} \quad i = 1, \dots, 3 \quad (4.57)$$

In Figure 4.5,  $L_1$  to  $L_3$  represent the dynamic loads and their equations are given in Equation (4.57).

As explained in Subsection 3.4.1, the damping for the synchronous generators is considered as

$$P_{Di} = -0.6 \dot{\delta}_i \quad i = 1, \dots, 3 \quad (4.58)$$

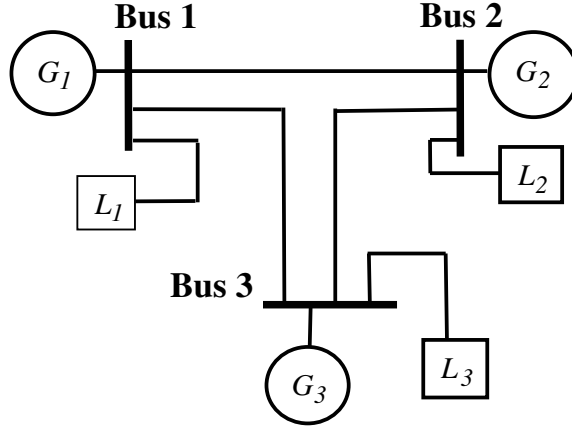


Figure 4.5: A simplified diagram of the test power system including a dynamic load at each generator terminal

The state variable vector for this system is presented by

$$X = \begin{bmatrix} \delta_1 & \delta_2 & \delta_3 & \dot{\delta}_1 & \dot{\delta}_2 & \dot{\delta}_3 & P_{L1} & P_{L2} & P_{L3} \end{bmatrix}^T \quad (4.59)$$

The state space representation for the test system can be written as

$$\dot{X} = \mathbf{A}_I X + \mathbf{B}U \quad (4.60)$$

where

$\mathbf{A}_I$  = the system matrix including loads

$U$  = the vector of the input sources

The system matrix  $\mathbf{A}_I$  can be formed by using (2.10) as

$$\mathbf{A}_I = \begin{bmatrix}
0 & 0 & 0 & 1 & 0 & 0 & 0 & 0 & 0 \\
0 & 0 & 0 & 0 & 1 & 0 & 0 & 0 & 0 \\
0 & 0 & 0 & 0 & 0 & 1 & 0 & 0 & 0 \\
\sum_{i=2}^3 P_{s1i} & -P_{s12} & -P_{s13} & -0.6 & 0 & 0 & -\frac{1}{J_1} & 0 & 0 \\
-P_{s21} & \sum_{\substack{i=1 \\ i \neq 2}}^3 P_{s2i} & -P_{s23} & 0 & -0.6 & 0 & 0 & -\frac{1}{J_2} & 0 \\
-P_{s31} & -P_{s32} & \sum_{\substack{i=1 \\ i \neq 3}}^3 P_{s3i} & 0 & 0 & -0.6 & 0 & 0 & -\frac{1}{J_3} \\
0 & 0 & 0 & b_1 & 0 & 0 & a_1 & 0 & 0 \\
0 & 0 & 0 & 0 & b_2 & 0 & 0 & a_2 & 0 \\
0 & 0 & 0 & 0 & 0 & b_3 & 0 & 0 & a_3
\end{bmatrix} \quad (4.61)$$

The input matrix  $\mathbf{B}$  and the input vector  $\mathbf{U}$  and are considered as

$$\mathbf{B} = \begin{bmatrix}
0 & 0 & 0 & -\frac{B1}{J_1} & 0 & 0 & 0 & 0 & 0 \\
0 & 0 & 0 & 0 & -\frac{1}{J_2} & 0 & 0 & 0 & 0 \\
0 & 0 & 0 & 0 & 0 & -\frac{1}{J_3} & 0 & 0 & 0
\end{bmatrix} \quad (4.62)$$

$$\mathbf{U} = [u_1 \quad u_2 \quad u_3]^T \quad (4.63)$$

where  $u_1$  to  $u_3$  are the three white noise sources.

The test system is simulated for 30 minutes with a sampling frequency of 10 Hz. The first step according to the algorithm in Section 4.6, is the identification of the power system eigenvalues. The power system resonant frequencies and loads are identified using the CBMSI presented in Chapter 3. Since the generators of the test system are the same as the generators of

the test system in Section 3.4.2, the identified resonant frequencies are the same as those previously given in Table 3.1.

In the next step, the dynamic load transfer functions are identified according to Equation (4.28). The frequency response of the identified model for load 2, is shown in Figure 4.4. The identified dynamic load parameters as well as the chosen values are given in Table 4.1. The chosen values in this table represent the known values for the dynamic load parameters.

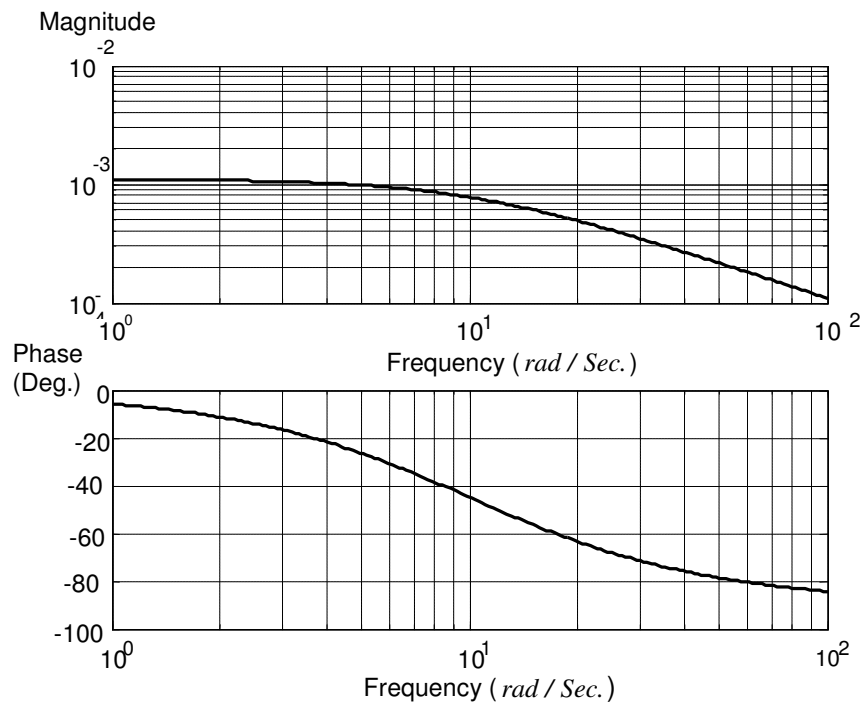


Figure 4.6: The frequency response of the identified model of load 2 for the test power system

As Table 4.1 illustrates, the estimated values of the load parameters agree with the actual values. This shows the validity of the load model identification.

Table 4.1: The chosen and estimated the loads parameters for the test power system

	Load Parameter	Chosen	Estimated
Load $L_1$	$b_1$	$0.035$	$0.0348$
	$a_1$	$15$	$14.919$
Load $L_2$	$b_2$	$0.011$	$0.0110$
	$a_2$	$10$	$10.0216$
Load $L_3$	$b_3$	$0.21$	$0.0209$
	$a_3$	$7$	$7.0134$

The sensitivity of the eigenvalues of the test power system to the presence of all loads is also calculated using Equation (4.17). These values as well as actual sensitivity are shown in Table 4.2. The actual sensitivity in this table illustrates the difference in the power system eigenvalue when there is no load with the case in which the loads are present.

Table 4.2: The actual and estimated sensitivity of the power system eigenvalues when all loads are varied

Resonant Frequency	Sensitivity with the Chosen Load Parameters	Estimated Sensitivity
$f = 1.4 \text{ Hz}$	$-0.0116 + j0.0107$	$-0.0102 + j0.0098$
$f = 2.1 \text{ Hz}$	$-0.0177 + j0.0329$	$-0.01722 + j0.0313$

As shown in Table 4.2, the actual and estimated values of the sensitivity are close. This indicates that the ESL method is capable of accurate estimation.

The results given in Table 4.2 also indicate:

- The load has increased the damping for both modes, real part of the sensitivity values are negative.
- However, the increase in the imaginary component of the modes shows that the load has caused a small increase in modal frequencies.
- At  $2.1\text{ Hz}$ , the influence of the load on frequency is stronger than the influence on damping.

It is worthwhile to quantify load contribution to damping. By evaluating the identified load transfer function at the resonant frequency, the contribution to damping is quantified. The contributions of the loads  $L_1$  to  $L_3$  to damping at  $f = 1.4\text{ Hz}$  and  $f = 2.1\text{ Hz}$  are shown in Tables 4.3

Table 4.3: The value of load contribution to damping for the test power system

	Load Contribution to Damping at $f = 1.4\text{ Hz}$ (Neper per second)	Load Contribution to Damping at $f = 2.1\text{ Hz}$ (Neper per second)
Load $L_1$	<i>0.0152</i>	<i>0.0174</i>
Load $L_2$	<i>0.0054</i>	<i>0.0053</i>
Load $L_3$	<i>0.0102</i>	<i>0.0085</i>

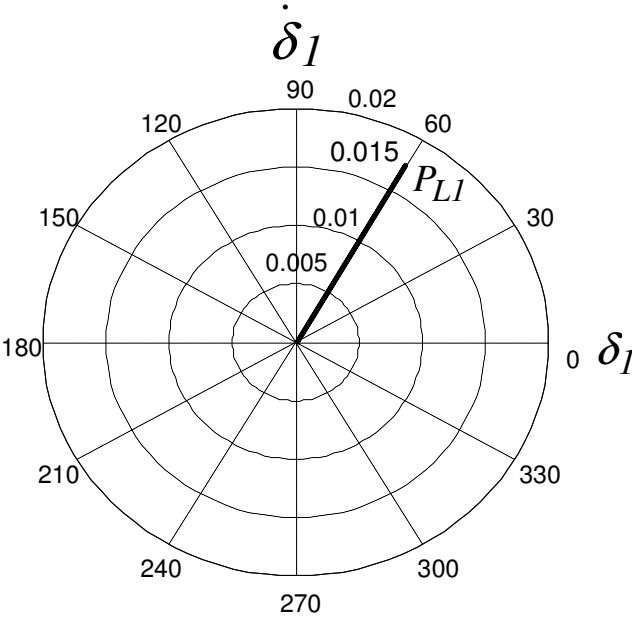


Figure 4.7: The plot of the contribution of the load  $L_I$  to damping at  $f = 1.4 \text{ Hz}$  for the test power system

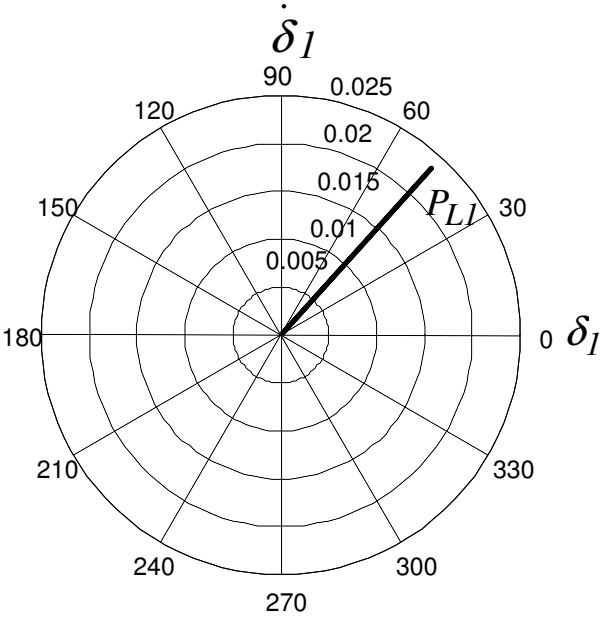


Figure 4.8: The plot of the contribution of the load  $L_I$  to damping at  $f = 2.1 \text{ Hz}$  for the test power system

Since the identified dynamic load parameters shown in Table 4.2 are very close to the actual value, the estimated value of the load contribution in Table 4.3 are also very close to the actual values. For this reason, the actual value contributions are not shown in Table 4.3. Figures 4.7 and 4.8 represent graphically the contribution of load  $L_1$  to damping at  $f = 1.4 \text{ Hz}$  and  $f = 2.1 \text{ Hz}$ .

The results of the simulation show:

- The three loads in both resonant frequencies have a positive contribution to damping and their presence in the test power system improve the damping.
- At any of the two frequencies, the load  $L_1$  makes the greatest contribution and the load  $L_2$  has the smallest contribution to damping.
- For the load  $L_3$ , the contribution at  $f = 1.4 \text{ Hz}$  is greater than the contribution at  $f = 2.1 \text{ Hz}$ .

## 4.8 Results of ESL Method on Real Data <sup>1</sup>

This part is devoted to analysis of the data measured on the interconnected Australian network. The data was used in Section 3.5.2 to find the eigenvalues and the mode shape of the Australian electricity network. As explained in Section 3.5.2, the real data consists of voltage magnitude and angle of the four major load centers: Brisbane, Sydney, Adelaide and Melbourne. In addition to this, the magnitude and angle of the current of one feeder from a substation located in Brisbane were measured. The

---

1- The real data was provided by Powerlink Queensland.

measurement in Brisbane was made on a feeder supplying a small portion of the Brisbane load which is largely residential and it is referred to in this section as the Brisbane feeder load. The aim is to determine to what extent this load contributes to damping or from a sensitivity analysis context, what is the sensitivity of the eigenvalues of the power system with respect to the Brisbane feeder load. The duration of the data was one hour with a sampling frequency of  $5 \text{ Hz}$ . The power system resonant frequencies are found using multi-site curve fitting to the *FFT* of autocorrelations of the COI referenced voltage angles of the four major load centers which are shown in Table 3.8. In the next step, the load model of the feeder from Brisbane is identified. The load model is represented by a transfer function from the rate change of the Brisbane bus voltage angle ( $\dot{\delta}$ ) to the  $P_L$  of the substation. Therefore, according to Equation (4.28) the identified load model,  $H_L$ , is obtained from

$$H_L(\omega) = \frac{\Im \left[ C_{\dot{\delta}_B P_L}(\tau) \right]}{\Im \left[ R_{\dot{\delta}_B \dot{\delta}_B}(\tau) \right]} \quad (4.64)$$

where  $C_{\dot{\delta}_B P_L}(\tau)$  is the cross-correlation of the rate of Brisbane bus

voltage angle changes and  $P$  of the feeder, and  $R_{\dot{\delta}_B \dot{\delta}_B}(\tau)$  is the

autocorrelation of the rate of Brisbane bus voltage angle changes. Using Equation (4.64) and fitting a model gives the Brisbane feeder load transfer function in the Laplace domain as

$$\mathbf{H}_L(s) = \frac{0.001 s^3 + 0.0066 s^2 + 0.0092 s + 0.0374}{s^6 + 6.3535 s^5 + 207.9877 s^4 + 1291.3000 s^3 + 222.80 s^2 + 1888.4 s + 6388.0} \quad (4.65)$$

By evaluating Equation (4.65) at the identified resonant frequencies, the  $V$  vector in Equation (4.10) can be formed.

According to (4.17) the sensitivity is determined using the right and left modal matrices. The value of the identified transfer function between the voltage angle of Brisbane and the other load centers bus voltage angle, at the identified resonant frequencies are utilized to form the right modal matrix. Using real data, it is difficult to find the single common mode,  $\lambda_c$ , because the presence of governors and dynamic load response creates a higher order model. However, a simple first order model can be fitted and fortunately the accuracy of the oscillatory mode response is not dependent on accuracy of the common mode fit.

By taking the inverse of the right modal matrix, the left modal matrix is specified. Finally, the sensitivity of the power system resonant frequencies with respect to the load of the Brisbane feeder are determined according to Equation (4.17) by using the results of the previous steps. The values of the sensitivity of the eigenvalues are depicted in Table 4.4. As is shown in the table, the sensitivity of the load decreases the damping of mode 2, but causes an increase in the damping of mode 1 and 3. For mode 2 in particular, the entire contribution of the load is to change the damping rather than the frequency of this mode.

Table 4.4: The sensitivity of the eigenvalues of the real data with respect to the Brisbane feeder load

Resonant Frequency	The value of the sensitivity
$f = 0.299 \text{ Hz}$	$-0.0011 + j0.0039$
$f = 0.439 \text{ Hz}$	$0.0021 + j0.0005$
$f = 0.740 \text{ Hz}$	$-0.0012 + j0.0007$

The value of the Brisbane feeder load contribution to damping is shown in Table 4.5. Also, the Brisbane feeder load contribution to damping at the three resonant frequencies graphically is shown in Figures 4.9 to 4.11. As can be seen from Table 4.5 and Figures 4.9 to 4.11, since this load is very small compared to the total load in the network, the contribution of this load to damping for all of the modes is very small. Also the Brisbane feeder load has a positive contribution at the first and third modes, but has a negative contribution at the second mode. Also the contribution of the Brisbane feeder load to damping at the first mode is smaller than that to the other modes.

Table 4.5: The value of load contribution to damping at the three identified resonant frequencies

	Brisbane Feeder Load Contribution to Damping (Neper per second)
$f = 0.299 \text{ Hz}$	$4.11e-6$
$f = 0.439 \text{ Hz}$	$-5.46e-6$
$f = 0.740 \text{ Hz}$	$5.73e-6$

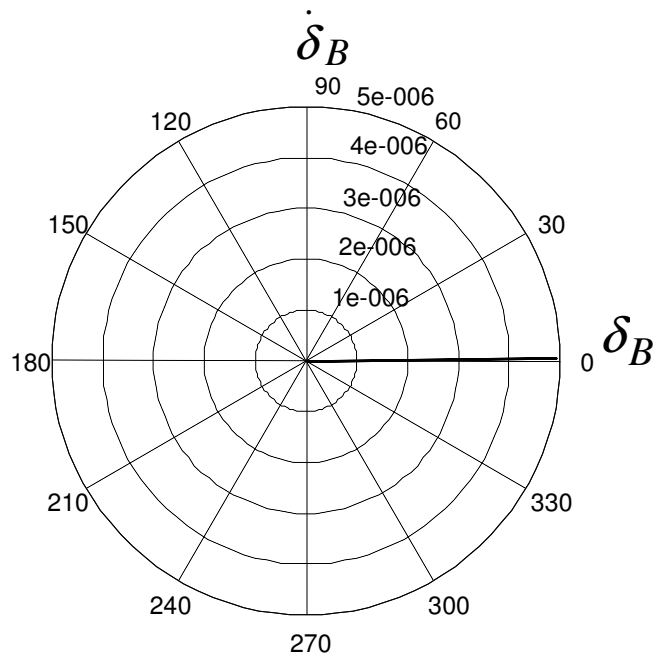


Figure 4.9: The Brisbane feeder load contribution to damping at

$$f = 0.299 \text{ Hz}$$

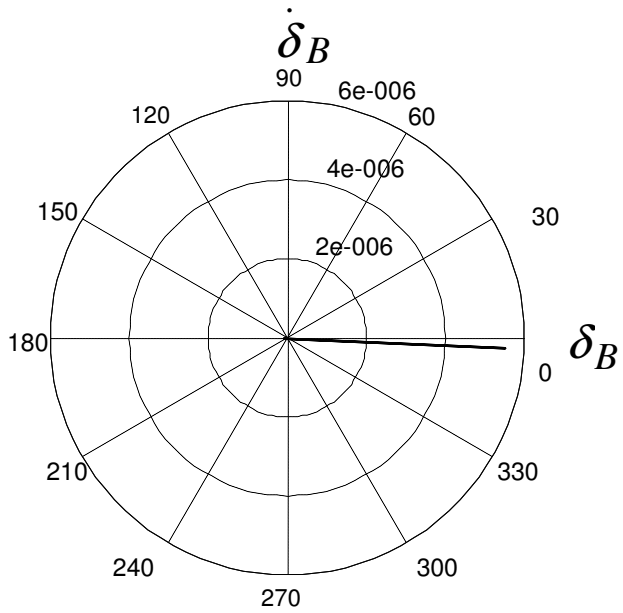


Figure 4.10: The Brisbane feeder load contribution to damping

$$\text{at } f = 0.439 \text{ Hz}$$

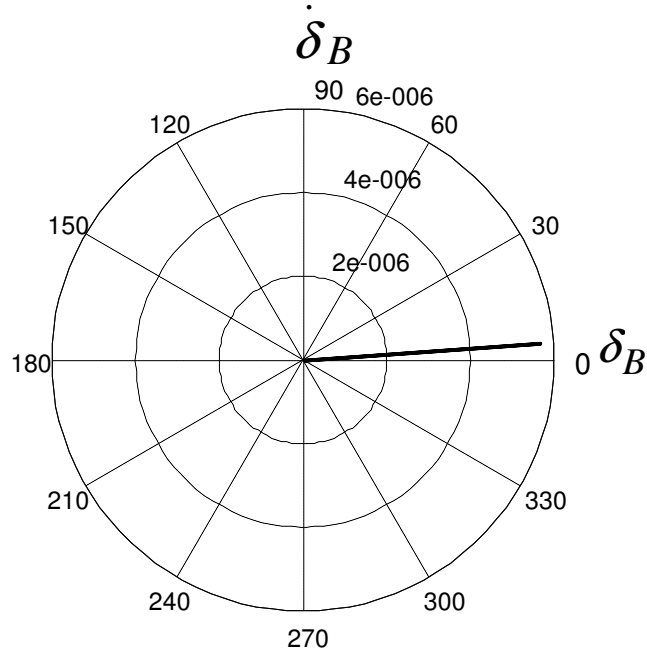


Figure 4.11: The Brisbane feeder load contribution to damping

at  $f = 0.740 \text{ Hz}$

## 4.9 Summary

In this chapter, the eigenvalue sensitivity to load (ESL) method is developed to identify the load contribution to damping of a multi-machine power system. In the method, the resonant frequencies of a test power system are first identified. Then the transfer function representing the relationship between the rate of bus voltage angle changes and the load power is then determined using cross-correlation and autocorrelation functions. Evaluating the identified transfer function at resonant frequencies of the IAO yields the right eigenvectors. Finally, by using the right and left

eigenvectors and using load models, the sensitivity of the eigenvalues with respect to the load are obtained.

The ESL method is simulated on a test power system consisting of three buses and nine lines. In the test system, three dynamic loads are considered and each load is connected to the generator terminals. In the simulation after identifying the loads model, the sensitivity of the power system eigenvalues with respect to the loads are determined. Also, the contribution of the load to damping of the test system is quantified. The results of the sensitivity analysis and quantification of the load contribution to damping show a good agreement with the actual values.

To illustrate the applicability of the method, the contribution of a Brisbane feeder load in Australia to damping of the major modes of the Australian electricity network is determined. In this method, the model of one feeder of a substation in Brisbane namely the Brisbane feeder load, is identified and then sensitivity of the eigenvalues of IAO of the Australian power system with the Brisbane feeder load is computed. Finally, the contribution of the Brisbane load to damping at the three identified resonant frequencies is quantified and it is shown that the Brisbane load has a positive contribution for the first and third mode and has a negative contribution for the second mode.

In Chapter 5, the effect of SVC on active power is investigated and it is demonstrated analytically that the SVC is capable of improving load contribution to damping.



## **Chapter 5: SVC Contribution to Damping**

### **5.1 Introduction**

As explained in Section 2.9, the static var compensators (SVC) were first used in power systems to maintain the voltage, but it was found that they can also be used to improve the damping of the inter-area oscillations (IAO) of the power systems. The model of the SVC was described in section 2.8. There are many kinds of SVC implementations. However, for analysis of this chapter, they are treated as variable capacitors that could have positive or negative values.

In Chapter 4, after identifying the load model, the contribution to damping was investigated and the sensitivity of power system eigenvalues with respect to load was determined. Also, the contribution of load to the damping of the IAO was quantified. The aim of this chapter is to determine the effect of SVC on load contribution to damping, i.e. the effect SVC reactive power has on the load's active power. This effect is investigated in the context of closed loop feedback. A procedure for redesigning an SVC controller is presented to achieve maximum contribution of load to damping

i.e. the load contribution should be in phase with speed changes of the synchronous generator at each resonant frequency.

In this chapter, firstly the main aspects of SVC contribution to damping are explained. Next, a method is developed to redesign the SVC controller on the basis of complete testing. An algorithm then is presented to redesign the SVC controller to achieve maximum load contribution to damping based on complete testing. A test system is also employed to simulate the algorithm and demonstrate the change of contribution of an induction motor to damping, due to the presence of the SVC.

In the next section, the redesigning of SVC controller based on normal operation is given by analysing the effect of reactive power of SVC on the measured active power of the load. A method is developed to find the transfer function between the reactive power of the SVC and the measured power on the basis of the cross-correlation and autocorrelation functions. Finally the algorithm is applied to the real data of the Australian electricity network to determine the effect of SVC at the Blackwall substation on measured power flow past this substation.

## **5.2 The Basic Concepts of SVC Contribution to Damping**

The basic concepts regarding the influence of SVC on damping are explained by considering a simple case including an induction motor in parallel to an SVC. At first, consider the output of the SVC is zero. If the active power used by the induction motor and the rate of voltage angle

changes are denoted by  $P_L$  and  $\dot{\delta}$ , respectively, then as explained in Section 4.2, due to the inertia of the induction motor, there is a phase shift between  $P_L$  and  $\dot{\delta}$  as shown in Figure 5.1.a. Notice from this figure, that, the load partly contributes to damping. Knowing this phase shift between  $P_L$  and  $\dot{\delta}$  along with the given values of the controller parameters, help the designer of the SVC controller to redesign the parameters of the SVC controller to have maximum load contribution to damping, i.e. to achieve maximum alignment of  $P_L$  with  $\dot{\delta}$  as shown in Figure 5.1.b [11].

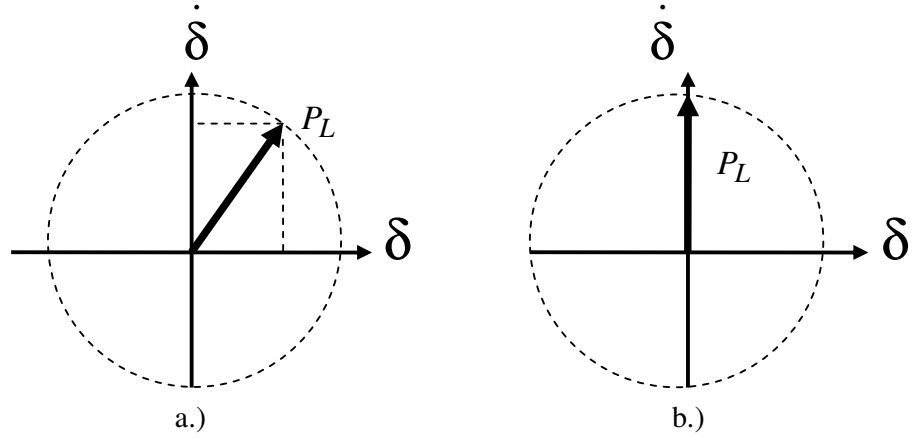


Figure 5.1: The effect of load to damping, a.) SVC with given controller parameters, b.) SVC with the updated controller parameters

Figure 5.2 shows the block diagram model of the power system including both load dynamic and SVC feedback. The feedforward transfer function  $\mathbf{G}(s)$ , represents the power system dynamic response. The inner feedback in this figure shows the effect of load dynamics on the measured

power  $P$ , and the outer feedback demonstrates the effect of SVC feedback on  $P$ . The label  $H_{SVC}(s)$  represents the transfer function of the SVC with output  $Q$ . The effect of reactive power,  $Q$ , on the measured load power is denoted by  $T(s)$ . As mentioned in Chapter 4, the transfer function  $H_L(s)$  expresses the effect of the rate of voltage angle changes on the measured load power.

In this figure  $w$  and  $z_I$  are local and remote load perturbation and  $d_2$  is direct white noise perturbation. The SVC is fed by two inputs:  $\delta$  and  $z_2$ . In small signal analysis,  $V_{ref}$ , which is one input of SVC block diagram, is omitted. In this system  $w$ ,  $z_I$  and  $z_2$  are uncorrelated white noise sources.

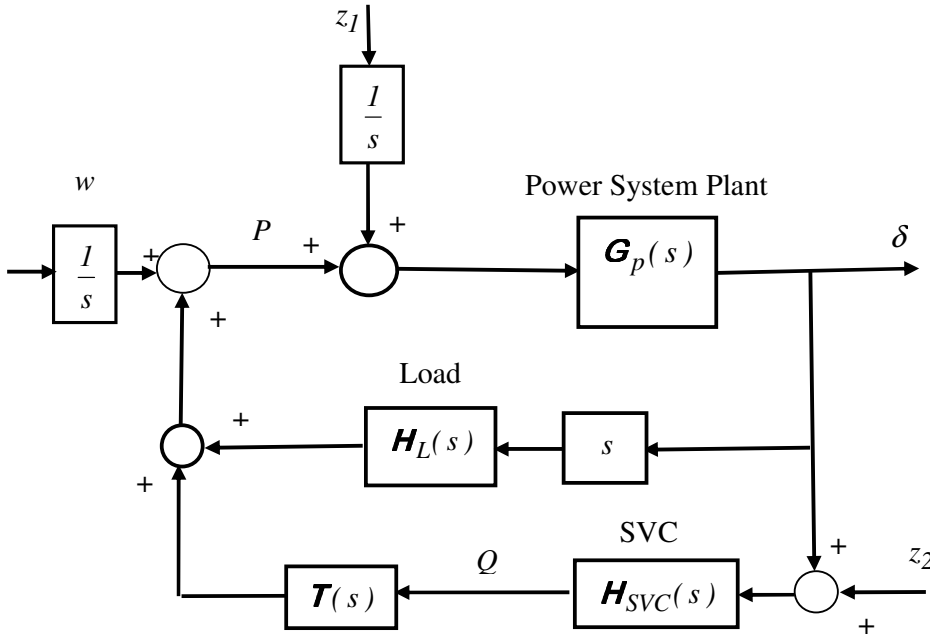


Figure 5.2: Power system block diagram including the effect of reactive power of SVC on the measured power

Two different methods are considered for redesigning the SVC controllers in this chapter. The first method explained in Section 5.3, is based on mainly “On” and “Off” situations of an SVC. In this method the load contribution to damping when there is no SVC, is compared to the case when there is SVC. These two cases are computed to find the new design for an SVC controller. Knowing the SVC contribution to damping with the existing setting leads to a method for redesigning the SVC controller to achieve maximum SVC contribution to damping. This method has some drawbacks, for example it is a costly test to arrange safely, and sometimes it is impractical to put the SVC out of service for testing purposes.

On the other hand, for the redesigning method based on normal operation, which is discussed in Sections 5.6 and 5.7, firstly the effect of reactive power of the SVC on the measured active power is identified using the normal operation data, then the desired phase shift of the SVC to have maximum damping is determined.

## **5.3 SVC Controller Redesign Based on Complete Testing**

### **5.3.1 The Essence of Redesign of SVC controller**

As described in Section 5.2, redesigning the parameters of the SVC controller can change the contribution of the induction motor load to damping. In fact, the variations in active power of the induction motor, change the power flow of the generators, and this influences damping of the synchronous generator [9]. To illustrate the method of redesigning of the

SVC controller based on complete testing, consider Figure 5.3. This shows a single machine connected to an infinite bus via a transmission line, and an SVC and an induction motor are connected to the same bus. In this figure  $SG$  and  $IM$  represent synchronous generator and induction machine, respectively. Also  $Z_a$  and  $Z_b$  characterize the line impedances. The equivalent impedance of the induction motor and SVC is denoted by  $Z_c$ . The change in power flow of the generator caused by induction motor changes is labelled by  $P_I$ , and  $P_L$  is the electric power to the induction motor transferred to the rotor. Consider the case where there is no SVC, in that case if there is a step change of the voltage at the induction motor terminals, there will be some changes of power in the motor and as a result the motor slip changes. During this step, there is a mismatch between electrical and mechanical power of the induction motor which restores the slip and consequently the load recovers to the new steady state speed determined by the inertia of motor plus shaft load. This indicates the system response to step voltage change and it creates a phase shift response between electric power of the induction motor  $P_L$  and the rate of changes of voltage bus angle at bus 3. This also implies a phase shift between shift between the rate of generator bus voltage angle,  $\dot{\delta}$  (or  $j\omega\delta$ ), and the power flow of the generator,  $P_I$ , caused by the induction motor changes. This phase shift at the resonant frequency is shown in Figure 5.4.a. As can be seen from Figure 5.4.a, when there is no SVC,  $P_I$  has a component in direction of  $j\omega\delta$ , therefore it participates in damping. However, when there

is an SVC with a particular feedback controller, the contribution of  $P_l$  to the system damping can be increased as shown in Figure 5.4.b.

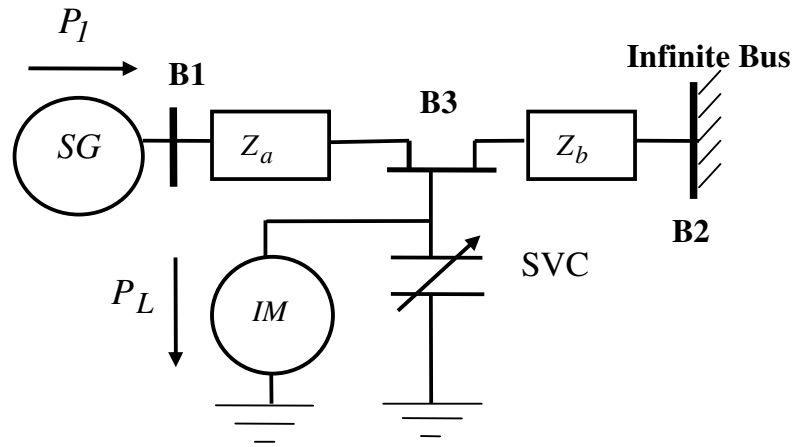


Figure 5.3: The diagram of a single machine connected to the infinite bus with SVC and induction motor

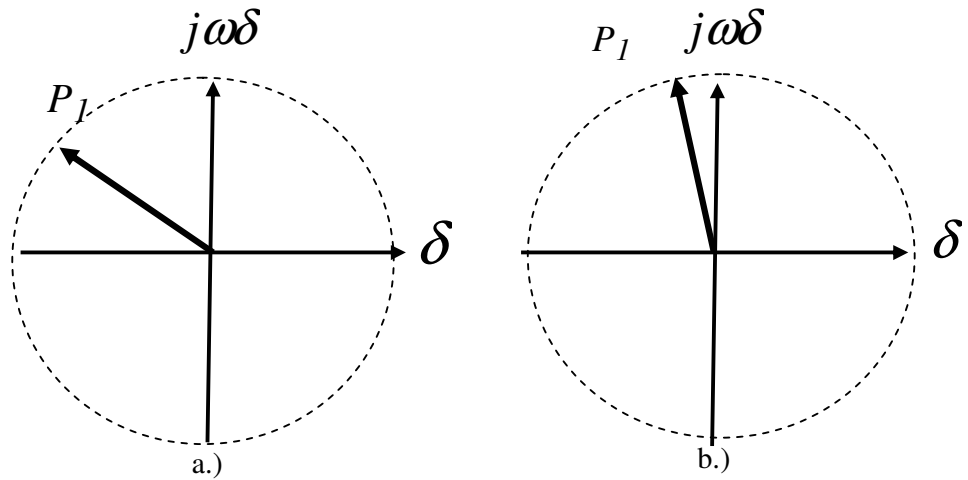


Figure 5.4: The phase shift diagram of contribution of  $P_l$  to damping, a.) without SVC, b.) with SVC

### 5.3.2 Theory of Redesign of SVC controller

In the following, the equations for SVC redesign based on complete testing are derived.

Regarding Figure 5.3, The mechanical equation for the synchronous generator and the induction motor in small signal analysis can be written as

$$J_g \ddot{\delta}_g = P_{mg} - P_l - D_g \dot{\delta}_g \quad p.u. \quad (5.1)$$

$$J_m \ddot{\delta}_m = P_{mm} - P_{ind} - D_m \omega_r \quad p.u. \quad (5.2)$$

where:

$\omega_r$  = mechanical speed of the induction motor

$J_m$  and  $J_g$  = inertia of the synchronous generator and the induction motor,

respectively

$\delta$  = the generator bus voltage angle

$P_{mg}$  and  $P_{mm}$  = the synchronous generator mechanical power and the

induction motor mechanical power, respectively

$D_g$  and  $D_m$  = damping coefficient of the synchronous generator and

induction motor respectively

$P_{ind}$  = input electrical power of the induction motor in the air gap

transferred to the rotor

Equation (5.2) represents the induction motor by steady state equivalent circuit. This assumes that the electrical transients are much faster than the mechanical transients in the induction motor [1, 64]. Assuming that the SVC is controlled as [97,105-106]

$$Y_{SVC} = \bar{k}_1 \delta_3 + k_2 \dot{\delta}_3 + k_3 (V_3 - V_{3ref}) \quad (5.3)$$

At a particular resonant frequency  $\omega_k$  we have

$$\dot{\delta}_3 = j\omega_k \delta_3 \quad (5.4)$$

where  $\dot{\delta}_3$  is the rate of voltage angle changes of Bus 3 in Figure 5.3. Since we are dealing with small signals and steady state, any feedback of voltage in the third term of Equation (5.3) can be represented as a component in the first term in Equation (5.3). In fact, the voltage changes in Bus 3 are in phase with the voltage angle at bus 3 rather than rate of change of voltage angle at this bus. In this regard, and by using Equation (5.4), Equation (5.3) becomes

$$Y_{SVC} = k_1 \delta_3 + k_2 j\omega \delta_3 \quad (5.5)$$

which can be represented as

$$Y_{SVC} = K_{SVC} \angle \theta \omega_k \delta_3 \quad (5.6)$$

It should be noted that  $K_{SVC}$  in Equation (5.6) is limited and it is related to the maximum size of SVC. The electric power of the induction motor  $P_{ind}$  in Equation (5.1) is calculated from

$$P_{ind} = R_r \left| \frac{V_3}{Z_{in}} \right|^2 \frac{1-S}{S} \quad (5.7)$$

where  $Z_{in}$ ,  $R_r$  and  $S$  are input impedance, rotor resistance, and slip of the induction motor, respectively. The slip of the induction motor is computed from

$$S = \frac{\dot{\delta}_{3-\omega_r}}{\dot{\delta}_3} \quad (5.8)$$

The expression for  $P_I$  in Equation (5.1) can be found by using star-delta transformation to give the circuit in Figure 5.5.

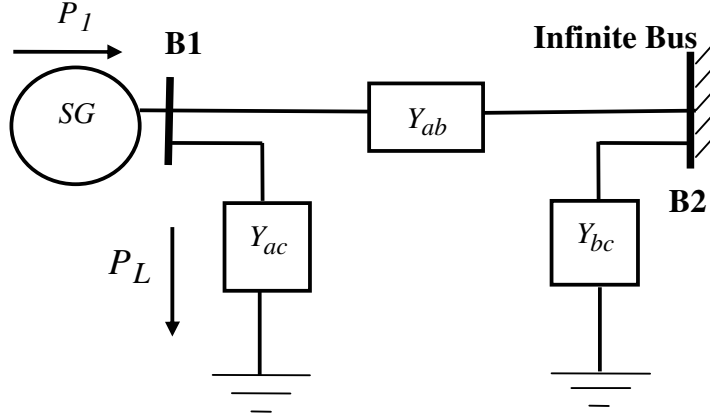


Figure 5.5: The delta equivalent of Figure 5.3

Therefore according to Figure 5.5, the expression for  $P_I$  can be written as

$$P_I = |V_I|^2 G_{ca} + |V_I|^2 G_{ab} - |V_I||V_2|G_{ab} \cos(\delta) - |V_I||V_2|B_{ab} \sin(\delta) \quad (5.9)$$

where  $G_{ab}$  and  $B_{ab}$  are conductance and susceptance of  $Y_{ab}$ , respectively.

Also  $G_{ca}$  is the conductance of  $Y_{ca}$ .

Thus the differential Equations (5.1) and (5.2), with regard to the relation given for SVC in Equation (5.3), characterize the system.

In the next section, the algorithm of redesign of the SVC controller based on complete testing is discussed. Following simulation of the system response to transients, the transfer function between each of three elements i.e.  $P_I$ ,  $P_{ind}$  and  $Y_{SVC}$ , and  $\delta$  are determined using the cross-correlation and autocorrelation functions. The phase shifts between each of the elements

and  $\delta$  will be determined by evaluating the corresponding transfer function at the resonant frequency of the IAO. With this information, the phase shift diagram is plotted to assess the current performance of the SVC in damping and what decision should be made in control design of the SVC, to have maximum contribution to damping.

## 5.4 Algorithm of the SVC Controller Redesign Based on Complete Testing

The suggested method consists of the following steps:

### Step 1: Power system resonant frequency identification

The resonant frequencies of the IAO of the power system are identified using the correlation based method explained in Chapter 3.

### Step 2: Transfer function determination

Using the method explained in Chapter 4, the transfer function between each of the three elements, i.e. SVC,  $P_{ind}$ ,  $P_I$ , and  $\delta$  are identified from the following equations

$$H_{\delta SVC}(\omega) = \frac{\Im[R_{\delta SVC}(\tau)]}{\Im[R_{\delta \delta}(\tau)]} \quad (5.10)$$

$$H_{\delta P_{ind}}(\omega) = \frac{\Im[R_{\delta P_{ind}}(\tau)]}{\Im[R_{\delta \delta}(\tau)]} \quad (5.11)$$

$$H_{\delta P_I}(\omega) = \frac{\Im[R_{\delta P_I}(\tau)]}{\Im[R_{\delta\delta}(\tau)]} \quad (5.12)$$

where

$H_{\delta SVC}(\omega)$  = the transfer function between  $\delta$  and SVC

$H_{\delta P_{ind}}(\omega)$  = the transfer function between  $\delta$  and  $P_{ind}$

$H_{\delta P_I}(\omega)$  = the transfers function between  $\delta$  and  $P_I$

### Step 3: Determining the Phase Shift Diagram:

Each of the three identified transfer functions is evaluated at the resonant frequency  $\omega_{res}$

$$V_{SVC} = H_{\delta SVC}(\omega) \Big|_{\omega=\omega_{res}} \quad (5.13)$$

$$V_{P_I} = H_{\delta P_I}(\omega) \Big|_{\omega=\omega_{res}} \quad (5.14)$$

$$V_{P_{ind}} = H_{\delta P_{ind}}(\omega) \Big|_{\omega=\omega_{res}} \quad (5.15)$$

The results can be used to plot the phase shift diagram.

### Step 4: Extracting the information for redesigning the SVC controller

The magnitudes and phases obtained in the previous step are used to plot the phase shift diagram. Therefore, the damping contribution of the induction motor in the presence of the SVC is determined [10]. The information obtained from this phase shift diagram is used to redesign the SVC

controller to get maximum load contribution to damping. If the analysis results in following vectors for SVC and  $P_l$

$$V_{SVC,\delta} = K'_{SVC} \angle \theta_{SVC} \delta \quad (5.16)$$

$$V_{P_l\delta} = K_{P_l} \angle \theta_{P_l} \delta \quad (5.17)$$

then, the compensated angle  $\theta_c$  for  $V_{P_l\delta}$  to have maximum contribution of  $P_l$  to damping can be found from

$$\theta_c = 90 - \theta_{P_l} \quad (5.18)$$

Therefore, the vector  $V_{SVC,\delta}$  should rotate by  $\theta_c$  degrees as

$$V_{SVC,\delta} = K'_{SVC} \angle (\theta_{SVC} + \theta_c) \delta \quad (5.19)$$

With regard to the relationship between  $\delta$  and  $\delta_3$ , the new setting for SVC can be found using Equations (5.5) and (5.19), and it can be implemented using lag-lead compensators.

## 5.5 Simulation Results for Redesign SVC Controller Based on Complete Testing

In this section, a test power system is considered to assess the performance of an SVC on the load contribution to damping. As explained before, due to induction motor changes, there are some changes in real power flow of the generator,  $P_l$ . In this regard, the algorithm of the SVC controller redesign on the basis on complete testing is simulated on the test power system depicted in Figure 5.3. As shown in Equation (5.5) the variable parameters of the SVC are  $k_1$  and  $k_2$ . In this simulation, the effect of coefficients  $k_1$  and

$k_2$  of the SVC controller on contribution of  $P_I$  to damping is examined. The specifications of the elements of the test system are given in Appendix B.

In the simulation, the power system is given the specified run from initial conditions corresponding to steady state. The state variables are the generator rotor angle changes ( $\delta$ ), the rate of generator rotor angle changes ( $\dot{\delta}$ ), and the speed of the rotor of the induction motor,  $\omega_r$ , the model incorporates the dynamic relation for the SVC as in Equation (5.5).

In the first step of the simulation, the resonant frequencies of IAO of the test system are identified, using the CBMSI method explained in Chapter 3. The identified resonant frequency of the test system is  $0.518 \text{ Hz}$ . The magnitude plot of the *FFT* of autocorrelation of the changes of generator bus voltage angle,  $\delta$ , is shown in Figure (5.6).

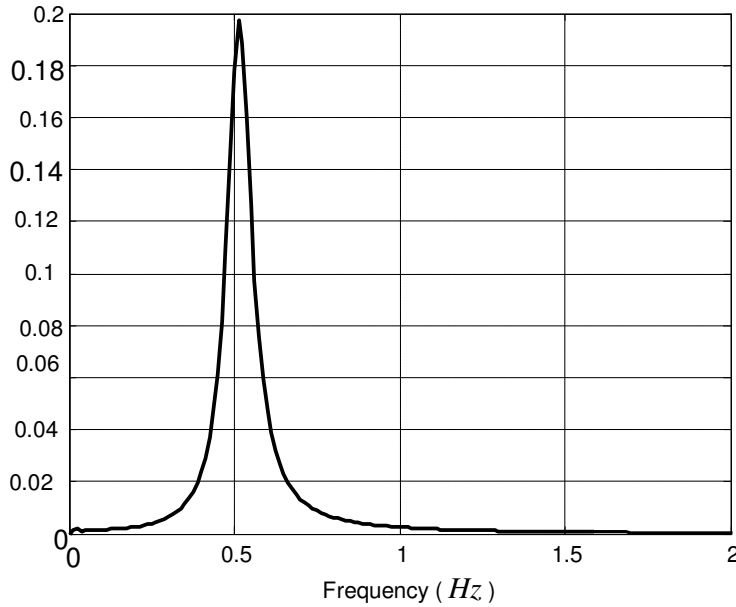


Figure 5.6: The magnitude of the *FFT* of autocorrelation of the generator bus voltage angle changes for the test power system

In the next step, the transfer function from  $\delta$  to each of the three elements,  $P_{ind}$ , SVC and  $P_I$  are identified on the basis of autocorrelation and cross-correlation functions. For instance, the magnitude and angle of the identified transfer function from  $\delta$  and SVC is depicted in Figure 5.7 at the identified resonant frequency.

According to the findings of the previous step, the phase shift angles between  $\delta$  and each of the three elements,  $P_{ind}$ ,  $Q$  of the SVC and  $P_I$ , are computed by evaluating the corresponding transfer function at the resonant frequency  $f = 0.518$ . Figure 5.8 shows the phase shift diagram for the power system.

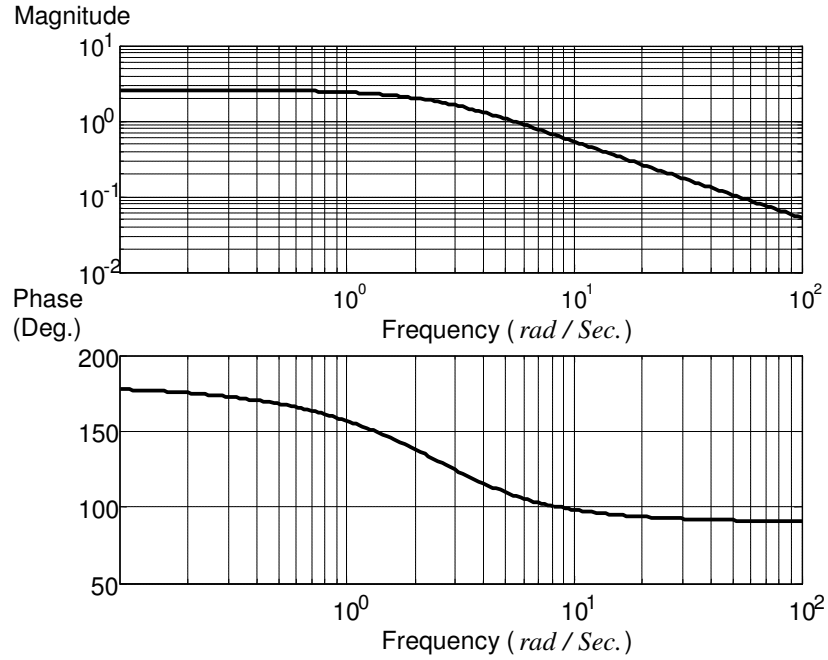


Figure 5.7: The magnitude and phase of identified transfer function between  $Q$  of the SVC and  $\delta$  for the test power system

To demonstrate the performance of the algorithm, the system is first evaluated at  $k_1 = 0$  and  $k_2 = 0.3$  and this case is compared with the case that both gains  $k_1$  and  $k_2$  are zero. The program is run for the two different cases. Then, the corresponding vectors are defined as

$$\Delta VP_{ind} = VP_{ind}|_{k_2=0.3, k_1=0} - VP_{ind}|_{k_2=0, k_1=0} \quad (5.20)$$

$$\Delta VSVC = VSVC|_{k_2=0.3, k_1=0} - VSVC|_{k_2=0, k_1=0} \quad (5.21)$$

$$\Delta VP_I = VP_I|_{k_2=0.3, k_1=0} - VP_I|_{k_2=0, k_1=0} \quad (5.22)$$

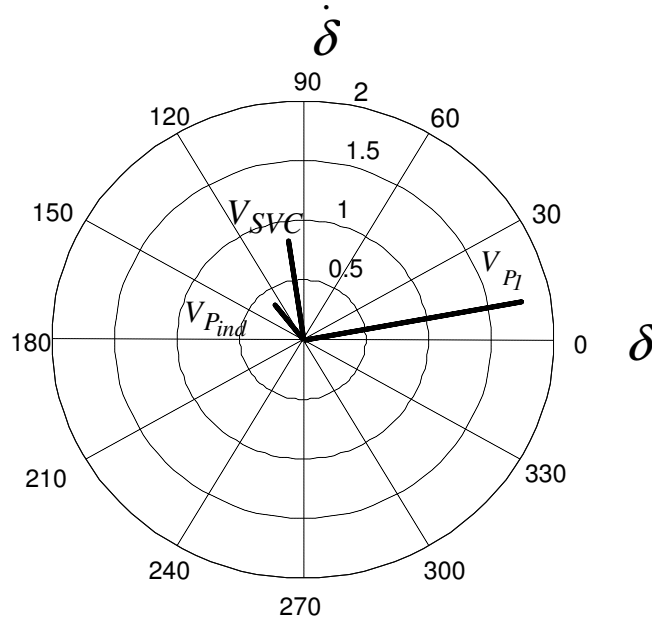


Figure 5.8: The phase shift fit diagram of the test power system (for SVC:

$$k_1 = 0 \text{ and } k_2 = 0.3)$$

The values of the vector changes are shown in Table 5.1. With respect to Table 5.1 the vector diagram is depicted in Figure 5.9. As can be seen from Table 5.1 and Figure 5.9, when  $k_1 = 0$ , increasing the value of  $k_2$  in the

SVC, increases  $P_I$ 's contribution. In fact,  $\Delta VP_I$  indicates the change in generator power flow due to the variation of  $P_{ind}$  when the SVC is present.

As shown in Figure 5.9,  $\Delta VP_I$  is not fully aligned with  $\dot{\delta}$  and has an angle of  $\theta$  with respect to  $\dot{\delta}$ . In order to reach the best contribution to damping, the design of SVC controller should be changed.

Table 5.1: The change in the vectors when  $k_2$  increases for the test power system

	$\Delta VP_{ind}$	$\Delta VSVC$	$\Delta VP_I$
<i>Magnitude</i>	0.2075	0.8375	0.1212
<i>Phase(Deg.)</i>	-83.4561	97.8635	98.4445

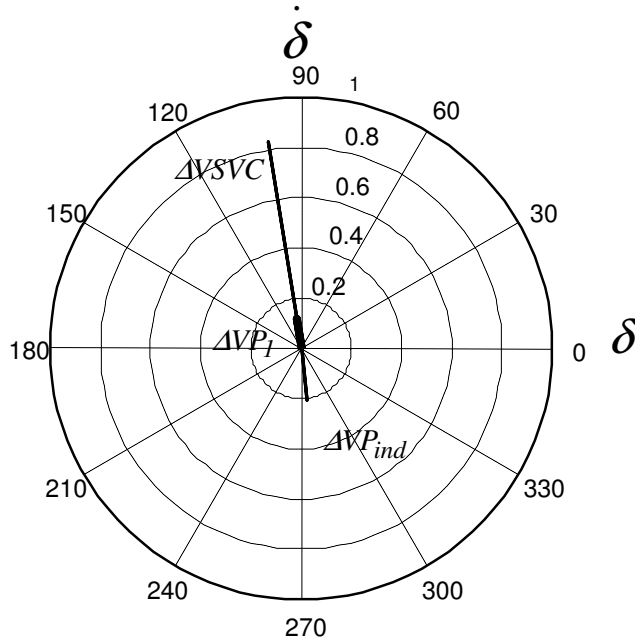


Figure 5.9: The phase shift of the change in the vectors when  $k_2$  increases from 0 to 0.3, meanwhile  $k_I = 0$ , for the test power system

To achieve maximum contribution to damping, the vector  $\Delta VP_I$  in Figure 5.9 should be rotated clockwise so that the vector  $\Delta VP_I$  is fully aligned with the  $j\omega\delta$  axis by  $\theta$  degrees. In the other words, we move  $K_{SVC}\angle 90$  to  $K_{SVC}\angle(90-\theta)$ , which can be implemented as

$$k_1 = K_{SVC} * \sin(\theta) \quad \text{and} \quad k_2 = K_{SVC} * \cos(\theta) \quad (5.23)$$

With the new values of  $k_1$  and  $k_2$ , SVC maximises the  $P_I$ 's contribution to damping. In fact, it compensates the phase shift created by the induction motor.

## 5.6 SVC controller Redesign Based on Normal Operation (Simplified Case)

In the previous section, the redesign of the SVC controller was described based on complete testing. In this section, the effect of the reactive power of the SVC on active power is investigated in normal operation. To study this effect, consider the simplified version of Figure 5.2 which is shown in Figure 5.10. In this figure, the inner feedback is included in  $G_P^*(s)$ .

The ultimate aim is to have all the changes of  $P$  in phase with  $\dot{\delta}$  to get maximum contribution of  $P$  to damping. In order to achieve this, the transfer function  $T(\omega)$  should be known, then, the SVC controller can be redesigned to achieve this aim.

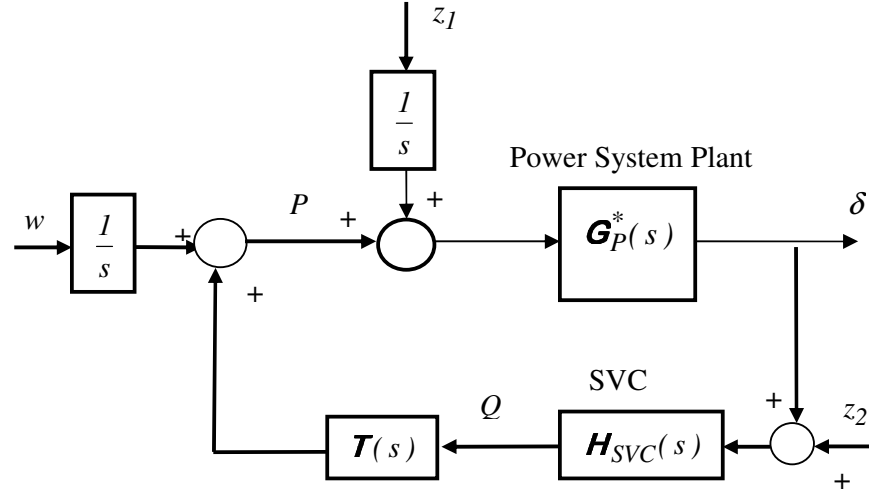


Figure 5.10: Power system block diagram representing the effect of reactive power of SVC on the load measured power

For the system shown in Figure 5.10, the transfer function between  $Q$  and  $P$  can be found from

$$H_{QP}(\omega) = \frac{\Im[C_{QP}(\tau)]}{\Im[R_{QQ}(\tau)]} \quad (5.24)$$

where

$C_{QP}(\tau)$  = the cross-correlation of  $Q$  and  $P$

$R_{QQ}(\tau)$  = the autocorrelation of  $P$

$\tau$  = time lag

The response of  $Q$  and  $P$  to the system inputs in Figure 5.10 can be found by using the superposition law. In this regard, the response of  $Q$  can be

found by adding the  $Q$  responses, when each input is applied separately.

The same procedure is performed to find the response of  $P$ .

$$Q = \int_{-\infty}^{\infty} h_{11}(\xi_{11}) w(t - \xi_{11}) d\xi_{11} + \int_{-\infty}^{\infty} h_{12}(\xi_{12}) z_1(t - \xi_{12}) d\xi_{12} \\ + \int_{-\infty}^{\infty} h_{13}(\xi_{13}) z_2(t - \xi_{13}) d\xi_{13} \quad (5.25)$$

$$P = \int_{-\infty}^{\infty} h_{21}(\xi_{21}) w(t - \xi_{21}) d\xi_{21} + \int_{-\infty}^{\infty} h_{22}(\xi_{22}) z_1(t - \xi_{22}) d\xi_{22} \\ + \int_{-\infty}^{\infty} h_{23}(\xi_{23}) z_2(t - \xi_{23}) d\xi_{23} \quad (5.26)$$

where

$h_{11}$  = the impulse response of the system when only  $w$  is present and  $Q$  is output

$h_{21}$  = the impulse response of the system when only  $w$  is present and  $P$  is output

$h_{12}$  = the impulse response of the system when only  $z_1$  is present and  $Q$  is output

$h_{22}$  = the impulse response of the system when only  $z_1$  is present and  $P$  is output

$h_{13}$  = the impulse response of the system when only  $z_2$  is present and  $Q$  is output

$h_{23}$  = the impulse response of the system when only  $z_2$  is present and  $P$  is output

Assuming both  $P$  and  $Q$  are wide-sense stationary, then (see Appendix A)

$$C_{QP}(\tau) = E[Q(t)P(t+\tau)] \quad (5.27)$$

$$R_{QQ}(\tau) = E[Q(t)Q(t+\tau)] \quad (5.28)$$

where  $E$  is the expected value.

Substituting (5.25) and (5.26) into (5.27) and (5.28), respectively, gives

$$C_{QP}(\tau) = E \left\{ \left[ \int_{-\infty}^{\infty} h_{11}(\xi_{11}) w(t - \xi_{11}) d\xi_{11} + \int_{-\infty}^{\infty} h_{12}(\xi_{12}) z_1(t - \xi_{12}) d\xi_{12} \right. \right. \\ \left. \left. + \int_{-\infty}^{\infty} h_{13}(\xi_{13}) z_2(t - \xi_{13}) d\xi_{13} \right] \left[ \int_{-\infty}^{\infty} h_{21}(\xi_{21}) w(t + \tau - \xi_{21}) d\xi_{21} \right. \right. \\ \left. \left. + \int_{-\infty}^{\infty} h_{22}(\xi_{22}) z_1(t + \tau - \xi_{22}) d\xi_{22} + \int_{-\infty}^{\infty} h_{23}(\xi_{23}) z_2(t + \tau - \xi_{23}) d\xi_{23} \right] \right\} \quad (5.29)$$

$$R_{QQ}(\tau) = E \left\{ \left[ \int_{-\infty}^{\infty} h_{11}(\xi_{11}) w(t - \xi_{11}) d\xi_{11} + \int_{-\infty}^{\infty} h_{12}(\xi_{12}) z_1(t - \xi_{12}) d\xi_{12} \right. \right. \\ \left. \left. + \int_{-\infty}^{\infty} h_{13}(\xi_{13}) z_2(t - \xi_{13}) d\xi_{13} \right] \left[ \int_{-\infty}^{\infty} h_{11}(\xi_{11}) w(t + \tau - \xi_{11}) d\xi_{11} \right. \right. \\ \left. \left. + \int_{-\infty}^{\infty} h_{12}(\xi_{12}) z_1(t + \tau - \xi_{12}) d\xi_{12} + \int_{-\infty}^{\infty} h_{13}(\xi_{13}) z_2(t + \tau - \xi_{13}) d\xi_{13} \right] \right\} \quad (5.30)$$

With the assumption that the expectation and integration operation are interchangeable [107], we take expected value from the internal terms of the integrals in (5.29) to yield

$$\begin{aligned}
C_{QP}(\tau) = & \int_{-\infty}^{\infty} \int_{-\infty}^{\infty} h_{11}(\xi_{11}) h_{21}(\xi_{21}) E\{w(t-\xi_{11}) w(t+\tau-\xi_{21})\} d\xi_{11} d\xi_{21} \\
& + \int_{-\infty}^{\infty} \int_{-\infty}^{\infty} h_{11}(\xi_{11}) h_{22}(\xi_{22}) E\{w(t-\xi_{11}) z_1(t+\tau-\xi_{22})\} d\xi_{11} d\xi_{22} \\
& + \int_{-\infty}^{\infty} \int_{-\infty}^{\infty} h_{11}(\xi_{11}) h_{23}(\xi_{23}) E\{w(t-\xi_{11}) z_2(t+\tau-\xi_{23})\} d\xi_{11} d\xi_{23} \\
& + \int_{-\infty}^{\infty} \int_{-\infty}^{\infty} h_{12}(\xi_{12}) h_{21}(\xi_{21}) E\{z_1(t-\xi_{12}) w(t+\tau-\xi_{21})\} d\xi_{12} d\xi_{21} \\
& + \int_{-\infty}^{\infty} \int_{-\infty}^{\infty} h_{12}(\xi_{12}) h_{22}(\xi_{22}) E\{z_1(t-\xi_{12}) z_1(t+\tau-\xi_{22})\} d\xi_{12} d\xi_{22} \\
& + \int_{-\infty}^{\infty} \int_{-\infty}^{\infty} h_{12}(\xi_{12}) h_{23}(\xi_{23}) E\{z_1(t-\xi_{12}) z_2(t+\tau-\xi_{23})\} d\xi_{12} d\xi_{23} \\
& + \int_{-\infty}^{\infty} \int_{-\infty}^{\infty} h_{13}(\xi_{13}) h_{21}(\xi_{21}) E\{z_2(t-\xi_{13}) w(t+\tau-\xi_{21})\} d\xi_{13} d\xi_{21} \\
& + \int_{-\infty}^{\infty} \int_{-\infty}^{\infty} h_{13}(\xi_{13}) h_{22}(\xi_{22}) E\{z_2(t-\xi_{13}) z_1(t+\tau-\xi_{22})\} d\xi_{13} d\xi_{22} \\
& + \int_{-\infty}^{\infty} \int_{-\infty}^{\infty} h_{13}(\xi_{13}) h_{23}(\xi_{23}) E\{z_2(t-\xi_{13}) z_2(t+\tau-\xi_{23})\} d\xi_{13} d\xi_{23}
\end{aligned} \tag{5.31}$$

Note that the impulse responses have been taken out of the expectation operators in (5.31). This is because the impulse responses are not random variables, and are treated as constants.

Since  $w$ ,  $z_1$  and  $z_2$  are uncorrelated white noise, the following equations hold for all values of time lag  $\tau$ , [24]

$$E[w(t) z_1(t+\tau)] = 0 \tag{5.32}$$

$$E[z_1(t) z_2(t+\tau)] = 0 \tag{5.33}$$

$$E[w(t) z_2(t+\tau)] = 0 \tag{5.34}$$

By using Equations (5.32)-(5.34), Equation (5.31) can be simplified as

$$\begin{aligned}
C_{QP}(\tau) = & \int_{-\infty}^{\infty} \int_{-\infty}^{\infty} h_{11}(\xi_{11}) h_{21}(\xi_{21}) R_{ww}(\tau + \xi_{11} - \xi_{21}) d\xi_{11} d\xi_{21} \\
& + \int_{-\infty}^{\infty} \int_{-\infty}^{\infty} h_{12}(\xi_{12}) h_{22}(\xi_{22}) R_{z_1 z_1}(\tau + \xi_{12} - \xi_{22}) d\xi_{12} d\xi_{22} \quad (5.35) \\
& + \int_{-\infty}^{\infty} \int_{-\infty}^{\infty} h_{13}(\xi_{13}) h_{23}(\xi_{23}) R_{z_2 z_2}(\tau + \xi_{13} - \xi_{23}) d\xi_{13} d\xi_{23}
\end{aligned}$$

where  $R_{ww}$ ,  $R_{z_1 z_1}$  and  $R_{z_2 z_2}$  are the autocorrelation of  $w(t)$ ,  $z_1(t)$  and  $z_2(t)$ , respectively.

Applying the definition of convolution to Equation (5.35), then we have

$$\begin{aligned}
C_{QP}(\tau) = & R_{ww}(\tau) * h_{11}(-\tau) * h_{21}(\tau) + R_{z_1 z_1}(\tau) * h_{12}(-\tau) * h_{22}(\tau) \\
& + R_{z_2 z_2}(\tau) * R_{z_1 z_1}(\tau) * h_{13}(-\tau) * h_{23}(\tau) \quad (5.36)
\end{aligned}$$

where  $*$  represents the convolution integral operator.

Similarly, we can derive

$$\begin{aligned}
R_{QQ}(\tau) = & R_{ww}(\tau) * h_{11}(-\tau) * h_{11}(\tau) + R_{z_1 z_1}(\tau) * h_{12}(-\tau) * h_{12}(\tau) \\
& + R_{z_2 z_2}(\tau) * R_{z_1 z_1}(\tau) * h_{12}(-\tau) * h_{12}(\tau) \quad (5.37)
\end{aligned}$$

Taking the Fourier transform of (5.36) and (5.37) gives

$$\begin{aligned}
\mathbf{C}_{QP}(\omega) = & \mathbf{R}_{ww}(\omega) \mathbf{H}_{11}(-\omega) \mathbf{H}_{21}(\omega) + \mathbf{R}_{z_1 z_1}(\omega) \mathbf{H}_{12}(-\omega) \mathbf{H}_{22}(\omega) \\
& + \mathbf{R}_{z_2 z_2}(\omega) \mathbf{H}_{13}(-\omega) \mathbf{H}_{23}(\omega) \quad (5.38)
\end{aligned}$$

$$\begin{aligned}
\mathbf{R}_{QQ}(\omega) = & \mathbf{R}_{ww}(\omega) \mathbf{H}_{11}(-\omega) \mathbf{H}_{11}(\omega) + \mathbf{R}_{z_1 z_1}(\omega) \mathbf{H}_{12}(-\omega) \mathbf{H}_{12}(\omega) \\
& + \mathbf{R}_{z_2 z_2}(\omega) \mathbf{H}_{13}(-\omega) \mathbf{H}_{13}(\omega) \quad (5.39)
\end{aligned}$$

Since  $w(t)$ ,  $z_1(t)$  and  $z_2(t)$  are white noise, their power spectral densities are constant, so,  $\mathbf{R}_{ww}(\omega)$ ,  $\mathbf{R}_{z_1 z_1}(\omega)$  and  $\mathbf{R}_{z_2 z_2}(\omega)$  can be found from

$$\mathbf{R}_{ww}(\omega) = W \quad (5.40)$$

$$\mathbf{R}_{z_1 z_1}(\omega) = Z_1 \quad (5.41)$$

$$\mathbf{R}_{z_2 z_2}(\omega) = Z_2 \quad (5.42)$$

where  $W$ ,  $Z_1$  and  $Z_2$  are real positive constants.

Using (5.40)-(5.42), Equations (5.38) and (5.39) become

$$\begin{aligned} \mathbf{C}_{QP}(\omega) = & W \mathbf{H}_{11}(-\omega) \mathbf{H}_{21}(\omega) + Z_1 \mathbf{H}_{12}(-\omega) \mathbf{H}_{22}(\omega) \\ & + Z_2 \mathbf{H}_{13}(-\omega) \mathbf{H}_{23}(\omega) \end{aligned} \quad (5.43)$$

$$\begin{aligned} \mathbf{R}_{QQ}(\omega) = & W \mathbf{H}_{11}(-\omega) \mathbf{H}_{11}(\omega) + Z_1 \mathbf{H}_{12}(-\omega) \mathbf{H}_{12}(\omega) \\ & + Z_2 \mathbf{H}_{13}(-\omega) \mathbf{H}_{13}(\omega) \end{aligned} \quad (5.44)$$

Equations (5.43) and (5.44) can be simplified to

$$\mathbf{C}_{QP}(\omega) = \mathbf{H}_a(\omega) W + \mathbf{H}_b(\omega) Z_1 + \mathbf{H}_c(\omega) Z_2 \quad (5.45)$$

$$\mathbf{R}_{QQ}(\omega) = \mathbf{H}_d(\omega) W + \mathbf{H}_e(\omega) Z_1 + \mathbf{H}_f(\omega) Z_2 \quad (5.46)$$

where

$$\mathbf{H}_a(\omega) = \mathbf{H}_{11}(-\omega) \mathbf{H}_{21}(\omega) \quad (5.47)$$

$$\mathbf{H}_b(\omega) = \mathbf{H}_{12}(-\omega) \mathbf{H}_{22}(\omega) \quad (5.48)$$

$$\mathbf{H}_c(\omega) = \mathbf{H}_{13}(-\omega) \mathbf{H}_{23}(\omega) \quad (5.49)$$

$$\mathbf{H}_d(\omega) = \mathbf{H}_{11}(-\omega) \mathbf{H}_{11}(\omega) \quad (5.50)$$

$$\mathbf{H}_e(\omega) = \mathbf{H}_{12}(-\omega) \mathbf{H}_{12}(\omega) \quad (5.51)$$

$$\mathbf{H}_f(\omega) = \mathbf{H}_{13}(-\omega) \mathbf{H}_{13}(\omega) \quad (5.52)$$

The transfer function  $\mathbf{H}_{QP}(\omega)$  is determined by replacing the numerator and denominator in Equation (5.24) by Equations (5.45) and (5.46), respectively. Therefore, we have

$$\mathbf{H}_{QP}(\omega) = \frac{\mathbf{H}_a(\omega)W + \mathbf{H}_b(\omega)Z_1 + \mathbf{H}_c(\omega)Z_2}{\mathbf{H}_d(\omega)W + \mathbf{H}_e(\omega)Z_1 + \mathbf{H}_f(\omega)Z_2} \quad (5.53)$$

or

$$\begin{aligned} \mathbf{H}_{QP}(\omega) = & \frac{\mathbf{H}_a(\omega)W}{\mathbf{H}_d(\omega)W + \mathbf{H}_e(\omega)Z_1 + \mathbf{H}_f(\omega)Z_2} \\ & + \frac{\mathbf{H}_b(\omega)Z_1}{\mathbf{H}_d(\omega)W + \mathbf{H}_e(\omega)Z_1 + \mathbf{H}_f(\omega)Z_2} \\ & + \frac{\mathbf{H}_c(\omega)Z_2}{\mathbf{H}_d(\omega)W + \mathbf{H}_e(\omega)Z_1 + \mathbf{H}_f(\omega)Z_2} \end{aligned} \quad (5.54)$$

When the load disturbances in the feeder being examined are much smaller than the remote load disturbance, i.e.  $W \ll Z_1$ , and when the input disturbance of the SVC is much smaller than the remote load disturbance, i.e.  $Z_1 \ll Z_2$ , the transfer function  $\mathbf{H}_{QP}$  can be approximated by

$$\mathbf{H}_{QP} = \frac{\mathbf{H}_b(\omega)}{\mathbf{H}_e(\omega)} \quad (5.55)$$

After substituting  $\mathbf{H}_b(\omega)$  from (5.48) and  $\mathbf{H}_e(\omega)$  from (5.51) and then simplifying, then

$$\mathbf{H}_{QP}(\omega) = \mathbf{T}(\omega) \quad (5.56)$$

Thus, under the condition that  $W$  and  $Z_2$  are much smaller than  $Z_1$ , the transfer function  $\mathbf{H}_{QP}$  can be identified. The assumptions are justified in many cases in power systems. It is obvious that in a large network, the total

disturbances are often much greater than the local load of a bus being examined. Also, the total load disturbance in the system is very large compared to the white noise disturbance fed to the SVC.

## 5.7 SVC controller Redesign Based on Normal Operation (General Case)

In the previous section the transfer function  $\mathbf{T}(\omega)$  was identified under the assumptions that the effect of  $W$  and  $Z_2$  are much smaller than  $Z_1$ . With this assumption according to Figure 5.2 the effect of  $w$  and  $z_2$  were considered negligible compared to  $z_1$ . This situation can be true for many cases. In this section, we consider the more general case where all three signals  $w$ ,  $z_1$  and  $z_2$  are potentially of equivalent size. For instance, when the total load in Brisbane is being examined, its perturbations are of the same order of magnitude as other loads in the network. Regarding Figure 5.2, the SVC block has two inputs, one input comes from the plant including feedback paths and the other is the white noise  $d_2$ . These two inputs affect the identification of  $\mathbf{T}(\omega)$ .

It is worthwhile to note that, since  $w$  and  $z_2$  are uncorrelated white noise, the white noise  $w_1$  has no effect on identification of the transfer function between  $Q_w$  and  $P_r$ .

By considering the white noise part of  $Q$ , which is ; labelled  $Q_w$ , the system is treated as open loop in terms of  $Q_w$  and  $\mathbf{T}(\omega)$ .

### 5.7.1 System Description

In this section, we are aiming to examine the relationship between SVC and measured load power in normal operation considering the three signals  $w$ ,  $z_1$  and  $z_2$  are present. In the other words, we examine how the SVC reactive power affects the measured load power in the normal operation when local and remote load perturbations as well as the white noise for SVC are present. This relationship is shown by  $T(\omega)$  in Figure 5.10. This effect is examined in more detail through the test power system shown in Figure 5.11. This figure shows a test power system including a synchronous machine connected to the infinite bus. In this figure, an induction motor in parallel to an SVC, are connected near the generator terminals via impedance  $Z_b$ . For this system,  $SG$  and  $IM$  are synchronous generator and induction machine, respectively. Also  $Z_a$  and  $Z_b$  are the line impedances. The measured power  $P$  shows the changes of the power flow of the synchronous generator caused by the changes of electric power of the induction motor. The induction motor changes are created by the changes of the SVC reactive power. For this test system, the characteristic of the SVC changes is represented by a white noise. The specifications of the elements of the test power system are given in Appendix C. This figure represents case where the SVC modulates the load which consists only of induction motor.

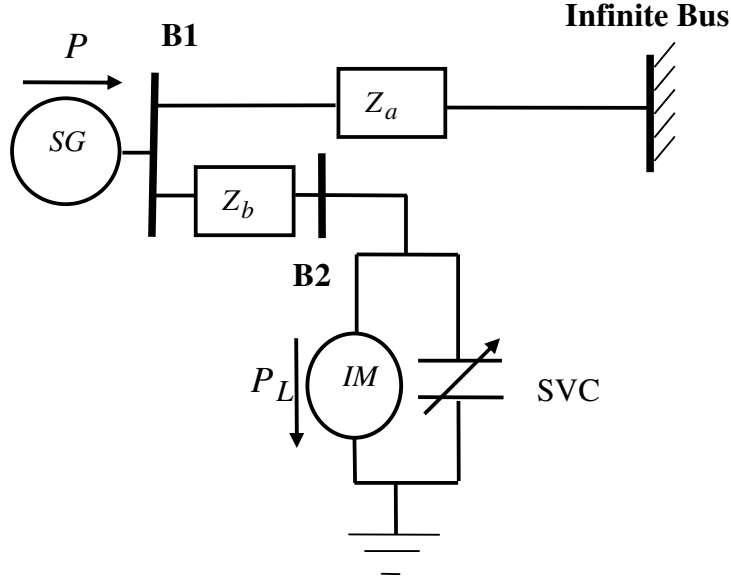


Figure 5.11: A load modulated test system to investigate the effect of the reactive power of SVC on active power

### 5.7.2 Examination of Approaches to Analyse

The aim of this section is to find the transfer function between the white noise part of the reactive power of the SVC and the measured power.

At first the white noise part of the SVC reactive power ( $Q_w$ ) is determined.

To find  $Q_w$ , a model is built with the bus voltage angle ( $\delta$ ) as the input and the measured SVC reactive power ( $Q$ ) as the output. Then, the model output due to the input of  $\delta$  is calculated. The difference between the model output and the measured reactive power of the SVC ( $Q$ ) gives us  $Q_w$  (see Figure 5.2). This model is the best representation of the effect of  $\delta$  on the SVC reactive power. In the simulation,  $Q_w$  is modelled with a white noise.

As shown in Figure 5.2, two components are incorporated in the measured power  $P$ . The first component that affect the measured power comes from

$z_2$  and is called  $P_r$ . This component is of interest. The second component in the measured power comes  $\delta$  through two feedbacks as shown in Figure 5.2 and is called  $P_p$ .

As explained before  $w_I$  has no effect on identification of the transfer function between  $Q_w$  and  $P_r$ , since  $w$  and  $z_2$  are uncorrelated white noise sources.

In order to find the effect of white noise part of the SVC reactive power on the measured active power, the effect of the second component in the measured power  $P$ , should be eliminated. To extract the model for  $T(\omega)$  without the errors that can be induced by the presence of the feedback loops two approaches are suggested which are explained as follows:

#### **Partial Fraction Expansion Approach:**

In this approach, the transfer function between the white noise part of the SVC reactive power  $Q_w$ , and measured power  $P$ , is identified. This transfer function includes the feed back effects of  $\delta$  on the measured power,  $P$  and obtained from

$$T_t(\omega) = \frac{\mathfrak{S}[C_{Q_w P}(\tau)]}{\mathfrak{S}[R_{Q_w Q_w}(\tau)]} \quad (5.57)$$

Using the partial fraction expansion method,  $T_t(\omega)$  can be decomposed into terms corresponding to the poles of the plant with the feedback loops, and poles of  $T(\omega)$  as

$$\mathbf{T}_t(\omega) = \mathbf{F}(\omega) + \mathbf{T}_p(\omega) \quad (5.58)$$

where  $\mathbf{F}(\omega)$  is the transfer function formed by the eigenvalues corresponding to poles of  $\mathbf{T}(\omega)$  and it has the same poles of  $\mathbf{T}(\omega)$ . Also,  $\mathbf{T}_p(\omega)$  shows the effect of second component in the measured power  $P$ , which was previously called  $P_P$ . Knowing the poles of the plant with the feedback loops present, we can identify the other eigenvalues as the poles of  $\mathbf{T}(\omega)$ .

#### **Decorrelation Approach:**

In this approach, at first the feedback effects of system angle on the measured power  $P$  are identified and then removed from the measured power  $P$  to give  $P_r$ . Then, the transfer function  $\mathbf{T}(\omega)$  can be found from

$$\mathbf{T}(\omega) = \frac{\Im[C_{Q_w P_r}(\tau)]}{\Im[R_{Q_w Q_w}(\tau)]} \quad (5.59)$$

where  $P_r$  is the measured power after the decorrelating the effect  $P_P$  from the measured power  $P$ .

To decorrelate  $P_P$  from the measured power  $P$ , we build a model with  $P_P$  as the input and  $P$  as the output. Then, the model output due to the input of  $P_P$  is computed. The difference between the output model and measure power gives us  $P_r$ . The model is the best representation of  $P_P$  formed by the two feedback paths.

The decorrelation method has the advantage that it identifies the transfer function  $T(\omega)$  completely. However, the decorrelation approach requires a significant length of data to achieve accuracy.

## 5.8 Identification of System in Normal Operation with SVC

In this section the algorithm and result of the simulation for determining the information between  $Q_w$  and  $P_r$  are given using the two approaches presented in the previous section.

### 5.8.1 Algorithm and Simulation of the Partial Fraction Expansion Approach

The algorithm of finding the effect of the white noise part of the SVC reactive power on the measured power using the partial fraction expansion method has the following steps:

**Step1: Finding the power system resonant frequencies**

**Step 2: Determination of the white noise part of the SVC reactive power**

**Step3: Identifying the transfer function  $T_t(\omega)$  according to Equation (5.57)**

**Step 4: Identifying the transfer function  $F(\omega)$  using partial fraction expansion method**

In order to validate the algorithm based on the partial fraction expansion approach, the algorithm is applied to the system of Figure 5.11. In this simulation the SVC is the white noise and time duration for the simulation is 20 seconds. Applying the algorithm yields  $T_t$  in the Laplace domain as

$$\mathbf{T}_t(s) = \frac{-1.8996s^2 - 31.4912s - 953.171}{s^3 + 19.02s^2 + 798.1s + 10954} \quad (5.60)$$

The frequency response of  $\mathbf{T}_t(\omega)$  is shown in Figure 5.12. Using partial fraction expansion, Equation (5.60) is changed to

$$\mathbf{T}_t(s) = \frac{-1.01}{s + 14.8733} + \frac{-0.8896s - 14.0752}{s^2 + 4.1429s + 736.4858} \quad (5.61)$$

The second term in Equation (5.61) corresponds to the IAO of the test power system caused by the load changes. Thus, the transfer function  $\mathbf{F}$  which has the poles of  $\mathbf{T}$ , is the first term in Equation (5.61). Therefore

$$\mathbf{F}(s) = \frac{-1.01}{s + 14.8733} \quad (5.62)$$

The frequency response of  $\mathbf{F}(\omega)$  is shown in Figure 5.13.

To validate the results, the synchronous generator is frozen in Figure 5.11 by choosing a very large value for the inertia of the generator. In this case, the dynamics in measured  $P$  come only from the induction motor dynamics excited by the SVC changes. In this situation, changes in the measured power  $P$  created by the SVC changes only, and  $P$  is equal to  $P_r$ , because, the inertia of the synchronous generator does not incorporate in the measured power  $P$ . Using Equation (5.57) gives the transfer function for  $\mathbf{T}$  in the Laplace domain as

$$\mathbf{T}(s) = \frac{-0.7724}{s + 13.8671} \quad (5.63)$$

The pole of  $\mathbf{F}(s)$  in Equation (5.62) is close to the pole of  $\mathbf{T}(s)$  in Equation (5.63) and thus, the algorithm is validated. Figure 5.14 also shows the transfer function of  $\mathbf{T}(\omega)$  when the synchronous generator is frozen.

Magnitude

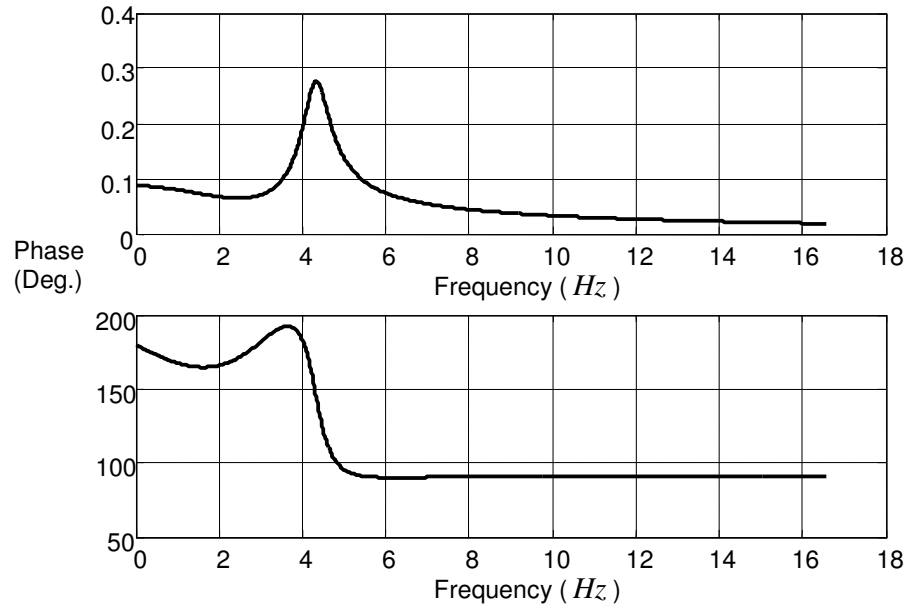


Figure 5.12: The frequency response of the identified transfer function

$$T_t(\omega)$$

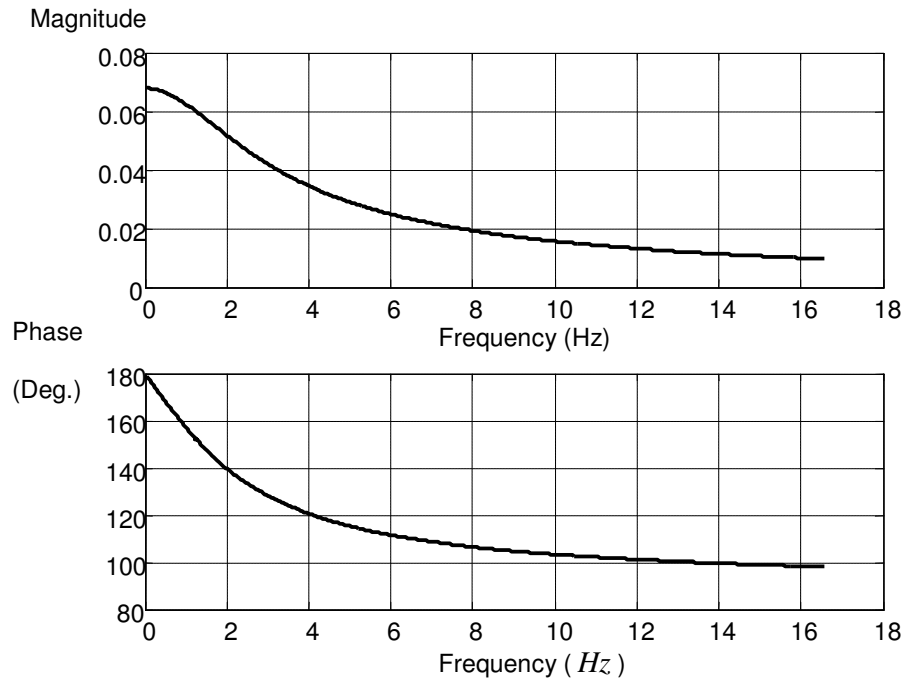


Figure 5.13: The frequency response of the identified transfer function

$$F(\omega) \text{ obtained using partial fraction expansion approach}$$

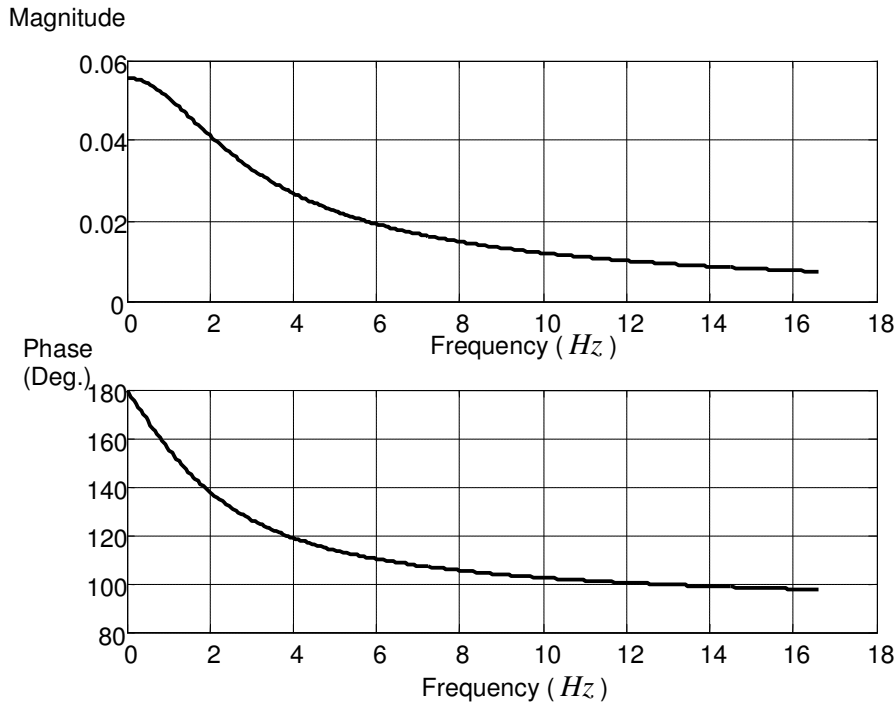


Figure 5.14: The frequency response of the identified transfer function

$T(\omega)$  obtained when the synchronous generator is frozen

### 5.8.2 Algorithm and Simulation of the Decorrelation Approach

When the a large number of the recorded data is available, it is recommended to use the decorrelation approach. The algorithm of this method has the following steps.

**Step 1: Determination of the white noise part of the SVC reactive power**

**Step2: Determining  $P_r$  by decorrelating the load effect from the measured power  $P$**

**Step 3: Identifying  $T(\omega)$  using Equation (5.59)**

Applying this algorithm to the test power system shown in Figure 5.11 gives the transfer function for  $T$  which can be represented in the Laplace domain as

$$\mathbf{T}(s) = \frac{-0.6522}{s + 14.6565} \quad (5.64)$$

In order to validate the algorithm of the decorrelation approach, Equation (5.64) is compared with Equation (5.63) obtained for the case when the synchronous generator is frozen. Comparing the parameters of Equations (5.64) and (5.63) reveals that the parameters of (5.64) are close to the parameters of Equation (5.63), this shows the validity of the algorithm. The frequency response  $\mathbf{T}(\omega)$  obtained from normal operation is shown in Figure 5.15.

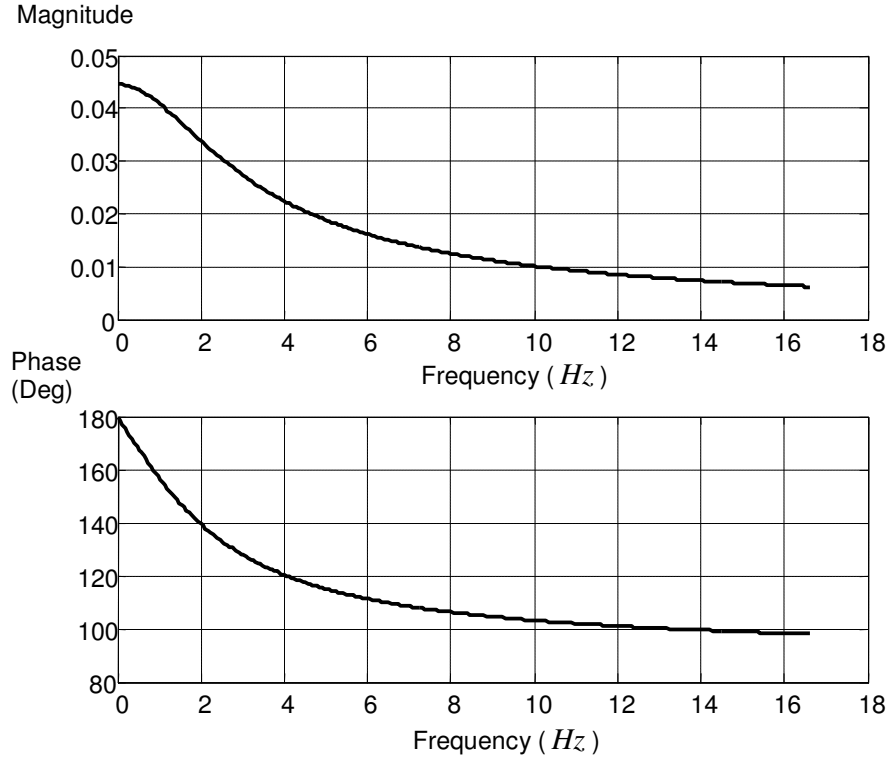


Figure 5.15: The identified transfer function  $\mathbf{T}(\omega)$  obtained when the generator is running using the decorrelation approach

### 5.9 Real Data Analysis<sup>1</sup>

In this part, the application of the suggested algorithm to the real data is investigated. The data was gathered from the Blackwall SVC near Brisbane. The data duration was 180 seconds. The reactive power  $Q$  of SVC at Blackwall substation for one snapshot is depicted in Figure 5.16, and Figure 5.17 indicates the power flow past the SVC to Brisbane.

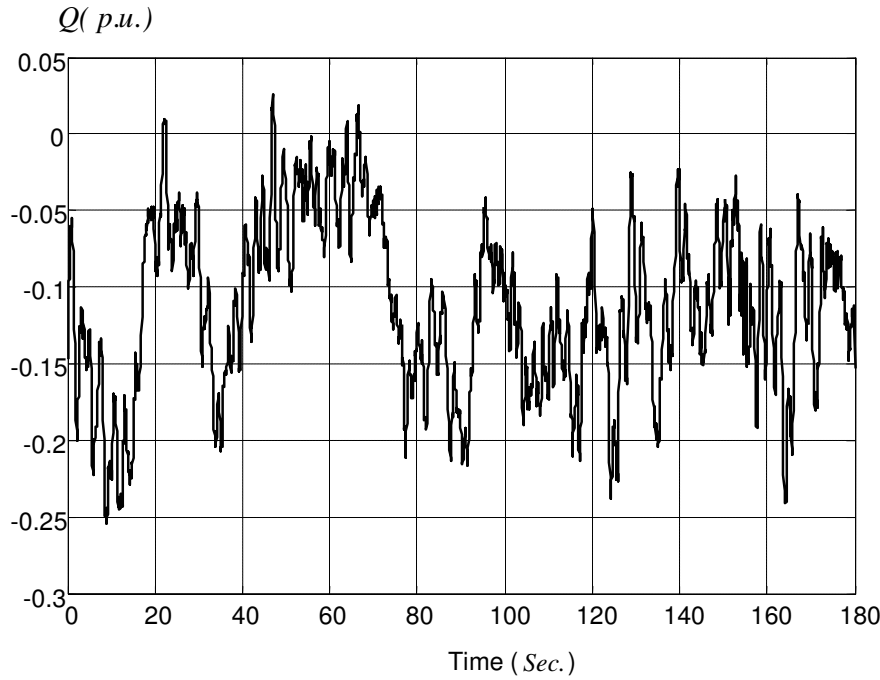


Figure 5.16: The reactive power of SVC from Blackwall substation

In the first step, the reactive power of the SVC was decorrelated from the dependency on Brisbane voltage angle. In fact, according to Figure 5.2, there is a dependency of the Brisbane bus voltage angle on the SVC reactive power  $Q$ . This dependency can be removed by extracting the white noise part of  $Q$ .

---

<sup>1</sup>The real data was provided by Powerlink Queensland.

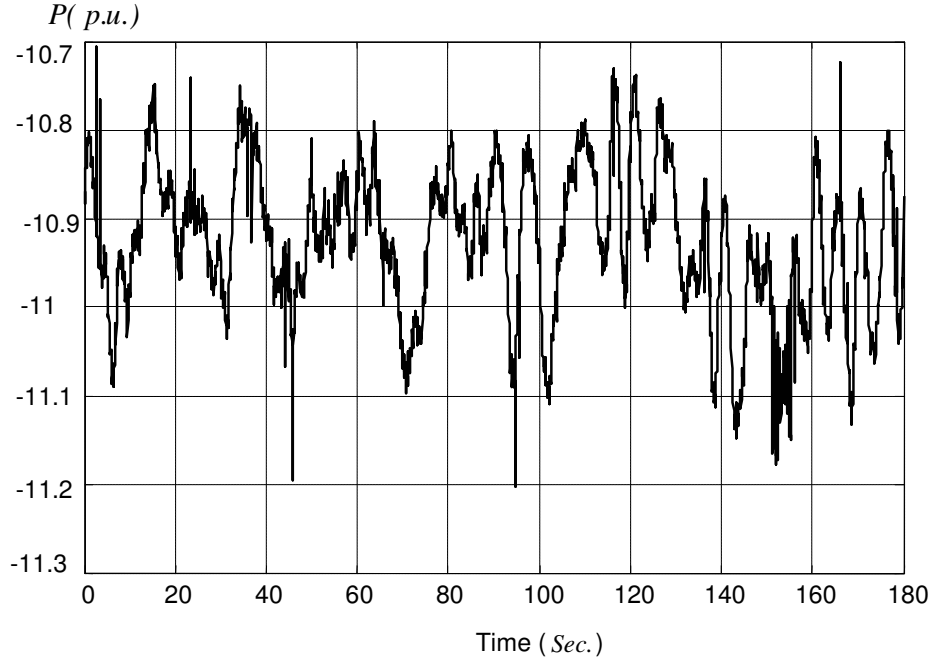


Figure 5.17: The active power flow past Blackwall substation to Brisbane

In the measured power  $P$ , however, there is still a dependency on the voltage bus angle. As explained in Subsection 5.8.1, this issue can also be resolved using the partial fraction expansion method. This means that if some power system resonant frequencies are present in the identified transfer function, the partial fraction expansion method can be used to extract the desired transfer function.

The transfer function between the white noise part of  $Q$  and measured power  $P$ , is found according to Equation (5.57) using the cross-correlation and autocorrelation functions. This identified transfer function  $T_t$  in the Laplace domain can be represented as

$$\mathbf{T}_t(s) = \frac{-0.2524s^3 - 2.6135s^2 - 3.6784s + 6.6714}{s^4 + 9.4211s^3 + 25.3233s^2 + 47.2425s + 48.4735} \quad (5.65)$$

The frequency response of the identified transfer function shown in Equation (5.65), is illustrated shown in Figure 5.18.

By comparing the roots of the denominator of Equation (5.65) and the identified power resonant frequencies in Table 3.8, it is found that there is one power system resonant frequency in the transfer function  $\mathbf{T}_t$  given in Equation (5.65). According to Equation (5.58), the transfer function  $\mathbf{T}_t$  can be decomposed to two terms:  $\mathbf{T}_p$  and  $\mathbf{F}$ , using partial fraction expansion.

Transfer functions  $\mathbf{T}_p$  and  $\mathbf{F}$  can be computed as

$$\mathbf{T}_p(s) = \frac{-0.5615s - 0.0325}{s^2 + 1.1367s + 4.1039} \quad (5.66)$$

$$\mathbf{F}(s) = \frac{0.3091s + 1.7191}{s^2 + 8.2844s + 11.8116} \quad (5.67)$$

The frequency response of  $\mathbf{T}_p(\omega)$  and  $\mathbf{F}(\omega)$  are illustrated in Figures 5.19 and 5.20, respectively. The poles of the transfer function  $\mathbf{F}$  in Equation (5.67) represents the poles of transfer function between white reactive power of the SVC and measured power  $P$ .

If the length of the recorded data is sufficient, then the decorrelation approach can be applied to the real data to the find transfer function  $\mathbf{T}(\omega)$ .

The obtained information regarding the effect of white noise power of the SVC reactive power on the measured power, can be used to design the SVC controller based on the normal operation to achieve the maximum damping of the IAO.

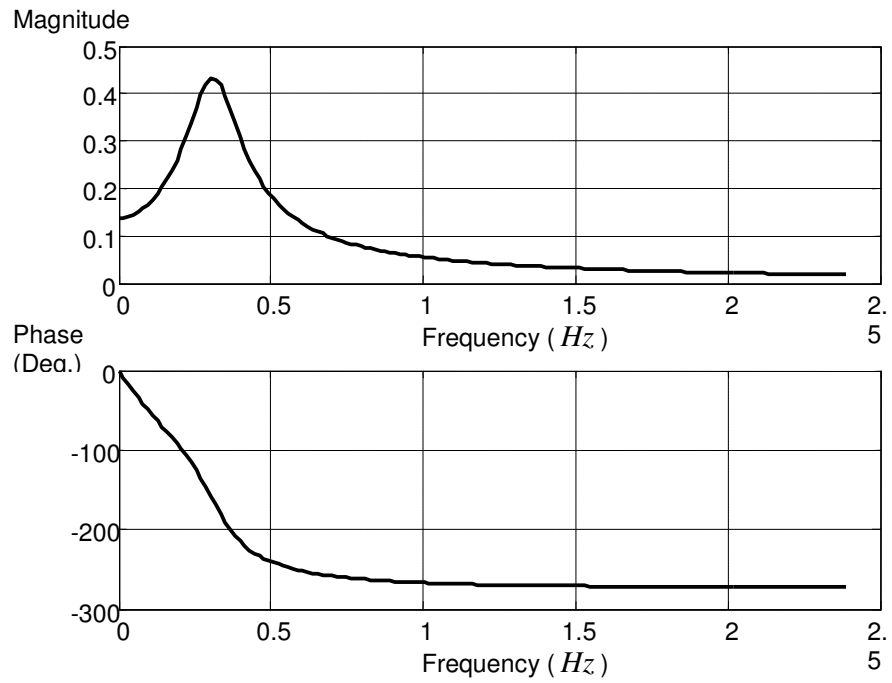


Figure 5.18: The frequency response of the identified transfer function

$T_t(\omega)$  for the real data

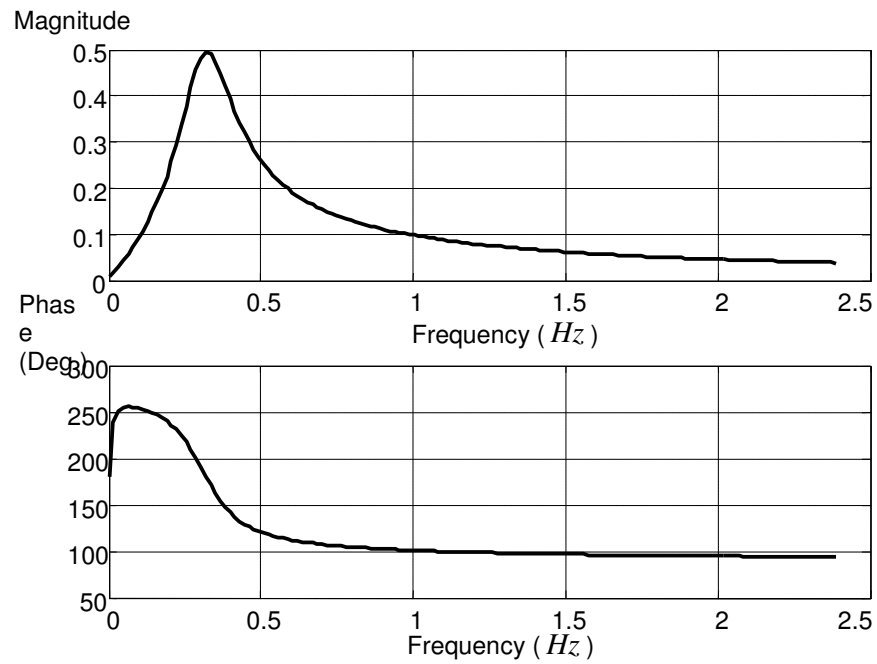


Figure 5.19: The frequency response of the identified transfer function

$T_p(\omega)$  for the real data

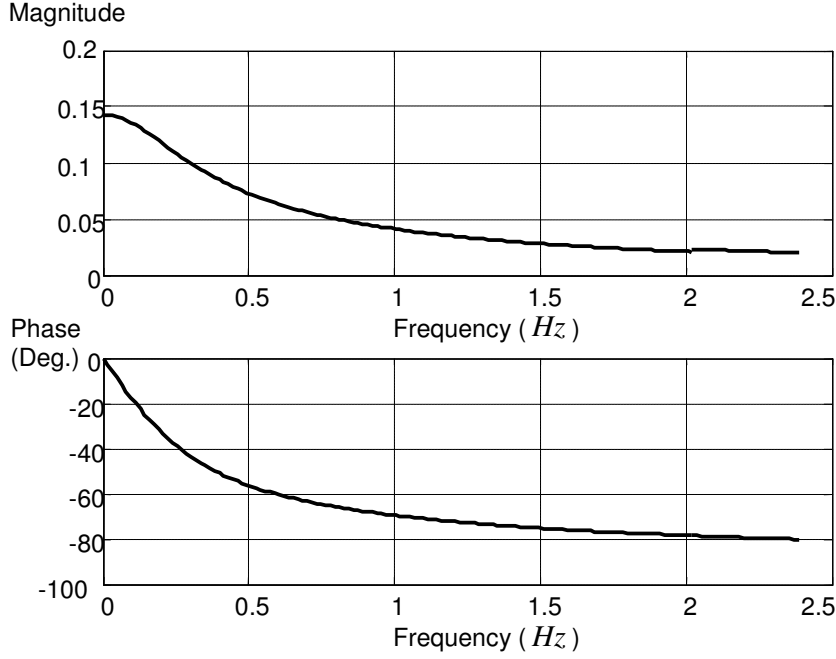


Figure 5.20: The frequency response of the identified transfer function

$\Gamma(\omega)$  for the real data

## 5.10 Summary

In this chapter, to examine the effect of SVC on damping of the IAO, two methods are proposed.

The first method is redesign of the SVC controller on the basis of complete testing. In this method, the CBMSI method is used to identify the resonant frequency of the oscillatory modes. Then, the involvement of real power flow of the generator in damping is determined in the presence of SVC. The effect of feedback signals from bus voltage angle and bus voltage angle changes is investigated by simulating the suggested algorithm. The results show that if the feedback signal is taken from the rate of bus voltage angle changes, the load contribution to damping can be improved. Indeed, without

the SVC, the load partly contributes to damping and SVC can modify this to achieve maximum contribution of load to damping.

The second method is redesign of the SVC controller based on normal operation. In this method, the transfer function representing the relationship between the white noise part of the reactive power of SVC and the measured power of the load is identified. To achieve maximum damping, measured power should be in phase with the speed changes of the synchronous generator, therefore, the desired phase shift of the SVC can be obtained using the phase angle of the identified transfer function at the resonant frequency. The results of simulating this method on a test system show the validity of the suggested algorithm. Finally, the effect of the reactive power of the SVC Blackwall of the Australian electricity network on the measured power supplied to Brisbane is examined.



## **Chapter 6: Summary, Conclusion and Recommendation for Future Research**

In this chapter a summary of the thesis is given, the main results of this research are explained and the major conclusions of the thesis are provided. Finally further research that may be carried out in the area of contribution of power system to damping of the inter-area oscillations (IAO) is described.

### **6.1 Summary**

In Chapter 3, in the first contribution of this thesis, the correlation based mode shape identification (CBMSI) is introduced to identify the power system eigenvalues of the IAO. It is demonstrated in this method that the eigenvalues can be identified from the power system response to impulse input or white noise input. Also it is shown when a combination of both impulse response and white noise are applied to the power system the

eigenvalues of the power system can be identified. The estimated results of the simulation agree with the actual values of the eigenvalues of the test power system. Then the CBMSI is applied to the real data of the Australian electricity network to find the eigenvalues and mode shapes. By using the result of this chapter, the resonant frequencies, damping and the mode shape plot of the power system can be updated continuously from normal operating data. This information provides continuous understanding of power system parameters, that can be useful to prevent or postpone emergency situations.

The quantification of load contribution using eigenvalue sensitivity to load (ESL) method is developed in Chapter 4. In this chapter in a closed loop representation of the power system, with the assumption that the local load disturbance is much smaller than the remote load disturbances, the load model is identified. The load model transfer function that relates the rate of the angle changes to the load power changes is identified on the basis of the cross-correlation and autocorrelation functions. Then, the load contribution to damping is determined using the ESL method. In the ESL method, the right and left eigenvector, the inertia of the generator and the value of the identified load model at identified resonant frequency, are employed to compute the sensitivity of the eigenvalues load contribution to damping. The algorithm presented in Chapter 4 is applied to a test system including three generators, nine lines and four loads to find the sensitivity of the power system eigenvalues with respect to the loads. The simulation results show there is a good agreement between actual values obtained from the

eigenvalues analysis and the estimated values determined from the ESL method. In the real data analysis the load of one feeder of a substation in Brisbane of Australia, which called the Brisbane feeder load, is examined. The contribution of this load to damping of each mode is identified separately. Also the sensitivity eigenvalues of the of Australian electricity network with respect the Brisbane load at each mode are identified. The method presented in this chapter, provides an understanding of the contribution of the specific load to damping and resonant frequency of the IAO. This contribution could be modified continuously. Identifying the load effect on damping, could lead to a choice of strategy in load management or load modulation in the contingency situation.

The effect of SVC on load contribution is examined in Chapter 5 and two methods for redesigning the SVC controller are developed in this chapter to increase the damping of the IAO. These two methods are SVC controller redesign based on complete testing and based on normal operation.

The SVC controller redesign based on complete testing uses “On” and “Off” control of the SVC to find the contribution of SVC and relates this to the SVC controllers parameters. This information can be used to find the new setting for parameters of the SVC controllers to achieve maximum damping of the IAO. The developed algorithm for SVC redesign based on complete testing is simulated on a test system and it is shown that through this method, a modification for the SVC controller parameters can be suggested by using particular feedback signals to achieve maximum contribution of the dynamic load to damping.

Next, the SVC controller redesign based on normal operation is developed. The effect of reactive power of the SVC on the measured power of the load is analyzed. The relationship between the white noise part of the SVC action and the measured power is described by a transfer function.

In the second test power system used in Chapter 5, a mainly load modulated test system is simulated to find the effect of reactive power of SVC on measured power. At first when the generator is running, a transfer function is extracted from the system response and system inputs. The system response consists of the dynamics of the induction motor and dynamic of the synchronous generator. Then transfer function which relates of SVC reactive power on the measured power excluding the synchronous generator dynamics is identified. To validate the results, the synchronous generator is frozen, and the transfer function is identified. The parameters of the identified transfer function when the generator is running is close to the parameters of the obtained transfer function when the generator is frozen and this demonstrates the validity of the algorithm. The SVC real data of the Australian electricity network is analyzed later in Chapter 5. In this analysis firstly the white noise part of the SVC reactive power is determined. Then, the effect of white noise part of the  $Q$  of SVC on the measured active power past the Blackwall Substation in Australia is investigated and the poles of the transfer functions between white noise part of the SVC and the measured active power are identified using the partial fraction expansion approach.

The method of the SVC controller design based on complete testing could

improve the SVC effect on the IAO, by redesigning the SVC controller. It has disadvantage of being costly process and sometimes it is difficult to put the SVC off-line. However the SVC controller redesign based on normal operation used the operating data to find the effect of the SVC reactive power on the measured load power. The resulting information can be used in redesigning of SVC controller to increase the damping of the IAO.

## 6.2 Conclusion

The conclusions arising from the studies in this thesis are as follows:

- This thesis makes three major contributions in developing
  - The CBMSI method to identify the power system resonant frequencies and mode shape,
  - The ESL method to identifying the load contribution to damping
  - A method of identification of SVC contribution to damping
- In the CBMSI method the power system eigenvalues and mode shape are determined using cross-correlation and autocorrelation functions.
- Load contribution to damping is quantified and the ESL method is used to find sensitivity of the power system eigenvalues with respect to the load.
- The redesign of SVC controller based on complete testing is presented. This method provides information for redesigning the SVC controller to increase the damping of the IAO.
- The contribution of SVC is investigated and the transfer function between the white noise part of reactive power of the SVC and the

active power is determined using cross-correlation and autocorrelation functions.

- The three contributions of this thesis are validated by simulating each method on a test system. The accuracy of the results of the simulation are good in that they are close to the chosen values. The methods developed in this thesis were applied to real data of the Australian electricity network to determine
  - The power system frequencies and mode shape plot at each identified resonant frequency.
  - Quantification of the Brisbane load to damping and sensitivity of the power system eigenvalues with respect to the Brisbane load.
  - Identification of the effect of the white noise part of the SVC of the Blackwell substation on the active power past this substation towards Brisbane.

## **6.3 Recommendation for Future Research**

The following areas are recommended for future work:

### **6.3.1 The Contribution of Automatic Voltage Regulator to Damping**

In this thesis the effect of load and SVC on damping are investigated. The influence of the automatic voltage regulator (AVR) to damping is one area to continue the current research.

The aim of an AVR is to continuously control the output voltage of a synchronous generator by adjusting the applied field voltage.

The effect of AVR on damping can be explained by considering the field of the generator. The field of the generator produces the magnetic flux and as the generator is running, the voltage is generated at the generator terminals. If the input voltage of the field of the generator is chosen proportional to the rate of the generator voltage angle changes  $\dot{\delta}$ , then, since the circuit of the field of the generator is inductive, therefore there is a time delay between the input voltage of the field and the produced magnetic flux  $\Phi$  of the field. Thus, at the IAO resonant frequency there is a phase shift between the produced flux and the field and input voltage of the field. When the input voltage of the field is chosen proportional to  $\dot{\delta}$ , then there is a phase shift between produced flux and  $\dot{\delta}$  as shown in Figure 6.1. In this case, similar to the SVC that discussed in Chapter 5, by taking appropriate feedback from terms related to  $\delta$  as well as terms related to  $\dot{\delta}$ , the input voltage can be adjusted, so that the produced flux is in phase with  $\dot{\delta}$ . In this case, the greatest contribution of AVR to damping can be provided. So the AVR contribution to damping should be able to be quantified and an algorithm should be developed to increase the AVR damping contribution to damping.

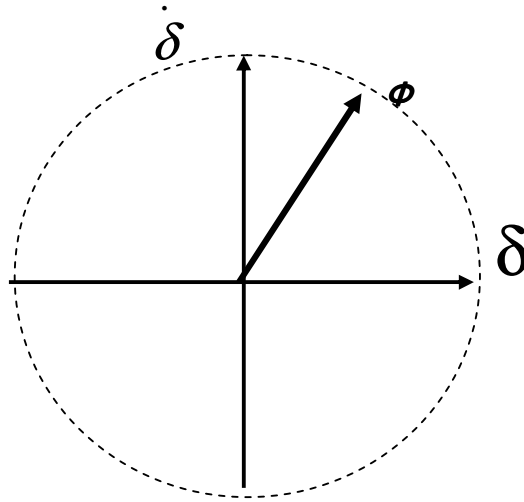


Figure 6.1: The contribution of produced magnetic flux load to damping

### **6.3.2 Examining the Effect of Location of Load on the Analysis of the Load Contribution to Damping**

In developing the load contribution method to damping, it is assumed that the load is connected to the generator terminals. This assumption is often acceptable, because in a large electricity network, many generators are clustered around a load considering a equivalent load, and the aggregated generator is often a reasonable representation of the real power system.

However it is more beneficial, if a more general case in which load is not close to the generator terminals, is considered. Fig 6.2.a shows a simple case to illustrate the case when a load is connected between the two generators. In that case the diagram can be changed to Figure 6.2.b. In fact, the changes in the load connected between generators  $i$  and  $j$  can be mapped to the reduced admittance matrix of the system. A more general case would have a

mesh of load buses and generator buses and changes in the load will affect several generators.

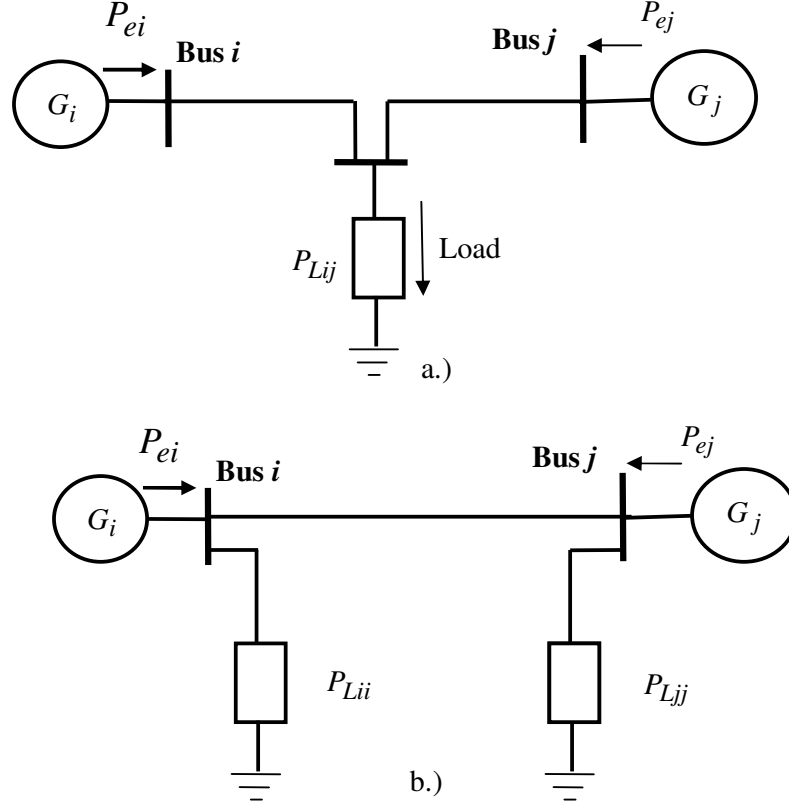


Figure 6.2: a.) Diagram of the connection of the general dynamic load  $P_{Lij}$  between generator  $i$  and generator  $j$ , b.) the simplified diagram

In forming the equation in the state space mode, the Equations (2.10) and (4.17) should be modified. In this modification two factors should be considered.

The first factor is the representation of the dynamic loads in terms of the state variables. Therefore, one challenging issue is the load identification and in doing this, the block diagram in Figure 5.2, should be investigated.

The second factor indicates how the dynamic load changes are shared between the groups of generators with intermediate loads. For example, in Figure 6.2 the changes in the load  $P_{Lij}$  can be mapped to the changes of the reduced Y bus matrix of the system. Therefore Equation (4.7) for the case that the loads are not connected to the generator terminals can be modified as

$$\begin{bmatrix} \dot{\delta} \\ \delta \end{bmatrix} = \mathbf{A} \begin{bmatrix} \delta \\ \dot{\delta} \end{bmatrix} + \begin{bmatrix} 0 \\ \boldsymbol{\alpha} \end{bmatrix} \mathbf{S} [\mathbf{K}_1 \quad \mathbf{K}_2] \begin{bmatrix} \delta \\ \dot{\delta} \end{bmatrix} \quad (6.1)$$

where

$\mathbf{A}$  = the system matrix in the state space model with the dimension of  $2n \times 2n$

$\boldsymbol{\alpha}$  = the matrix of load factor with dimension of  $n \times n$

$\mathbf{K}_1$  and  $\mathbf{K}_2$  = the matrices with dimension of  $n \times n$  that show the dynamic representation of the loads in terms of  $\delta's$  and  $\dot{\delta}'s$

$\mathbf{S}$  = the allocation matrix with dimension of  $n \times n$  that show how the loads admittances are shared between the generators

Therefore more study is needed to determine the sensitivity of  $k^{th}$  eigenvalue with respect to the  $k^{th}$  active load  $P_{Lk}$  which is connected in the mesh network.

### **6.3.3 Investigation the effect of other AC Transmission Devices to Damping**

The SVC contributes to damping both directly and indirectly. The direct contribution is called line modulation and the indirect modulation is called load modulation. In the line modulation effect by the SVC, the variation of the capacitor of SVC changes the line impedance and therefore it contributes to damping directly. However in the load modulation effect by the SVC, capacitor changes the SVC leads to changes of the voltage of the dynamic loads, and therefore the contribution of the load to damping changes.

In this thesis, the effect of SVC and or shunt controlled capacitor considering mainly load modulation, is examined. Another area for further investigation, is to work on the line modulated performance of the SVC and how the contribution of the line modulated SVC to damping can be quantified.

Other flexible AC transmission Systems (FACTS) devices can be investigated to the effect of these devices to damping.

The contribution of the thyristor series controlled capacitor (TCSC), is another area for continuing this research [108-111]. In the case of TCSC, firstly the contribution of the TCSC to damping with the existing control design can be evaluated in terms of line modulation. Then, a method needs to be developed to redesign the TCSC control design to achieve the maximum contribution to damping.

The unified power flow controller (UPFC) is another FACTS device that could be investigated in future to find out how it contributes to damping of the IAO [112-115]. UPFC is a FACTS device which is capable of controlling power system parameters such as voltage terminal and line impedance. UPFC has two applications in power systems. The first application is to regulated power flow and the second application is to improve the damping of the IAO. A UPFC consists of the combination of static synchronous capacitors (STATCOM) and static synchronous series compensator, (SSSC) that are connected by a DC voltage link. The insights gained from SVC and TCSC contribution to damping, would help to develop a method for quantifying the UPFC contribution to damping.

### **6.3.4 Characterization of the Time Variation of Load**

With the methods developed in Chapters 3 and 4, the power system utilities are now able to continuously monitor the load model from disturbances created by the background customer load variations. Consequently, the identified load model could be used to update the setting of the FACTS control design and thus improve the contribution of the device to damping, if it is necessary.

## References

- [1] P. Kundur, *Power System Stability and Control*, 1994.
- [2] P. W. Sauer and M. A. Pai, *Power System Dynamic and Stability*. New Jersey: Prentice Hall, 1998.
- [3] D. J. Hill, "Nonlinear dynamic load models with recovery for voltage stability studies," *Power Systems, IEEE Transactions on*, vol. 8, pp. 166-176, 1993.
- [4] M. Banejad, G. Ledwich, P. O'Shea, and E. Palmer, "On Line determination of mode shape of a power system," presented at The 6th International Transmission and Distribution Conference: Distribution 2001, Brisbane, 2001.
- [5] M. Banejad and G. Ledwich, "Correlation-based mode shape determination of a power system," presented at 2002 IEEE International Conference on Acoustics, Speech and Signal Processing: ICASSP2002, Orlando, Florida, USA, 2002.
- [6] M. Banejad and G. Ledwich, "Quantification of load contribution in damping of a power system," presented at 17th International Power System Conference, Tehran, Iran, 2002.
- [7] M. Banejad and G. Ledwich, "Correlation-based identification of the effects of the loads on oscillatory modes," presented at the Australian Universities Power System Engineering Conference: AUPEC 2002, Melbourne, Australia, 2002.

- [8] M. Banejad and G. Ledwich, "Investigation of load contribution in damping in a multi-machine power system based on sensitivity analysis," presented at Australian Universities Power System Engineering Conference: AUPEC 2003, Christchurch, New Zealand, 2003.
- [9] M. Banejad and G. Ledwich, "Improving the SVC contribution in damping of low Frequency oscillations of a power system," presented at The 7th International Transmission and Distribution Conference: Distribution 2003, Adelaide, Australia, 2003.
- [10] M. Banejad and G. Ledwich, "On the effect of SVC control design of damping of low frequency oscillations," presented at The 38th Universities Power Engineering conference: UPEC2003, Thessaloniki, Greece, 2003.
- [11] M. Banejad and G. Ledwich, "Analysis of SVC contribution to damping of a power system including induction motor effects," presented at The 6th International Power Engineering Conference, Singapore, 2003.
- [12] K. Ogata, *Modern control engineering*, 4th ed. Upper Saddle River, NJ: Prentice Hall, 2001.
- [13] J. H. Chow, *Time-scale modeling of dynamic networks with applications to power systems*. Berlin New York: Springer-Verlag, 1982.
- [14] E. G. Cate and D. P. Gelopuls, "Time frame notion and time frame of the models in transient, mid-term and long-term stability programs,"

- Power Apparatus and Systems, IEEE Transactions on*, vol. Pas-103, pp. 143-151, 1984.
- [15] P. M. Anderson and A. A. Fouad, *Power system control and stability*: A John Wiley & Sons INC Publication, 2003.
  - [16] G. Rogers, *Power System Oscillations*. Massachusetts: Kluwer Academic Publisher, 2000.
  - [17] F. L. Pagola, I. J. Perez-Arriaga, and G. C. Verghese, "On sensitivities, residues and participations: applications to oscillatory stability analysis and control," *Power Systems, IEEE Transactions on*, vol. 4, pp. 278-285, 1989.
  - [18] K. W. Wang, C. Y. Chung, C. T. Tse, and K. M. Tsang, "Multimachine eigenvalue sensitivities of power system parameters," *Power Systems, IEEE Transactions on*, vol. 15, pp. 741-747, 2000.
  - [19] J. L. Sancha and I. J. Perez-Arriaga, "Selective modal analysis of power system oscillatory instability," *Power Systems, IEEE Transactions on*, vol. 3, pp. 429-438, 1988.
  - [20] K. R. Padiyar, *Power System dynamics, Stability and Control*: Interline Publishing Private Limited, 1996.
  - [21] I. A. Hiskens and J. V. Milanovic, "Locating dynamic loads which significantly influence damping," *Power Systems, IEEE Transactions on*, vol. 12, pp. 255-261, 1997.
  - [22] L. Rouco and F. L. Pagola, "Eigenvalue sensitivities for design of power system damping controllers," presented at Decision and Control, 2001. Proceedings of the 40th IEEE Conference on, 2001.

- [23] L. Rouco, "Design of damping controllers of static series voltages source using eigenvalue sensitivities," presented at Transmission and Distribution Conference and Exposition, 2001 IEEE/PES, 2001.
- [24] P. Z. Peebles, *Probability, Random Variables, and Random Signal Principles*: McGraw-Hill Book Company, 2001.
- [25] A. Papoulis, *Probability, Random Variables, and Stochastic Processes*. New York: McGraw-Hill, 2002.
- [26] H. Stark and J. W. Woods., *Probability and random processes with applications to signal processing*, 3rd ed. Upper Saddle River, NJ: Prentice Hall, 2001.
- [27] J. G. Proakis and D. G. Manolakis., *Digital signal processing: principles, algorithms, and applications*. Prentice Hall: Upper Saddle River, N.J, 1996.
- [28] J. P. Norton, *An introduction to identification*. New York: Academic Press, 1986.
- [29] S. S. Soliman and M. D. Srinath., *Continuous and discrete signals and systems*, 2nd ed. Upper Saddle River, NJ: Prentice Hal, 1998.
- [30] G. J. Rogers, "A Fundamental aspects of low frequency inter-area oscillations," *IEEE Power Engineering Society: Inter- Area Oscillations in Power Systems*, pp. 13-17, 1994.
- [31] H. Breulmann, E. Grebe, and M. Losing, "Analysis and damping of inter-area oscillations in the UCTE/Central power system," *Cigre, Session 2000*, 2000.

- [32] V. Vittal, N. Bhatia, and A. A. Fouad, "Analysis of the inter-area mode phenomenon in power systems following large disturbances," *IEEE Power Engineering Society: Inter- Area Oscillations in Power Systems*, pp. 33-39, 1994.
- [33] M. Klein, G. J. Rogers, and P. Kundur, "A fundamental study of inter-area oscillations in power systems," *Power Systems, IEEE Transactions on*, vol. 6, pp. 914-921, 1991.
- [34] M. Bounou, S. Lefebvre, and R. P. Malhame, "A spectral algorithm for extracting power system modes from time recordings," *Power Systems, IEEE Transactions on*, vol. 7, pp. 665-683, 1992.
- [35] D. R. Ostojic, "Spectral monitoring of power system dynamic performances," *Power Systems, IEEE Transactions on*, vol. 8, pp. 445-451, 1993.
- [36] R. Niu and e. al., "Power System Random Oscillation Studies Using Frequency Spectrum Method," presented at The Fifth International Power Engineering Conference (PEC 2001), Singapore, 2001.
- [37] M. J. Corinthios, "A Fast Z-Transformation Algorithm for System Identification," vol. vol. 26, no.11, 1977.
- [38] F. P. Demello, P. J. Nolan, T. F. Laskowaski, and J. M. Undreill, "Coordinated Application of Stablizers in Multi-machine Systems," *Power Apparatus Systems, IEEE Transactions on*, vol. PAS-99, pp. 892-901, 1980.

- [39] A. Feliachi, X. Zhang, and C. S. Sims, "Power system stabilizers design using optimal reduced order models. II. Design," *Power Systems, IEEE Transactions on*, vol. 3, pp. 1676-1684, 1988.
- [40] P. Kundur, M. Klein, G. J. Rogers, and M. S. Zywno, "Application of power system stabilizers for enhancement of overall system stability," *Power Systems, IEEE Transactions on*, vol. 4, pp. 614-626, 1989.
- [41] M. Klein, G. J. Rogers, and P. Kundur, "Analytical investigation of factors influencing power systems Stabiliser," *IEEE Power Engineering Society: Inter- Area Oscillations in Power Systems*, pp. 144-150, 1994.
- [42] S. M. Kay, *Modern Spectral Estimation*: Prentice-Hall, 1988.
- [43] J. F. Hauer, C. J. Demeure, and L. L. Scharf, "Initial results in Prony analysis of power system response signals," *Power Systems, IEEE Transactions on*, vol. 5, pp. 80-89, 1990.
- [44] J. F. Hauer, "Application of prony analysis to determination of modal content and equivalent models for measured power system response," *Power Systems, IEEE Transactions on*, vol. vol. 6. no. 3, 1991.
- [45] D. J. Trudnowski, J. R. Smith, T. A. Short, and D. A. Pierre, "An application of Prony methods in PSS design for multi-machine systems," *Power Systems, IEEE Transactions on*, vol. 6, pp. 118-126, 1991.
- [46] C. E. Grund, J. J. Paserba, J. F. Hauer, and S. L. Nilsson, "Comparison of Prony and eigenanalysis for power system control

- design," *Power Systems, IEEE Transactions on*, vol. 8, pp. 964-971, 1993.
- [47] J. R. Smith, F. Fatehi, C. S. Woods, J. F. Hauer, and D. J. Trudnowski, "Transfer function identification in power system applications," *Power Systems, IEEE Transactions on*, vol. 8, pp. 1282-1290, 1993.
  - [48] D. J. Trudnowski, J. M. Johnson, and J. F. Hauer, "Making Prony analysis more accurate using multiple signals," *Power Systems, IEEE Transactions on*, vol. 14, pp. 226-231, 1999.
  - [49] J. J. Sanchez-Gasca and J. H. Chow, "Performance Comparison of Three Identification Methods for the Analysis of Electromechanical Oscillations," *Power Systems, IEEE Transactions on*, vol. 14, pp. 995-1002, 1999.
  - [50] G. Ledwich and E. Palmer, "Modal Estimation from Normal Operation of Power Systems," presented at IEEE Power System Winter Meeting Conference, 2000.
  - [51] R. L. Cresap and J. F. Hauer, "Emergence of a new swing modes in the western power system," *Power Apparatus Systems, IEEE Transactions on*, vol. Pas-100, pp. 3017-3024, 1981.
  - [52] C. Jing, J. D. McCalley, and M. Kommareddy, "An energy approach to analysis of interarea oscillations in power systems," *Power Systems, IEEE Transactions on*, vol. 11, pp. 734-740, 1996.

- [53] A. R. Messina, M. Ochoa, and E. Barocio, "Use of energy and power concepts in the analysis of the inter-area mode phenomenon," *Electric Power Systems Research*, vol. 59, pp. 111-119, 2001.
- [54] IEEE Task Force on Load Representation for Dynamic Performance, "Load representation for dynamic performance analysis [of power systems]," *Power Systems, IEEE Transactions on*, vol. 8, pp. 472-482, 1993.
- [55] IEEE Task Force on Load Representation for Dynamic Performance, "Standard load models for power flow and dynamic performance simulation," *Power Systems, IEEE Transactions on*, vol. 10, pp. 1302-1313, 1995.
- [56] P. C. Krause and . *Analysis of Electric Machinery*. New York: IEEE Press, 1985.
- [57] S. Ahmed-Zaid and M. Taleb, "Structural modeling of small and large induction machines using integral manifolds," *Energy Conversion, IEEE Transactions on*, vol. 6, pp. 529-535, 1991.
- [58] P. V. Kokotovic and P. W. Sauer, "Integral manifold as a tool for reduced-order modeling of nonlinear systems: A synchronous machine case study," *Circuits and Systems, IEEE Transactions on*, vol. 36, pp. 403-410, 1989.
- [59] R. Hung and H. W. Dommel, "Synchronous machine models for simulation of induction motor transients," *Power Systems, IEEE Transactions on*, vol. 11, pp. 833-838, 1996.

- [60] A. M. Stankovic and B. C. Lesieutre, "Parametric variations in dynamic models of induction machine clusters," *Power Systems, IEEE Transactions on*, vol. 12, pp. 1549-1554, 1997.
- [61] G. W. Stewart, "Stochastic perturbation theory," *SIAM Review*, vol. 32, pp. 597-610, 1990.
- [62] T. Y. J. Lem and R. T. H. Alden, "Comparison of experimental and aggregate induction motor responses," *Power Systems, IEEE Transactions on*, vol. 9, pp. 1895-1900, 1994.
- [63] T. Omata and K. Uemura, "Aspects of voltage responses of induction motor loads," *Power Systems, IEEE Transactions on*, vol. 13, pp. 1337-1344, 1998.
- [64] T. Thiringer and J. Luomi, "Comparison of reduced-order dynamic models of induction machines," *Power Systems, IEEE Transactions on*, vol. 16, pp. 119-126, 2001.
- [65] R. K. Varma, R. M. Mathur, G. J. Rogers, and P. Kundur, "Modeling effects of system frequency variation in long-term stability studies," *Power Systems, IEEE Transactions on*, vol. 11, pp. 827-832, 1996.
- [66] J. Alvarez-Gallegos and R. J. Herrera-Alfonsin, "Sliding mode control of induction motors using singular perturbation techniques," presented at Control Applications, 1992., First IEEE Conference on, 1992.
- [67] X. Xu, R. M. Mathur, J. Jiang, G. J. Rogers, and P. Kundur, "Modeling of generators and their controls in power system

- simulations using singular perturbations," *Power Systems, IEEE Transactions on*, vol. 13, pp. 109-114, 1998.
- [68] X. Xu, R. M. Mathur, J. Jiang, G. J. Rogers, and P. Kundur, "Modeling effects of system frequency variations in induction motor dynamics using singular perturbations," *Power Systems, IEEE Transactions on*, vol. 15, pp. 764-770, 2000.
- [69] D. Karlsson and D. J. Hill, "Modelling and identification of nonlinear dynamic loads in power systems," *Power Systems, IEEE Transactions on*, vol. 9, pp. 157-166, 1994.
- [70] C.-J. Lin, A. Y.-T. Chen, C.-Y. Chiou, C.-H. Huang, H.-D. Chiang, J.-C. Wang, and L. Fekih-Ahmed, "Dynamic load models in power systems using the measurement approach," *Power Systems, IEEE Transactions on*, vol. 8, pp. 309-315, 1993.
- [71] M. A. Pai, P. W. Sauer, and B. C. Lesieutre, "Static and dynamic nonlinear loads and structural stability in power systems," *Proceedings of the IEEE*, vol. 83, pp. 1562-1572, 1995.
- [72] I. R. Navarro, O. Samuelsson, and S. Lindahl, "Influence of normalization in dynamic reactive load models," *Power Systems, IEEE Transactions on*, vol. 18, pp. 972-973, 2003.
- [73] A. Borghetti, R. Caldon, A. Mari, and C. A. Nucci, "On dynamic load models for voltage stability studies," *Power Systems, IEEE Transactions on*, vol. 12, pp. 293-303, 1997.

- [74] P. Ju, E. Handschin, and D. Karlsson, "Nonlinear dynamic load modelling: model and parameter estimation," *Power Systems, IEEE Transactions on*, vol. 11, pp. 1689-1697, 1996.
- [75] W. W. Price, K. A. Wirgau, A. Murdoch, J. V. Mitsche, E. Vaahedi, and M. El-Kady, "Load modeling for power flow and transient stability computer studies," *Power Systems, IEEE Transactions on*, vol. 3, pp. 180-187, 1988.
- [76] E. Vaahedi, H. M. Z. El-Din, and W. W. Price, "Dynamic load modeling in large scale stability studies," *Power Systems, IEEE Transactions on*, vol. 3, pp. 1039-1045, 1988.
- [77] W.-S. Kao, C.-T. Huang, and C.-Y. Chiou, "Dynamic load modeling in Taipower system stability studies," *Power Systems, IEEE Transactions on*, vol. 10, pp. 907-914, 1995.
- [78] W.-S. Kao, "The effect of load models on unstable low-frequency oscillation damping in Taipower system experience w/wo power system stabilizers," *Power Systems, IEEE Transactions on*, vol. 16, pp. 463-472, 2001.
- [79] D.-Q. Ma and P. Ju, "A novel approach to dynamic load modelling," *Power Systems, IEEE Transactions on*, vol. 4, pp. 396-402, 1989.
- [80] G. C. Goodwin and K. S. Sin, *Adaptive filtering prediction and control*. Englewood Cliffs, N.J.: Prentice-Hall, 1984.
- [81] I. A. Hiskens and J. V. Milanovic, "Load modelling in studies of power system damping," *Power Systems, IEEE Transactions on*, vol. 10, pp. 1781-1788, 1995.

- [82] J. V. Milanovic and I. A. Hiskens, "Effects of load dynamics on power system damping," *Power Systems, IEEE Transactions on*, vol. 10, pp. 1022-1028, 1995.
- [83] T. Smed and G. Andersson, "Utilizing HVDC to damp power oscillations," *Power Delivery, IEEE Transactions on*, vol. 8, pp. 620-627, 1993.
- [84] O. Samuelsson and B. Eliasson, "Damping of electro-mechanical oscillations in a multimachine system by direct load control," *Power Systems, IEEE Transactions on*, vol. 12, pp. 1604-1609, 1997.
- [85] I. Kamwa, R. Grondin, D. Asber, J. P. Gingras, and G. Trudel, "Active-power stabilizers for multimachine power systems: challenges and prospects," *Power Systems, IEEE Transactions on*, vol. 13, pp. 1352-1358, 1998.
- [86] I. Kamwa, R. Grondin, D. Asber, J. P. Gingras, and G. Trudel, "Large-scale active-load modulation for angle stability improvement," *Power Systems, IEEE Transactions on*, vol. 14, pp. 582-590, 1999.
- [87] O. Samuelsson, "Load modulation at two locations for damping of electro-mechanical oscillations in a multimachine system," presented at Power Engineering Society Summer Meeting, 2000. IEEE, 2000.
- [88] O. Samuelsson, "Load modulation for damping of electro-mechanical oscillations," presented at Power Engineering Society Winter Meeting, 2001. IEEE, 2001.
- [89] T. J. E. Miller, *Reactive Power Control in Electric Systems*. New York: John Wiley, 1982.

- [90] IEEE Special Stability Controls Working Group, "Static VAR compensator models for power flow and dynamic performance simulation," *Power Systems, IEEE Transactions on*, vol. 9, pp. 229-240, 1994.
- [91] S. C. Kapoor, "Dynamic Stability of Long transmission Systems with Static Compensators and Synchronous Machines," *Power Apparatus and Systems, IEEE Transactions on*, vol. vol. PAS-98, pp. pp. 124-134, 1979.
- [92] M. A. Choudhry, M. A. Reza, and K. A. Ellithy, "Design of a robust modulation controller over a wide range of load characteristics for AC/DC systems," *Power Systems, IEEE Transactions on*, vol. 5, pp. 212-218, 1990.
- [93] M. Noroozian and G. Adersson, "Damping of power system oscillations by use of controllable components," *Power Delivery, IEEE Transactions on*, vol. 9, pp. 2046-2054, 1994.
- [94] C.-H. Cheng and Y.-Y. Hsu, "Damping of generator oscillations using an adaptive static VAR compensator," *Power Systems, IEEE Transactions on*, vol. 7, pp. 718-725, 1992.
- [95] H. Okamoto, A. Kurita, and Y. Sekine, "A method for identification of effective locations of variable impedance apparatus on enhancement of steady-state stability in large scale power systems," *Power Systems, IEEE Transactions on*, vol. 10, pp. 1401-1407, 1995.

- [96] H. F. Wang and F. J. Swift, "Capability of the static Var compensator in damping power system oscillations," *Generation, Transmission and Distribution, IEE Proceedings*-, vol. 11, 1996.
- [97] H. F. Wang and F. J. Swift, "Application of the Phillips-Heffron model in the analysis of the damping torque contribution to power systems by SVC damping control," *International Journal of Electrical Power & Energy Systems*, vol. 18, pp. 307-313, 1996.
- [98] H. F. Wang and F. J. Swift, "A unified model for the analysis of FACTS devices in damping power system oscillations. I. Single-machine infinite-bus power systems," *Power Delivery, IEEE Transactions on*, vol. 12, pp. 941-946, 1997.
- [99] A. R. Messina, O. Begovich M, and M. Nayebzadeh, "Analytical investigation of the use of static VAR compensators to aid damping of inter-area oscillations," *International Journal of Electrical Power & Energy Systems*, vol. 21, pp. 199-210, 1999.
- [100] J. Chen, J. V. Milanovic, and F. M. Hughes, "Comparison of the effectiveness of PSS and SVC in Damping of Power System Oscillations," Budapest, 1999.
- [101] M. Noroozian, M. Ghandhari, G. Andersson, J. Gronquist, and I. Hiskens, "A robust control strategy for shunt and series reactive compensators to damp electromechanical oscillations," *Power Delivery, IEEE Transactions on*, vol. 16, pp. 812-817, 2001.
- [102] A. V. Oppenheim, A. S. Willsky, and I. T. Young, *Signals and systems*. Englewood Cliffs, N.J.: Prentice-Hall, 1983.

- [103] A. V. Oppenheim, R. W. Schaffer, and J. R. Buck, *Discrete-time signal processing*, 2nd ed. Upper Saddle River, N.J.: Prentice Hall, 1999.
- [104] E. C. Ifeachor and B. W. Jervis, *Digital signal processing : a practical approach*. Wokingham, England Reading, Mass: Addison-Wesley, 1993.
- [105] Q. Zhao and J. Jiang, "Robust SVC controller design for improving power system damping," *Power Systems, IEEE Transactions on*, vol. 10, pp. 1927-1932, 1995.
- [106] A. R. Messina, H. Hernandez, E. Barocio, M. Ochoa, and J. Arroyo, "Coordinated application of FACTS controllers to damp out inter-area oscillations," *Electric Power Systems Research*, vol. 62, pp. 43-53, 2002.
- [107] G. R. Cooper and C. D. McGillem, *Probabilistic methods of signal and system analysis*, 2nd ed. New York: Holt Rinehart and Winston : CBS College Publishing, 1986.
- [108] N. Yang, Q. Liu, and J. D. McCalley, "TCSC controller design for damping interarea oscillations," *Power Systems, IEEE Transactions on*, vol. 13, pp. 1304-1310, 1998.
- [109] X. Zhou and J. Liang, "Overview of control schemes for TCSC to enhance the stability of power systems," *Generation, Transmission and Distribution, IEE Proceedings-*, vol. 146, pp. 125-130, 1999.
- [110] T. Yu and P. I. So, "Coordinated control of TCSC and SVC for system damping improvement," presented at Electric Utility

- Deregulation and Restructuring and Power Technologies, 2000. Proceedings. DRPT 2000. International Conference on, 2000.
- [111] G. Chunlin, T. Luyuan, and W. Zhonghong, "Stability control of TCSC between interconnected power networks," presented at Power System Technology, 2002. Proceedings. PowerCon 2002. International Conference on, 2002.
- [112] C.-T. Chang and Y.-Y. Hsu, "Design of UPFC controllers and supplementary damping controller for power transmission control and stability enhancement of a longitudinal power system," *Generation, Transmission and Distribution, IEE Proceedings-*, vol. 149, pp. 463-471, 2002.
- [113] W. Bo and Z. Yan, "Damping subsynchronous oscillation using UPFC-a FACTS device," presented at Power System Technology, 2002. Proceedings. PowerCon 2002. International Conference on, 2002.
- [114] S. A. Nabavi Niaki and M. Reza Iravani, "Application of unified power flow controller (UPFC) for damping interarea oscillations," presented at Transmission and Distribution Conference and Exhibition 2002: Asia Pacific. IEEE/PES, 2002.
- [115] N. Tambey and M. L. Kothari, "Damping of power system oscillations with unified power flow controller (UPFC)," *Generation, Transmission and Distribution, IEE Proceedings-*, vol. 150, pp. 129-140, 2003.

## Appendix A:

### Some Signal Processing Aspects

In this appendix some aspects of signal processing used in this thesis are explained [24-27].

#### A.1 Random Variable, Random Process and Ensemble

A random variable  $X$  is defined as a function that maps any outcome  $\xi$  of a sample space  $\Omega$  into a real number  $x$ , with the two necessary conditions. Firstly, the set  $\{X \leq x\}$  will be an outcome of  $\Omega$  for any real number. Secondly,  $P\{X = -\infty\} = 0$  and  $P\{X = \infty\} = 0$ , where  $P$  represents the probability of the event (page 74 of [25]).

Similarly, a random process is a rule that maps any outcome  $\xi$  of a sample space  $\Omega$  into a function  $X(t, \xi)$  (page 373 of [25]).

When  $t$  and  $\xi$  are variables, the random process  $X(t, \xi)$  shows an ensemble of time functions. Each time function of the ensemble is called realization or ensemble member (page 180 of [24]).

#### A.2 Cross-correlation and Autocorrelation

If  $X(t)$  and  $Y(t)$  are two real wide-sense stationary processes, the cross-correlation function of  $X(t)$  and  $Y(t)$  are to be found from the following equation

$$C_{XY}(\tau) = E[X(t)Y(t+\tau)] \quad (\text{A.1})$$

where  $E$  is the expected value.

If  $X(t)$  and  $Y(t)$  are real and jointly ergodic processes then the time cross-correlation process  $x(t)$  and  $y(t)$  can be computed from

$$C_{xy}(\tau) = \lim_{T \rightarrow \infty} \frac{1}{2T} \int_{-T}^T x(t) y(t+\tau) d\tau \quad (\text{A.2})$$

where  $x$  and  $y$  the ensemble members of  $X(t)$  and  $Y(t)$ , respectively.

Similarly, If  $X(t)$  is a real wide-sense stationary processes, then the autocorrelation function of  $X(t)$  can be obtained found from

$$R_{XX}(\tau) = E[X(t) X(t+\tau)] \quad (\text{A.3})$$

If  $X(t)$  is a real and ergodic process then the time autocorrelation function of  $x(t)$  can be calculated from

$$R_{xx}(\tau) = \lim_{T \rightarrow \infty} \frac{1}{2T} \int_{-T}^T x(t) x(t+\tau) d\tau \quad (\text{A.4})$$

where  $x$  is an ensemble member of  $X(t)$ .

### **A.3 Power Spectrum Density and Cross-Power spectrum Density**

if  $X(t)$  a real stationary processes of order of two, then the power density spectrum of  $X$  is the Fourier transform [29] of autocorrelation of  $X$  that can be found from the following Equation as

$$P_{XX}(\omega) = \int_{-\infty}^{\infty} R_{XX}(\tau) e^{-j\omega\tau} d\tau \quad (\text{A.5})$$

Similarly, if  $X(t)$  and  $Y(t)$  are two real wide-sense stationary processes, then the cross-power density spectrum of  $X$  and  $Y$  is the Fourier transform of cross-correlation of  $X$  and  $Y$  that can be computed from

$$\mathbf{P}_{XY}(\omega) = \int_{-\infty}^{\infty} C_{XY}(\tau) e^{-j\omega\tau} d\tau \quad (\text{A.6})$$

#### A.4 Evaluation of a linear systems Response to a random Variable

##### Input

A system with a random variable input  $u(t)$  as the input and  $y(t)$  as the output is illustrated in Figure A.1.

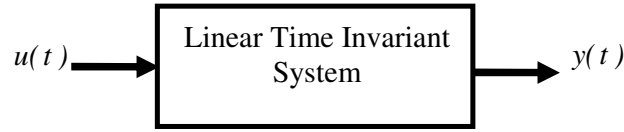


Figure A.1: A linear system with a random variable input

In Figure A.1,  $u(t)$  is an ensemble member of process  $U(t)$ . If the impulse response of this system is denoted by  $h(t)$  then we have

$$C_{uy}(\tau) = R_{uu} * h(\tau) \quad (\text{A.7})$$

or

$$C_{yy}(\tau) = R_{yu} * h(\tau) \quad (\text{A.8})$$

where  $*$  is the convolution integral operator.

By taking the Fourier transform from Equations (A.7) and (A.8), the transfer function of  $\mathbf{H}(\omega)$  can be found from one of the following equations

$$\mathbf{H}(\omega) = \frac{\mathfrak{F}[C_{uy}(\tau)]}{\mathfrak{F}[R_{uu}(\tau)]} \quad (\text{A.9})$$

or

$$\mathbf{H}(\omega) = \frac{\Im[C_{yy}(\tau)]}{\Im[R_{yu}(\tau)]} \quad (\text{A.10})$$

With regard to Equations (A.5) and (A.6), Equations (A.9) and (A.10) are changed to Equations (A.11) and (A.12) respectively, as

$$\mathbf{H}(\omega) = \frac{\mathbf{P}_{uy}(\omega)}{\mathbf{P}_{uu}(\omega)} \quad (\text{A.11})$$

or

$$\mathbf{H}(\omega) = \frac{\mathbf{P}_{yy}(\omega)}{\mathbf{P}_{yu}(\omega)} \quad (\text{A.12})$$

where

$\mathbf{P}_{uu}(\omega)$  = power density spectrum of  $u$

$\mathbf{P}_{uy}(\omega)$  = cross-power density spectrum of  $u$  and  $y$

$\mathbf{P}_{yy}(\omega)$  = power density spectrum of  $y$

$\mathbf{P}_{yu}(\omega)$  = cross-power density spectrum of  $y$  and  $u$

## Appendix B

The specifications of test power system of Section 5.5 are as follows

### 1. Synchronous Generator and Transmission Lines

$$\text{Inertia} = J_G = 0.404$$

$$\text{Input mechanical power} = P_{mg} = 0.8$$

$$\text{Damping coefficient} = D_g = 0.003$$

$$Z_a = j0.3$$

$$Z_b = j0.2$$

The transient reactance of the synchronous generator is incorporated in  $Z_a$ .

### 2. Induction Motor

$$\text{Inertia} = J_m = 0.1120$$

$$\text{Stator resistance} = r_s = 0.0185$$

$$\text{Rotor resistance} = r_{rs} = 0.0073$$

$$\text{Stator leakage reactance} = x_s = 0.085$$

$$\text{Rotor leakage reactance} = x_r = 0.085$$

$$\text{Mechanical load} = P_{mm} = 0.1$$

$$\text{Damping coefficient} = D_m = 0.0027$$

All of the parameters in *p.u.* and the synchronous frequency is  $f_s = 60 \text{ Hz}$ .



## Appendix C

The specifications of test power system of Section 5.8 are as follows

### 1. Synchronous Generator and Transmission Lines

$$J_G = 0.404$$

$$P_{mg} = 0.8$$

$$D_g = 0.07$$

$$Z_a = j0.03$$

$$Z_b = j0.02$$

The transient reactance of the synchronous generator is neglected.

### 3. Induction Motor

$$J_m = 0.00224$$

$$r_s = 0.0185$$

$$r_r = 0.0132$$

$$x_s = 0.085$$

$$x_r = 0.085$$

$$P_{mm} = 0.1$$

$$D_m = 0.0027$$

All of the parameters in  $p.u.$  and  $f_s = 60 \text{ Hz}$ .